

# Integrated Single Photon Emitters

Junyi Lee,<sup>1</sup> Victor Leong,<sup>1</sup> Dmitry Kalashnikov,<sup>1</sup> Jibo Dai,<sup>1</sup> Alagappan Gandhi,<sup>2</sup> and Leonid Krivitsky<sup>1</sup>

<sup>1</sup>*Institute of Materials Research and Engineering, Agency for Science, Technology and Research (A\*STAR),*

*2 Fusionopolis Way, #08-03 Innovis, 138634 Singapore*

<sup>2</sup>*Institute of High Performance Computing, Agency for Science, Technology and Research (A\*STAR),*

*1 Fusionopolis Way, #16-16 Connexis North, 138632 Singapore*

(Dated: 30 July 2020)

The realization of scalable systems for quantum information processing and networking is of utmost importance to the quantum information community. However, building such systems is difficult because of challenges in achieving all the necessary functionalities on a unified platform while maintaining stringent performance requirements of the individual elements. A promising approach which addresses this challenge is based on the consolidation of experimental and theoretical capabilities in quantum physics and integrated photonics. Integrated quantum photonics devices allow efficient control and read-out of quantum information while being scalable and cost effective. Here we review recent developments in solid-state single photon emitters coupled with various integrated photonic structures, which form a critical component of future scalable quantum devices. Our work contributes to the further development and realization of quantum networking protocols and quantum logic on a scalable and fabrication-friendly platform.

## CONTENTS

<b>I. Introduction</b>	<b>1</b>	C. Single photon emitters in Hexagonal Boron Nitride (hBN)	<b>23</b>
<b>II. Theoretical Background</b>	<b>2</b>	D. Deterministic Creation and Control of Single Photon Emitters in 2D Materials	<b>23</b>
A. The NV <sup>-</sup> center as an illustrative SPE	3	E. Enhancement of Emission from 2D Materials by Coupling into Resonant Modes	24
1. Photostability, saturated count rates and emission into ZPL	3	F. Coupling and Transfer of Emission from 2D Materials into Photonic Structures	24
2. Indistinguishability	5	<b>VII. Integration Approaches</b>	<b>25</b>
3. Single photon purity	6	A. Random Dispersion	26
B. Enhancement of ZPL emission using resonant cavities	7	B. Targeted Creation	27
<b>III. Integrated NV<sup>-</sup> centers in bulk diamond</b>	<b>9</b>	1. Irradiation and annealing in diamond	27
A. Integration with waveguides	9	2. Implantation and annealing in diamond	27
B. Integration with resonators	11	3. Laser writing and annealing in diamond	28
1. Diamond ring resonators	11	4. In-situ Lithography	29
2. Diamond 2-D photonic crystal cavities	11	C. Wafer Bonding	29
3. Diamond 1-D photonic crystals cavities	12	D. Pick-and-place	31
C. Larger scale integration	12	1. Transfer Printing	31
D. Deterministic integration	13	2. Microprobe	31
E. Outlook	15	<b>VIII. Conclusion and outlook</b>	<b>32</b>
<b>IV. Color centers in nanodiamonds</b>	<b>15</b>	<b>Data availability statement</b>	<b>33</b>
A. Fabrication	15	<b>Acknowledgments</b>	<b>33</b>
B. Integration with photonic structures	16	<b>References</b>	<b>34</b>
<b>V. Quantum Dots</b>	<b>18</b>	<b>I. INTRODUCTION</b>	
A. Introduction to Quantum Dots	18	The control and manipulation of physical objects at the quantum level has progressed considerably in the past decade. This quantum control promises fascinating advances to both technology and fundamental science. For	
B. As a Single-Photon Emitter	18		
C. Spin-Photon Interfaces	19		
D. Interfacing Multiple QDs	19		
<b>VI. 2-D materials</b>	<b>21</b>		
A. Introduction into 2D Materials	21		
B. Single photon emitters in Transitional Metal Dichalcogenides (TMDC)	22		

example, use of quantum phenomena in data systems allows one to speed up computation and database search algorithms and to develop highly secure communication networks<sup>1,2</sup>. A new class of devices are now in active development to fundamentally exploit the paradigm of quantum information and to make it accessible in practical applications.

A variety of physical systems have been identified as candidates for emerging quantum technologies, such as quantum dots, atomic defects in solids, atoms etc. Solid-state systems possess outstanding quantum optical properties that can be used to build practical quantum devices. Quantum information can be stored, for example, in the electron spin of a defect and the nuclear spin of nearby atoms with relatively long coherence times (a few ms) even at room temperature. During this time, it is feasible to record, manipulate, and read-out quantum information. Quantum logic can be implemented with incident microwave and RF fields, driving transitions between electron and nuclear sublevels. These blocks can interact with each other via photon-mediated interaction. Optical links connect the nodes as they enable reliable and fast transfer of quantum information.

Building the quantum data system outlined above requires, among other things, efficient interfaces between solid-state single photon emitters (SPEs) and optical networks. A scalable and cost efficient approach towards implementing such interfaces relies on the use of integrated photonics technologies. The stationary nodes that encode the quantum information (for example, a spin state of an atomic-like defect) can be interconnected via optical waveguides made of low-loss materials. Optically resonant micro- and nanostructures can enhance the coupling of photons emitted from the stationary nodes into waveguides. Moreover, enhancement can also be obtained in waveguide QED due to slow light effects. Photons can then be routed to different nodes on the same chip or between different chips to create quantum entanglement between the nodes. Furthermore, one can use compact and highly sensitive photodetectors fabricated on the same chip for the read-out of quantum information. Generation, transport, manipulation and detection of quantum information can all be accomplished on this scalable, intrinsically stable and fabrication-friendly platform.

Besides applications in quantum information processing, the same physics and engineering concepts can be further applied in quantum metrology and sensing<sup>3,4</sup>. Combining solid-state quantum systems with compact photonic devices will lead to the development of a new family of highly sensitive and compact temperature, stress, inertia, electric and magnetic field sensors with high spatial resolution. These sensors will find applications in microelectronics, bio-chemical, and healthcare industries.

In this paper, we review recent experimental efforts in developing integrated solid-state single photon sources, which serve as a key enabling component for scalable quantum devices. Broader reviews of other necessary

components in a quantum photonic chip are available elsewhere<sup>5,6</sup>. Due to the multi-disciplinary nature of integrating solid state SPEs onto photonic chips, we have strove to make this review accessible to a broad audience with varying backgrounds by giving a theoretical overview of important SPE metrics and providing details related to the fabrication and integration of SPEs with resonant photonic structures. A shorter review covering solid state SPEs of slightly different systems can be found in Ref. 7.

We start off with a review of the nitrogen vacancy (NV) defect center in diamond as an illustrative example of a solid state SPE in Section II. After describing its basic photo-physical properties, we then provide a generic theoretical framework for the interaction of resonant photonic structures with quantum emitters. We then proceed with a review of experiments that have integrated NV centers in bulk diamonds with optical waveguides and resonant structures before discussing their prospects of larger scale integration with other photonic components and different material platforms (Section III). In Section IV we describe the integration of color centers in nanodiamonds. The limitations and benefits of color centers in nanodiamonds versus those in bulk diamond are also discussed.

Section V is focused on integrated SPEs in Quantum Dots (QDs). Following a brief introduction into the photo-physics of QDs and their interaction with optical cavities, we describe methods for manipulating the QDs spin states. We then discuss experiments on interfacing multiple QDs coherently with the goal of generating entanglement between spatially separated QDs on the same chip.

In Section VI we discuss SPEs in 2D materials, namely in transitional metal dichalcogenides (TMDC) and hexagonal boron nitride (hBN). Following a brief overview of different types of 2D SPEs, we discuss their interfaces with resonant photonic structures.

In Section VII we discuss various techniques for the integration of solid state SPEs with nanophotonics structures. This section describes dedicated nanofabrication and mechanical nano-manipulation methods.

Finally, we present two benchmarking tables in Section VIII for comparing various experimentally integrated SPEs and resonators before concluding with a general outlook for the field.

## II. THEORETICAL BACKGROUND

Two-level quantum mechanical systems are natural candidates for true SPEs. At first sight, discrete energy levels within a solid-state system normally described by valence and conduction bands might seem at odds with intuition, but they can exist under special circumstances near a lattice defect or in quantum dots, where electrons are physically confined to such small spatial volumes that their eigen-energies are discrete. For many applications,

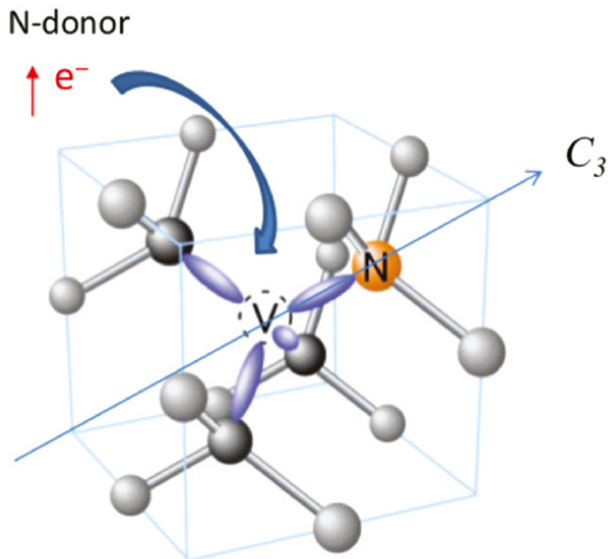


FIG. 1. Structure of the  $NV^-$  center. Grey circles denote carbon atoms. The vacancy is denoted with a dashed vacant circle while the nitrogen substitutional defect is shown as an orange circle.  $sp^3$  bonds are illustrated by grey rods while dangling bonds to the vacancy are drawn as purple ellipses. As shown in the figure, the NV center can have a  $C_{3v}$  symmetry about any of the equivalent  $\langle 111 \rangle$  directions in a diamond that it is aligned with. A  $NV^-$  state is negatively charged because it acquires and traps an additional electron from another donor. Reprinted from [Ádám Gali](#), “Ab initio theory of the nitrogen-vacancy center in diamond,” *Nanophotonics* **8**, 1907 - 1943 (2019) under the [CC BY 4.0](#) license.

however, it is not merely sufficient to have a two-level system since there are many other metrics to consider. In the following section, we use a nitrogen vacancy defect in diamond as an illustrative solid-state SPE to discuss these other considerations and to motivate the benefits of integrating solid-state SPEs with resonant photonic structures. Although we use the nitrogen vacancy defect in diamond as a concrete example, many of the challenges we point out are broadly applicable to quantum dots and 2-D materials, where these challenges can be similarly mitigated by their integration with photonic structures.

### A. The $NV^-$ center as an illustrative SPE

A nitrogen vacancy (NV) center in diamond consists of a nitrogen atom (a substitutional defect) that is paired together with a neighboring vacant site (see Fig. 1). The substitution-vacancy pair can be aligned along any of the equivalent  $\langle 111 \rangle$  directions in the crystal and typically, all four possible orientations of the NV centers are found in equal proportions although relatively recent work have successfully created preferentially oriented NV centers<sup>9-11</sup>. Although NV centers are known to exist in two distinct states (traditionally labeled as

$NV^0$  and  $NV^-$ )<sup>12</sup>, it is the  $NV^-$  state that has of late received the most attention due to its attractive optical and spin properties that have made it amenable to a variety of technological applications including quantum computation<sup>13</sup>, quantum information<sup>14</sup> and microscopic magnetic<sup>15</sup>, electric<sup>16</sup>, stress<sup>17</sup>, inertia<sup>18</sup> and even thermal<sup>19</sup> sensing. Figure 2 shows the energy levels of the ground ( $a_1^2e^2$ ) and first excited ( $a_1^1e^3$ ) molecular orbital (MO) configurations<sup>20</sup> of the  $NV^-$ . Since the NV center has a  $C_{3v}$  point symmetry with 2 one-dimensional irreducible representations ( $A_1$  and  $A_2$ ), and a two-dimensional irreducible representation ( $E$ )<sup>21,22</sup>, the nomenclature of the states and orbitals are typically given by their transformation properties under  $C_{3v}$ . The  $^3A_2$  orbital singlet ground state has been amply confirmed by electron paramagnetic resonance (EPR) in the dark<sup>23</sup>, optical hole burning<sup>24</sup>, optically detected magnetic resonance<sup>25,26</sup> (ODMR), and Raman heterodyne measurements<sup>27</sup> to be a spin triplet that is split, at zero magnetic field, by  $\approx 2.88$  GHz<sup>24,28</sup> into a spin singlet  $A_1$  (with  $m_s = 0$ ) and spin doublet  $E_x, E_y$  (with  $m_s = \pm 1$ ) state due to spin-spin interactions<sup>21,29,30</sup>.

Similarly, the orbital-doublet excited  $^3E$  state is also known to be a spin triplet via ODMR measurements<sup>31,32</sup>. The degeneracy of these states is likewise lifted by spin-spin and spin-orbit interactions<sup>21</sup> into  $E_x, E_y$  states with  $m_s = 0$ , and  $A_1, A_2, E_x$  and  $E_y$  states with  $m_s = \pm 1$  (see Fig. 2). Compared to the ground state however, the excited state is considerably more sensitive to shifts induced by lattice strains<sup>31-33</sup> and the exact ordering of its states are more variable. Nevertheless, it is clear from EPR measurements that the zero-phonon line at 637 nm is associated with a spin-triplet excited state and that the triplet state consists of a spin-singlet (i.e. the  $E_x, E_y$  states with  $m_s = 0$ ) and spin-doublet (consisting of  $A_1, A_2, E_x$  and  $E_y$  states with  $m_s = \pm 1$ ) state that are separated by a zero-field splitting  $D_{es}$  of  $\approx 1.42$  GHz<sup>31,32</sup>. Early uniaxial stress studies<sup>34</sup>, together with the measurements described above, indicate that the prominent zero-phonon line (ZPL) observed at 1.945 eV ( $\approx 637$  nm) is due to a  $^3A_2 \rightarrow ^3E$  transition (see Fig. 3). Moreover, for a NV in a low strain environment, the ZPL emission is mostly linearly polarized with the plane of polarization depending on the NV’s axial orientation, indicating that the transitions are mostly spin-conserving<sup>34,35</sup>.

### 1. Photostability, saturated count rates and emission into ZPL

Despite receiving less attention than the  $NV^-$ , the  $NV^0$  state can affect the dynamics of  $NV^-$  in important ways such as its photostability to which we now turn. An important characteristic of a SPE is its photostability. Although organic fluorescent dyes are an important class of single photon emitters, such sources have a significant disadvantage because of their susceptibility to photobleaching in which photochemical changes induced by

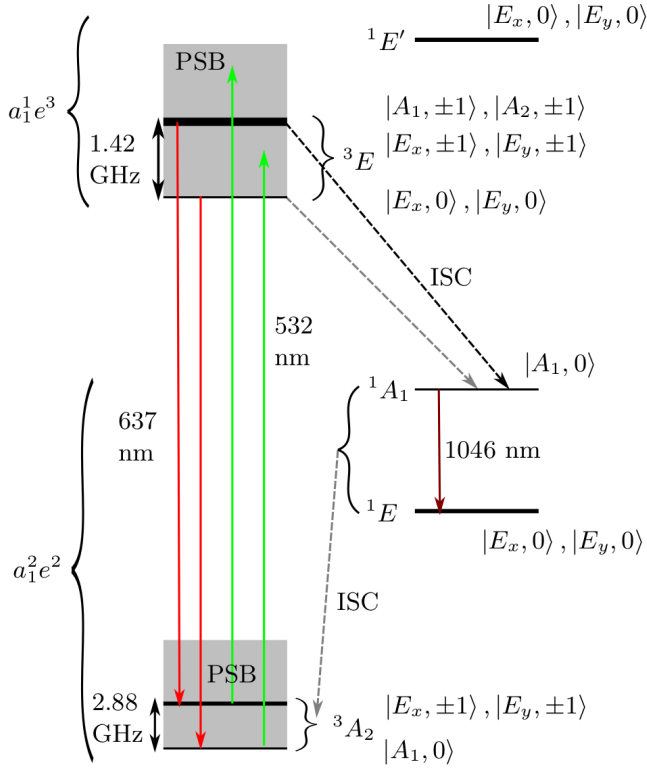


FIG. 2. Energy levels of the ground and first excited MO configuration of the NV<sup>-</sup>. States labeled here with a  $|n, m_s\rangle$  notation are spin-orbit states that transform according to a particular row of an irreducible representation of  $C_{3v}$  (labeled by  $n$ ; see Ref. 20 and 21), which are the convenient basis states to use in the presence of spin-orbit/spin-spin interactions. Note that they are linear combinations of states with definite azimuthal spin quantum numbers  $m_s$  and can hence have  $m_s = \pm 1$ . PSB denotes the phonon side band. Solid lines with single arrow heads denote optical transitions, while solid lines with double arrow heads denote microwave transitions. Non-radiative inter-system crossings (ISC)s are denoted by dashed lines. A darker ISC line between the  $m_s = \pm 1$  states of  ${}^3E$  to  ${}^1A_1$  is used to illustrate the faster ISC rate for that transition. Spacing of the energy levels are not drawn to scale.

the excitation light causes the emitter to degrade and permanently lose its fluorescence<sup>36</sup>. This is, for obvious reasons, undesirable for many quantum information and communication applications. Fortunately, SPEs like defect centers in diamond, 2-D materials and quantum dots are considerably more robust. However, despite the excellent photostability of the NV<sup>-</sup> center, it is known that the fluorescence of NV<sup>-</sup> can nevertheless be significantly (but mostly reversibly) quenched<sup>37–40</sup> (sometimes called *blinking*) when probed at high (typically pulsed) laser intensity and that this has been partially attributed to a spin-dependent ionization of NV<sup>-</sup> to NV<sup>0</sup><sup>41</sup>. Moreover, oscillations between NV<sup>-</sup> and NV<sup>0</sup> have been observed as a function of the excitation wavelength<sup>42</sup> and it is estimated that the NV center can be in the NV<sup>0</sup> state for ~

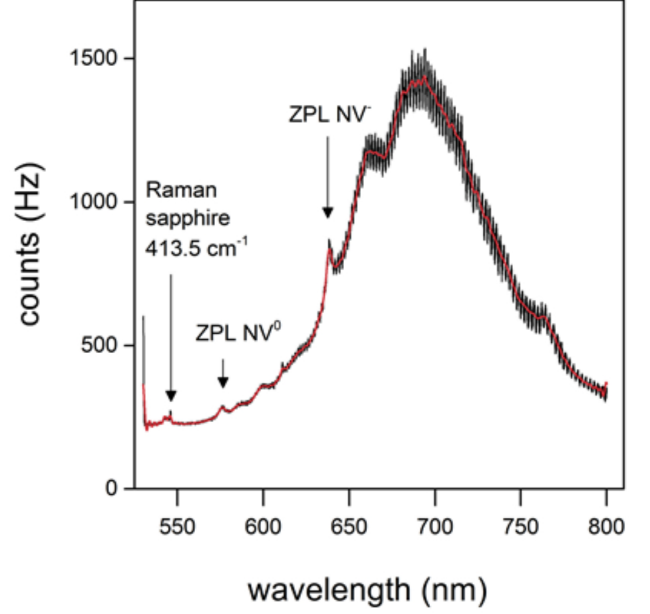


FIG. 3. Typical photoluminescence spectra of a NV center (on a sapphire substrate). Red-shifted emission to the ground state phonon sidebands constitute a large part of the spectrum and the NV ZPLs constitutes only a small fraction of the emission spectra. Reprinted with permission of Springer Nature Customer Service Center GmbH from Brenneis, Gaudreau, Seifert, Karl, Brandt, Huebl, Garrido, Koppens, and Holleitner, “Ultrafast electronic readout of diamond nitrogen-vacancy centres coupled to graphene,” *Nature Nanotechnology* **10**, 135-139 (2015), Copyright 2015.

30% of the time under usual operating conditions<sup>43</sup>. Nevertheless, these effects in NV may be mitigated by further annealing at 1200 °C<sup>44,45</sup>, and more generally, the equilibrium concentration<sup>46</sup> and stability of the NV<sup>-</sup> state depends on the Fermi level, which may be altered, among other things, by doping (N is itself a deep donor), irradiation, heating, photo-excitation, surface-termination, and annealing conditions<sup>12,47–51</sup>. Similarly, although the exact mechanisms may differ, quantum dots in nanocrystals are also susceptible to blinking<sup>52,53</sup>.

A related metric is the source’s saturated count rate at which point further increasing the excitation power no longer induces significantly more fluorescence. Generally, most applications would benefit from a brighter source since there are always losses in any real world application and in particular, repeat-until-succeed quantum information schemes<sup>55–57</sup> benefit from a higher rate of success with brighter sources. Table I lists some experimentally measured count rates that give an idea of the brightness of various sources. We caution however that the numbers do not enable a fair comparison between different references since the measured count rates is highly dependent on experimental conditions such as the collection optics/position, detection efficiency, exci-

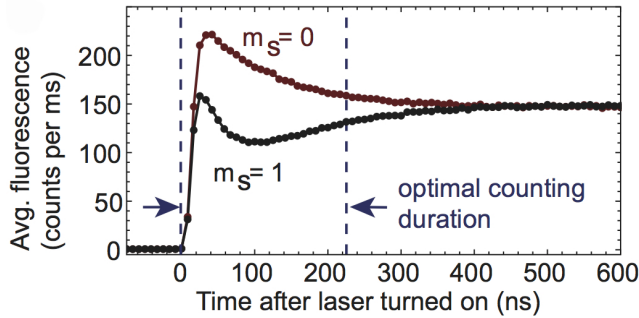


FIG. 4. Fluorescence from a  $\text{NV}^-$  center after initialization to either a  $m_s = 0$  or  $m_s = 1$  state. The spin dependent fluorescence is due to a much faster non-radiative inter-system crossing (ISC) from the  $m_s = \pm 1$  excited states to the  $^1\text{A}_1$  singlet state (see Fig. 2), and consequently, fluorescence at the ZPL is due mostly to radiative decays from the  $m_s = 0$  excited state<sup>60</sup>. This spin-selective depopulation of  $^3\text{E}$  to  $^1\text{A}_1$  also enables a  $\sim 80\%$  polarization of the  $m_s = 0$  ground state by optical pumping<sup>61,62</sup> that can then (if desired) be transferred to the  $m_s = \pm 1$  states by applying a microwave  $\pi$  pulse. Data in this trace was obtained after averaging over  $3 \times 10^7$  measurements. The optimal duration for photon counting can be obtained by using a maximum likelihood analysis to optimize the discrimination between  $m_s = 0$  versus  $m_s = 1$  states. Reprinted with permission from Ref. 63 © The Optical Society.

tation intensity etc. that are highly variable from one experiment to another.

Physically, the count rate from a single emitter is inversely proportional to its excited state lifetime that can, as we further discuss in section II B, be decreased by integrating the SPE with a resonator so that its rate of spontaneous emission into a resonant mode of the cavity is enhanced. This is useful for several reasons. Firstly, as Figure 3 illustrates, emission from the  $\text{NV}^-$ 's ZPL constitutes only a small fraction of its entire emission, with the majority of it coming from red-shifted transitions to the ground state phonon sidebands. The Debye-Waller factor, which quantifies this fraction, is particularly small for the  $\text{NV}^-$  and is approximately 0.04<sup>58,59</sup>. This is undesirable for many quantum information applications since coherent information may be lost to the phonon reservoir when transitions to the phonon sideband occurs. A small Debye-Waller factor is also undesirable for many nano-sensing applications involving the  $\text{NV}^-$  since many of them rely on the  $\text{NV}^-$ 's spin dependent ZPL emission to read out the  $\text{NV}^-$ 's spin state (see Fig. 4). Fortunately, by integrating the SPE with a resonator that has been engineered to be resonant at the SPE's ZPL, high count rates into the desired ZPL transition can be achieved.

## 2. Indistinguishability

Indistinguishability of photons is another important metric of SPEs designed for on-chip quantum infor-

mation applications such as linear optical quantum computing<sup>64</sup>, quantum teleportation<sup>65-67</sup> and entanglement swapping<sup>68,69</sup> that uses two-photon interference. In general, photons can be distinguished by their spectral/temporal shape as well as their polarization and time-of-arrival at a particular location. Although two identical but spatially separated two-level systems should in theory emit photons with the same spectral content, this is typically spoiled by the emitters' coupling to two different local environments. At short (compared to the radiative lifetime) time scales, interactions with the solid-state environment through, for example phonons, charge or spin noise<sup>70,71</sup>, perturb the energies of the two-level system and induces dephasing of the optical transitions which homogeneously broaden the linewidth and decrease the indistinguishability of emitted photons. On the other hand, slower interactions (relative to the radiative lifetime) will induce spectral diffusion of the emission wavelength and inhomogeneously broaden the linewidth (see Figures 5 and 17a). Moreover, the excitation wavelength can also affect the distinguishability of emitted photons.

In general, using a resonant excitation (637 nm for  $\text{NV}^-$ ) is more advantageous to the creation of indistinguishable photons since it eliminates timing jitters (which decreases indistinguishability) associated with relaxation through phonons<sup>72</sup>. Furthermore, higher frequency non-resonant excitation have a greater potential of ionizing defects around the SPE leading to larger charge fluctuations<sup>73</sup> that will in turn induce spectral diffusion. Consequently, resonant excitation is generally preferred for generating indistinguishable photons. However, we note that for the  $\text{NV}^-$ , resonant excitation cannot by itself generate ZPL photons continuously due to a permanent photoionization into the dark  $\text{NV}^0$  state<sup>74</sup>. However, this can be alleviated by using a weak ( $\sim 100$  nW) repump laser that is resonant with the  $\text{NV}^0$  ZPL (575 nm). Although a non-resonant 532 nm repump is also a popular choice, for reasons noted above, a weak resonant 575 nm repump is crucial to reducing longer term spectral diffusion by decreasing the probability of ionizing defects around the NV center<sup>74</sup> (see Fig. 5).

At short timescales, the photon's indistinguishability can be estimated by the metric<sup>75</sup>

$$\xi \equiv \frac{T_2}{2T_1} = \frac{1}{\Gamma T_1}, \quad (1)$$

where  $T_1$  is the emitter's radiative lifetime and  $T_2$  is the coherence time of the optical transition that is defined as<sup>75</sup>

$$\frac{1}{T_2} = \frac{1}{2T_1} + \frac{1}{T_2^*} = \frac{\Gamma}{2}. \quad (2)$$

$T_2^*$  here is the reciprocal of the dephasing rate  $\Gamma^* = 2/T_2^*$  that is causing *additional* (on top of the natural linewidth) homogeneous broadening while  $\Gamma$  is the (angular) FWHM of the emission's homogeneously broadened spectrum. We note that in general  $T_2 \leq 2T_1$  and

therefore,  $\xi \in [0, 1]$ . Experimentally, a common way to measure the indistinguishability of photons from a SPE is to measure the two-photon interference in a Hong-Ou-Mandel (HOM) type experiment<sup>76</sup> in which two indistinguishable photons arriving at a 50/50 beam-splitter at the same time should always end up in the same output port. In such a setup, coincidence counts of photons at both output ports should decrease to zero for two indistinguishable photons. It can be shown that Eq. (1) gives the efficiency (or the normalized size) of a HOM dip with  $\xi = 1$  corresponding to perfect distinguishability of the photons<sup>75</sup>. HOM interference between spatially separated defect centers have been experimentally demonstrated<sup>77–79</sup> and as Table I demonstrates, multiple integrated QDs have also demonstrated near ideal indistinguishability.

An intuitive way of understanding Eq. (1) is to see a transition with coherence time  $T_2$  as emitting a photon wavepacket of temporal width  $T_2/2$ , which sets the width of a HOM interference dip since that is the maximum temporal overlap between two distinct photons. Moreover, there is a time jitter of order  $T_1$  for the spontaneous emission to occur and therefore the probability of having two such distinct photon wavepacket interfere successfully is  $\sim T_2/(2T_1)$ . This suggests that one way of increasing the indistinguishability of photons from SPEs is to reduce their radiative lifetime  $T_1$  by placing them into a resonant cavity. For example, this has been successfully done for quantum dots in micropillar cavities where a HOM dip was successfully measured<sup>80,81</sup>. Moreover, such resonant cavities can be potentially used to implement other schemes for generating indistinguishable photons including cavity-assisted spin flip Raman transitions<sup>72,82</sup>. Furthermore, cavities can be used to select a particular polarization, which is also important for indistinguishability, and a particular spatial mode, which can make outcoupling to an in-plane waveguide easier. Table I summarizes some of the experimentally realized  $T_1$  values of integrated SPEs. We have also provided  $\Gamma^\dagger/(2\pi)$  values, which are the experimentally measured FWHM values that are not necessarily from homogeneously broadened lines.  $\xi^\dagger$ , which is calculated using Eq. (1) with  $\Gamma \rightarrow \Gamma^\dagger$  is also tabulated as a measure of indistinguishability.

Despite the utility of cavities described above, we acknowledge that they can only help with short term dephasing processes that homogeneously broaden the linewidth. For longer term fluctuations due, for example, to ionization of nearby defects that lead to local charge fluctuations<sup>78,83</sup> or drifting strains<sup>84</sup> that shift the energies of the excited states, a different strategy is required. Passive solutions include carefully fabricating the material with tailored annealing and surface treatments<sup>83</sup> while active solutions have also been investigated whereby the energies of the excited states are actively shifted via the Stark effect to stabilize the ZPL frequency<sup>84</sup>. Using these strategies, near life-time limited linewidths ( $\sim 13$  MHz) have been obtained for  $NV^-$

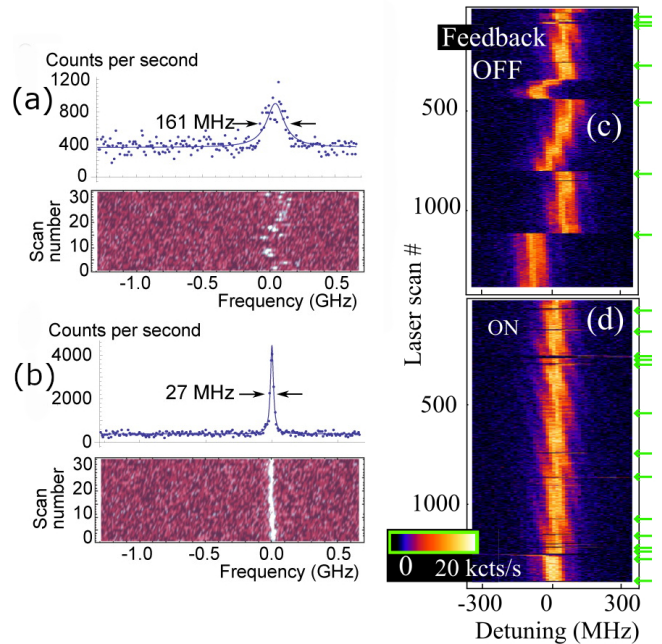


FIG. 5. (a), (b): Photoluminescence as a function of excitation frequency for a  $NV^-$  in an appropriately processed diamond. The  $NV^-$  is repumped at 532 nm for (a) and 575 nm for (b). Notice the significant decrease in spectral wandering for a resonant (of  $NV^0$ ) repump. Reprinted with permission from Chu, de Leon, Shields, Hausmann, Evans, Togan, Burek, Markham, Stacey, Zibrov, Yacoby, Twitchen, Loncar, Park, Maletinsky, and Lukin, “Coherent Optical Transitions in Implanted Nitrogen Vacancy Centers,” *Nano Letters* **14**, 1982-1986 (2014). Copyright 2014 American Chemical Society. Permission for further reuse should be directed to ACS.. (c), (d): Photoluminescence as a function of excitation frequency for a  $NV^-$  without (c) and with (d) active feedback of the ZPL transition. Reprinted from Acosta, Santori, Faraon, Huang, Fu, Stacey, Simpson, Ganesan, Tomljenovic-Hanic, Greentree, Prawer, and Beausoleil, “Dynamic Stabilization of the Optical Resonances of Single Nitrogen-Vacancy Centers in Diamond,” *Phys. Rev. Lett.* **108**, 206401 (2012) under the CC BY 3.0 license.

centers in bulk diamond at long time scales.

### 3. Single photon purity

Although a “single photon” can in principle be obtained by sufficiently attenuating a classical light source like a laser, there is a subtle but important difference between such attenuated sources and true SPEs: whereas a true SPE will never emit two photons at the same time, an attenuated source can occasionally deliver two photons in a single pulse. This is highly undesirable for some applications like quantum key distribution since security of the distributed key will be compromised in such cases and some of the key exchanged between the two parties will have to be discarded to ensure the security of the protocol<sup>85,86</sup>. An important metric that is typically used

to measure a source's single photon purity (in this sense) is the second order correlation function<sup>87</sup>

$$g^{(2)}(x_1, x_2) = \frac{\text{Tr}[\rho E^-(x_1) E^-(x_2) E^+(x_1) E^+(x_2)]}{\text{Tr}[\rho E^-(x_1) E^+(x_1)] \text{Tr}[\rho E^-(x_2) E^+(x_2)]}, \quad (3)$$

where  $x_i$  are space-time coordinates,  $\rho$  is the density matrix of the photons and  $E^\pm(x_i)$  are positive/negative frequency components of the electric field operator. Typically, the field is assumed to be stationary and we are only interested in the time difference  $\tau = x_2^0 - x_1^0$  so that Eq. (3) reduces to

$$g^{(2)}(\tau) = \frac{\langle I(t)I(t+\tau) \rangle}{\langle I(t) \rangle^2}, \quad (4)$$

where  $I(t)$  denotes the intensity (or count rate) and the brackets  $\langle \dots \rangle$  can be interpreted as a time average. Intuitively, Eq. (4) can be understood as the number of photons detected after a delay  $\tau$  from the detection of a preceding photon at time  $t$ , normalized by the average count rate. Since the field is assumed to be stationary,  $t$  drops out of the argument of  $g^{(2)}$ . Evidently, given that a true SPE can only emit a single photon at any particular instance of time,  $g^{(2)}(0)$  should equal zero for a true SPE since the number of photons detected immediately after the detection of one photon should be exactly zero. In reality, additional background photons from other sources as well as finite time resolution and timing jitter in photodetectors and time-to-digital converters result in a non-zero  $g^{(2)}(0)$ . For SPEs like NV centers, quantum dots and defects in 2-D materials, it is typically not possible to optically resolve two closely separated emitters and a  $g^{(2)}$  value of less than 0.5 is therefore typically used to discern whether emission is being collected from more than one emitter<sup>88</sup>. Table I lists some of the measured  $g^{(2)}(0)$  values of various SPEs from experiment. In cases where corrected  $g^{(2)}$  values are available, we give those that have been corrected for the timing response of the equipment used.

## B. Enhancement of ZPL emission using resonant cavities

We motivated in sections II A 1 and II A 2 how an enhanced spontaneous emission rate for SPEs is beneficial for numerous applications. In this section, we review how such an enhancement can be achieved by integrating SPEs with a resonant cavity.

Classical electromagnetism shows that the time-averaged power radiated by a dipole emitter can be written as

$$P = \frac{\omega}{2} \text{Im}[\mathbf{p}^* \cdot \mathbf{E}(\mathbf{r}_0)], \quad (5)$$

where  $\mathbf{p}$ ,  $\omega$ , and  $\mathbf{E}(\mathbf{r}_0)$  are the dipole moment, angular frequency and electric field at position  $\mathbf{r}_0$  respectively. The Purcell factor  $F$  of a dipole emitter gives the enhanced emission rate of an emitter in an optical cavity,

normalized with respect to its emission rate in free space (i.e. in the absence of the cavity). Using the well-known expression for  $\mathbf{E}_0(\mathbf{r}_0)$ , the electric field of a dipole in a homogeneous dielectric medium, the power radiated by a dipole in a homogeneous dielectric medium may be, from Eq. (5), succinctly written as  $P_0 = \mu_0 |\mathbf{p}|^2 n \omega^4 / (12\pi c)$ , where  $n$  is the refractive index of the dielectric medium and  $c$  is the speed of light<sup>89</sup>. With these expressions for  $P$  and  $P_0$ , the Purcell factor is given by  $F = P/P_0$ . One can also derive similar expressions for  $P$  and  $P_0$  using Fermi's golden rule. The quantum derivations will have an additional factor of 4, and this is related to fields from vacuum fluctuations<sup>90</sup>. Nevertheless, the factor cancels out in the ratio of  $F$  so that both classical and quantum derivations yield the same result.

When a dipole is placed in a structured dielectric medium like photonic crystal cavities, the corresponding electric field can be expressed as a sum of the dipole's own field  $\mathbf{E}_0(\mathbf{r})$  and the scattered electric field  $\mathbf{E}_s(\mathbf{r}_0)$ . Using  $F = P/P_0$  and the expression for  $P_0$ , it can be shown that

$$F = 1 + \frac{6\pi c}{\mu_0 n |\mathbf{p}|^2 \omega^3} \text{Im}[\mathbf{p}^* \cdot \mathbf{E}_s(\mathbf{r}_c)]. \quad (6)$$

Equation (6) may be evaluated by numerically simulating a dipole source in a finite-difference time-domain<sup>91</sup> (FDTD) simulation of Maxwell's equations where in general the field created by the dipole consists of its own field and the scattered field, but the scattered field  $\mathbf{E}_s(\mathbf{r})$  may be obtained by Fourier transforming the electric fields after the dipole excitation is switched off<sup>92</sup>.

The fields  $\mathbf{E}(\mathbf{r})$  and  $\mathbf{H}(\mathbf{r})$  are the total fields in the presence of the dipole emitter with current density

$$\mathbf{J}(\mathbf{r}) = -i\omega \mathbf{p} \delta(\mathbf{r} - \mathbf{r}_0), \quad (7)$$

where  $\mathbf{p}$  is the dipole moment and  $\delta(\mathbf{r})$  is the Dirac delta function.  $\mathbf{E}(\mathbf{r})$  and  $\mathbf{H}(\mathbf{r})$  obey Maxwell's equations for time harmonic fields

$$\nabla \times \mathbf{E}(\mathbf{r}) = i\omega \mu_0 \mathbf{H}(\mathbf{r}) \quad (8)$$

$$\nabla \times \mathbf{H}(\mathbf{r}) = \mathbf{J}(\mathbf{r}) - i\omega \epsilon(\mathbf{r}) \mathbf{E}(\mathbf{r}). \quad (9)$$

Let us assume the fields may be expanded using the quasi-normal modes of the optical cavity<sup>93-95</sup>. Under single-mode conditions the expansions can be written as

$$\mathbf{E} = \sum_n \alpha_n \mathbf{E}_n = \alpha_0 \mathbf{E}_0 \quad (10)$$

$$\mathbf{H} = \sum_n \alpha_n \mathbf{H}_n = \alpha_0 \mathbf{H}_0, \quad (11)$$

where  $\alpha_0$  is the expansion coefficient for the single mode<sup>96,97</sup>.  $\mathbf{E}_0$  and  $\mathbf{H}_0$  are the electric and magnetic field of the quasi-normal single mode and they obey (in the absence of free currents)

$$\nabla \times \mathbf{E}_0(\mathbf{r}) = i\tilde{\omega}_0 \mu_0 \mathbf{H}_0(\mathbf{r}) \quad (12)$$

$$\nabla \times \mathbf{H}_0(\mathbf{r}) = -i\tilde{\omega}_0 \epsilon(\mathbf{r}) \mathbf{E}_0(\mathbf{r}), \quad (13)$$

where  $\tilde{\omega}_0$  is the complex frequency of the quasi-normal mode. Applying Lorentz reciprocity theorem<sup>96</sup> to the set of fields  $(\mathbf{E}, \mathbf{H})$  and  $(\mathbf{E}_0, \mathbf{H}_0)$ , we have  $\int d^3\mathbf{r} \nabla \cdot (\mathbf{E} \times \mathbf{H}_0 - \mathbf{E}_0 \times \mathbf{H}) = 0$ . Subsequently, equations (8), (9), (12) and (13) can be combined as  $i(\omega - \tilde{\omega}_0) \int d^3\mathbf{r} (\mathbf{E} \cdot \epsilon(\mathbf{r})\mathbf{E}_0 - \mu_0\mathbf{H} \cdot \mathbf{H}_0) = \int d^3\mathbf{r} \mathbf{J} \cdot \mathbf{E}_0$ . Using this result and equations (7), (10) and (11), it can be shown that the complex expansion coefficient  $\alpha_0$  is

$$\alpha_0 = -\frac{\omega \mathbf{p} \cdot \mathbf{E}_0(\mathbf{r}_0)}{(\omega - \tilde{\omega}_0)I}, \quad (14)$$

where  $I$  is given by

$$I = \int d^3\mathbf{r} (\mathbf{E}_0 \cdot \epsilon(\mathbf{r})\mathbf{E}_0 - \mu_0\mathbf{H}_0 \cdot \mathbf{H}_0). \quad (15)$$

Using this integral, a mode volume  $V$  for the single mode can be defined as

$$V \equiv \frac{I}{2\epsilon_0 n^2 [\mathbf{E}_0(\mathbf{r}_0) \cdot \mathbf{p}]^2}, \quad (16)$$

where  $\epsilon_0$  is the vacuum permittivity and  $n^2$  is the square of the refractive index.

For cavities with high quality factor, the quasi-normal modes can be approximated to be normal modes where the integral  $I$  and the mode volume  $V$  are real-valued. If we assume that  $\mathbf{E}_0 \in \mathbb{R}$ , we see from equations (12) and (13) that  $\mathbf{H}_0 \in \mathbb{Im}$ , and therefore  $I = \int d^3\mathbf{r} (\epsilon |\mathbf{E}_0|^2 + \mu_0 |\mathbf{H}_0|^2) = 2 \int d^3\mathbf{r} \epsilon |\mathbf{E}_0|^2$ , where we have used the fact that  $\int d^3\mathbf{r} \epsilon |\mathbf{E}_0|^2 = \int d^3\mathbf{r} \mu_0 |\mathbf{H}_0|^2$  which follows from the identity

$$\nabla \cdot (\tilde{\mathbf{E}} \times \tilde{\mathbf{H}}) = \tilde{\mathbf{H}} \cdot \nabla \times \tilde{\mathbf{E}} - \tilde{\mathbf{E}} \cdot \nabla \times \tilde{\mathbf{H}}, \quad (17)$$

and the requirement that  $\int d^3\mathbf{r} \nabla \cdot (\mathbf{E}_0 \times \mathbf{H}_0^*) = 0$  for normal modes in which there is no out flow of energy from the cavity. By assuming a real  $I$  and using equations (10) and (5), it may be shown that the maximum Purcell factor on resonance (i.e.  $\omega = \omega_0 = \text{Re}[\tilde{\omega}_0]$ ) is given by

$$F_c = \frac{P}{P_0} = \frac{3}{4\pi^2} \left( \frac{\lambda_0}{n} \right)^3 \frac{Q}{V}, \quad (18)$$

where  $Q = \text{Im}[\tilde{\omega}_0]/(2\text{Re}[\tilde{\omega}_0])$  and  $\lambda_0 = c/(2\pi\omega_0)$ . In the case of a slight deviation off resonance, it is straightforward to show that  $F = F_c L_s(\omega)$ , where  $L_s(\omega)$  is the Lorentzian line shape function

$$L_s(\omega) = \frac{\omega_0^2}{\omega^2} \frac{\omega_0^2}{\omega_0^2 + 4Q^2(\omega - \omega_0)^2}. \quad (19)$$

Sauvan *et al.*<sup>96</sup> showed that for cavities with small quality factors, it is important to include the leakage part of the fields in the integral of  $I$ . Consequently, this leads to a complex volume, and in this case one can obtain a generalized  $F$

$$F = F_c L_s(\omega) \left( 1 + 2Q \frac{\omega - \omega_0}{\omega_0} \frac{\text{Im}[V]}{2\text{Re}[V]} \right), \quad (20)$$

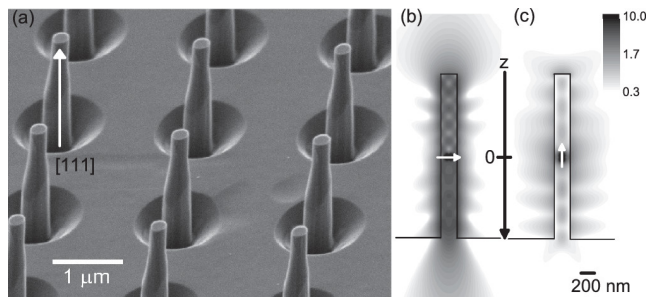


FIG. 6. (a) Scanning electron microscope (SEM) image of diamond nanopillars. (b), (c) FDTD simulations of the E-field's magnitude for orthogonal orientations of the optical dipole (shown with white arrows). Reprinted from Neu, Appel, Ganzhorn, Miguel-Sanchez, Lesik, Mille, Jacques, Tal-laire, Achard, and Maletinsky, "Photonic nano-structures on (111)-oriented diamond," Applied Physics Letters **104**, 153108 (2014), with the permission of AIP Publishing.

where  $F_c$  is now

$$F_c = \frac{3}{4\pi^2} \left( \frac{\lambda_0}{n} \right)^3 \frac{Q}{\text{Re}[V]}. \quad (21)$$

Equations (18) and (21) indicate that to maximize the spontaneous emission at the ZPL, it is necessary to achieve a high  $Q/V$  ratio at the ZPL wavelength. Typical cavity structures include microdisks<sup>99,100</sup>, micropillars<sup>101</sup>, nanopockets<sup>102–104</sup> and photonic crystals<sup>105</sup>. The whispering gallery modes of microdisk cavities can have very high quality factors of  $Q \sim 10^5$ , but relatively large mode volumes<sup>99</sup>. For micropillar resonators with integrated Bragg mirrors, very high  $Q > 250,000$  and small  $V < (\lambda/n)^3$  can be achieved, where  $\lambda$  is the wavelength and  $n$  is the refractive index<sup>101</sup>. Nanowires<sup>106</sup> and nanopillars<sup>98</sup> (see Fig. 6 for an example), like micropillars, are also efficient vertical-emitting photon sources when coupled with a quantum emitter such as a quantum dot or NV<sup>-</sup> center. Yet although they are useful for applications requiring outcoupling of light from the plane of the device, they are not as well suited for planar routing of light. Photonic crystal cavities (PCCs) present an appealing compromise between high  $Q$ , low  $V$ , and efficient in-plane coupling. PCCs commonly take the form of a membrane of material with a periodic lattice of air holes, where selected holes have been displaced to form a defect in the photonic crystal bandgap. A prominent example is the L3 cavity with three missing holes in a line (see Fig. 10 for an example), which supports polarized single modes with a relatively wide spectral margin<sup>105</sup>. For fabricated L3 cavities with embedded quantum dots (QDs) on a GaAs platform,  $Q \sim 10^4$  and  $V \sim (\lambda/n)^3$  has been demonstrated<sup>107,108</sup>, while an NV<sup>-</sup> center integrated with an all-diamond L3 cavity achieved a Purcell factor of 70<sup>109</sup>. A H1 PCC, which consists of a single central hole in a triangular 2D lattice, was also recently used to achieve a 43 fold spontaneous emission enhancement from an InGaAs quantum



dot in a GaAs cavity<sup>110</sup>.

For optimal coupling to the cavity, it is important for the quantum emitters, which may be modeled as dipole emitters, to be correctly oriented and positioned to match the cavity's mode and polarization. For example, light emission from a strain-free  $NV^-$  center has a single ZPL transition that may be modeled using a pair of orthogonal dipoles<sup>111</sup> (with equal strength of dipole moment) perpendicular to the NV axis while SiV centers, which have four ZPL transitions at cryogenic temperatures<sup>112,113</sup>, may be modeled as single dipole emissions. A misalignment of the optical dipole's orientation with respect to the cavity can significantly affect the modes it excites as Fig. 6 shows.

Cavities are not only useful for enhancing spontaneous emission but they are also useful in enhancing absorption, which can be beneficial under certain spin-to-charge<sup>114,115</sup>, spin-to-photocurrent<sup>54,116</sup> and magnetometry<sup>117,118</sup> read-out schemes. Besides enabling enhanced emission/absorption and out-of-plane waveguiding of quantum emitters, integrated photonic structures can also of course provide for in-plane waveguiding through conventional waveguides or line-defect PCC waveguides. In the following sections, we review various examples of integrated SPEs and different integration techniques that have been employed.

### III. INTEGRATED $NV^-$ CENTERS IN BULK DIAMOND

$NV^-$  centers have been successfully integrated with a variety of photonic structures in bulk diamond, which we here define as diamond substrates that are larger than nano-diamonds. Although nano-diamonds are in some ways easier to integrate with dissimilar photonic structures, they tend to suffer from poorer photostability and shorter coherence times due to their larger surface area to volume ratio that makes them particularly susceptible to surface effects. It is therefore desirable to integrate  $NV^-$  centers in bulk diamond to other photonic structures. These structures can be fabricated from the same bulk diamond substrate or they could be made of a dissimilar material and coupled to  $NV^-$  centers in a bulk diamond substrate evanescently. Moreover, with the advent of pick-and-place techniques, it is possible to envision  $NV^-$  in diamond photonic structures that are in turn coupled to other dissimilar material systems that could offer additional functionalities.

For fabricating all diamond photonic structures that contain only a single mode around the  $NV^-$  center's ZPL wavelength (637 nm), it is necessary to use thin membranes of diamond ( $n \approx 2.4$  at 637 nm) that are  $\sim 200$  nm thick. Although such membranes may be obtained from nanocrystalline diamond films grown on a substrate<sup>119,120</sup>, their optical quality is typically worse compared to bulk single-crystal diamonds due to increased absorption and scattering<sup>119</sup>. It is therefore preferable to obtain such thin diamond membranes from

(typically oxygen plasma) reactive ion etching (RIE) of bulk single-crystal diamonds<sup>121</sup>, which is a fabrication process that has been demonstrated to be compatible with moderately long  $NV^-$  spin coherence lifetimes of  $\gtrsim 100 \mu s$ <sup>122</sup> while also being consistent with low optical losses<sup>106,109</sup>. Moreover, RIE (with oxygen plasma) can be used to create surface-termination of the diamond membrane that encourages the conversion of  $NV^0$  to  $NV^-$  states<sup>51</sup>. To obtain good mode confinement, it is also typical to undercut the structures so as to achieve a large refractive index contrast between diamond and air. This may be achieved in several ways. For example, the diamond membrane can be first mounted on a sacrificial substrate, processed, and then made into a freestanding structure by a final isotropic etch step that removes the sacrificial substrate under the area of interest<sup>109,123</sup>. Alternatively, angular<sup>124,125</sup> and quasi-isotropic<sup>100,126,127</sup> RIE etching can also be employed to create such freestanding structures. Instead of creating a freestanding structure, another typical variation is to further etch the substrate to create a pedestal, which would reduce the leaking of fields into the substrate<sup>128</sup>.

Such all diamond photonic structures can then, in principle, be transferred to other dissimilar systems by using a pick-and-place technique to create a hybrid material platform. For example, this was demonstrated in Ref. 129 where  $NV^-$  containing diamond waveguides were transferred to a silicon platform containing SiN waveguides. GaP-diamond is another popular hybrid platform due to both the high refractive index of GaP ( $\approx 3.3$  at 637 nm) (compared to diamond  $\approx 2.4$  at 637 nm), and its relative ease of fabrication using standard semiconductor processing technology. In addition, unlike an all (bulk) diamond platform, which by inversion symmetry has a zero second-order non-linear susceptibility ( $\chi^{(2)}$ ) (we note however, that diamond has a non-zero third-order non-linear susceptibility  $\chi^{(3)}$  and that it has a relatively high non-linear refractive index that allows it to be harnessed for non-linear four-wave mixing processes<sup>130</sup>), GaP possesses a relatively large  $\chi^{(2)}$  that allows it to be used in non-linear processes such as second harmonic generation<sup>131</sup>. Moreover, unlike diamond which is forbidden by symmetry to have a bulk linear electro-optic coefficient<sup>132</sup>, GaP has a non-zero linear electro-optic coefficient ( $r_{41} \approx -0.97$  pm/V at 633 nm<sup>133</sup>) that enables it to be used for active electro-optic switching applications (as has been demonstrated in AlN material systems<sup>134,135</sup>), and as a III-VI semiconductor, GaP can potentially host on-chip integrated single-photon detectors as demonstrated on GaAs waveguides<sup>136</sup>. In the subsections below, we review some examples of integrated  $NV^-$ .

#### A. Integration with waveguides

$NV^-$  centers have been integrated with waveguides in a variety of ways. One direct approach is to fabricate an

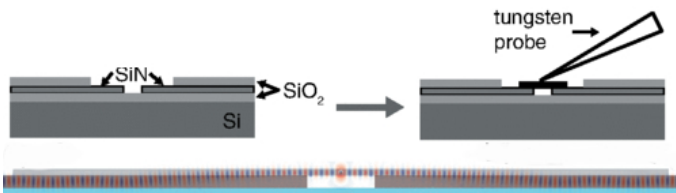


FIG. 7. Top: Schematic of single-mode diamond waveguides containing single  $NV^-$  centers suspended over single-mode SiN waveguides assembled using a tungsten probe. Bottom: Electric field profiles from FDTD simulations showing the transfer of mode from the suspended diamond waveguide (grey) into the underlying SiN waveguide (brown). Reprinted from Mouradian, Schröder, Poitras, Li, Goldstein, Chen, Walsh, Cardenas, Markham, Twitchen, Lipson, and Englund, “Scalable Integration of Long-Lived Quantum Memories into a Photonic Circuit,” *Phys. Rev. X* **5**, 031009 (2015) under the [CC BY 3.0](https://creativecommons.org/licenses/by/3.0/) license.

all-diamond waveguide on a thin diamond membrane using a mask and RIE etch. Since the diamond membrane will have randomly dispersed native  $NV^-$  centers, some of these diamond waveguides will, by chance, have  $NV^-$  centers in the approximately correct location within the waveguides. These  $NV^-$  integrated waveguides can then be post-selected and used to form more complex photonic circuits. This approach was taken in Ref. 129 where tapered diamond micro-waveguides were fabricated from a 200 nm thick single crystal diamond membrane with a Si mask and RIE etch. In this case, the Si mask was separately fabricated using well developed silicon fabrication processes and then transferred onto a diamond substrate using a mask transfer technique. Due to the mature silicon technology, such masks can be fabricated with stringent tolerances and their patterns can then be transferred to the diamond substrate after a RIE etch. The resulting diamond waveguides are then characterized by photoluminescence measurements and those that are found to have a single  $NV^-$  in the center of the waveguide, as verified by  $g^{(2)}(0)$  measurements, are selected and placed on top of an air gap in between SiN waveguides by a probe (see Fig. 7). Due to the air gap and taper of the diamond waveguides, up to 86% of the  $NV^-$ 's ZPL emission can be coupled to the SiN waveguides<sup>129</sup>. The background corrected saturated count rate from one end of the SiN waveguides was estimated to be  $1.45 \times 10^6$  photons/s and a  $g^{(2)}(0)$  as low as 0.07 was obtained. Photoluminescence excitation measurements of the  $NV^-$  revealed a FWHM of 393 MHz and ODMR Hahn-echo measurements revealed a relatively long spin coherence time of  $T_2 \approx 120 \mu\text{s}$ , which is, as in Ref. 137, close to the spin coherence time of  $NV^-$  centers in high quality bulk diamond crystals. This can likely be extended to the ms range if isotopically purified  $^{12}\text{C}$  carbon ( $^{13}\text{C}$  has a nuclear spin that decoheres the  $NV^-$  spin) is used instead<sup>138</sup>.

It is also possible to integrate  $NV^-$  with diamond waveguides using fs-laser writing. As discussed in section VII B 3, fs laser pulses are capable of creating  $NV^-$

centers in diamond. Moreover, as in the case of crystals like  $\text{LiNbO}_3$ <sup>139,140</sup> and sapphire<sup>141</sup>, it is possible to inscribe waveguides in diamond with fs laser writing. This may be accomplished by writing two parallel lines in diamond that results in graphitization of material within the focus leading to a decreased refractive index that in turn enables the confinement of an optical mode between the two laser written lines. In addition, the graphitized material, which has lower density, expands and causes stress-induced modification to the refractive index of the surrounding diamond that leads to vertical confinement of the optical mode<sup>142</sup>. Importantly, the laser inscribed waveguides in diamond survive annealing at 1000 °C<sup>143</sup>, which is commonly required for the formation of  $NV^-$  centers, but is not necessarily guaranteed as in the case of laser inscribed waveguides in sapphire<sup>141</sup>. Since the same fs laser system can be used to both create  $NV^-$  centers and write waveguides within bulk diamond, sub-micron relative positioning accuracy is possible between the  $NV^-$  center and waveguide. Using this technique, single  $NV^-$  centers, with a  $31 \pm 9\%$  probability of creation per 28 nJ pulse, were successfully incorporated into the midst of laser written diamond waveguides and waveguiding of their spontaneous emission was confirmed<sup>144</sup> (see Fig. 8). The measured  $g^{(2)}(0)$  values of such  $NV^-$  emission was as low as 0.07, confirming that single  $NV^-$  centers were indeed deterministically created in the waveguides<sup>144</sup>.

$NV^-$  centers in bulk diamond have also been integrated with GaP waveguides, although there has not, to our knowledge, yet been a demonstration of deterministic *single*  $NV^-$  integration with GaP waveguides. However,  $NV^-$  centers created by ion implantation in HPHT type Ib diamonds (at a depth of  $\approx 100\text{nm}$ ) have been evanescently coupled to a 120 nm thick GaP rib waveguide that was transferred onto diamond via epitaxial liftoff<sup>145</sup> after removal from its underlying  $\text{Al}_{0.8}\text{Ga}_{0.2}\text{P}$  sacrificial layer atop a GaP substrate<sup>146</sup>. Evanescent coupling between the  $NV^-$  and GaP waveguide was successfully observed when  $NV^-$  emission was detected after sending in a 532 nm excitation beam through the GaP waveguide<sup>146</sup>. The evanescent coupling requires that  $NV^-$  centers are created close to the diamond's surface and for gaps between GaP and the diamond substrate to be minimized. Indeed, a significant disadvantage of a (bulk) hybrid platform compared to an all-diamond one is that the  $NV^-$  centers cannot generally be placed in a maxima of the optical mode that would otherwise enable good optical coupling and an enhancement of spontaneous emission rates. To mitigate this,  $NV^-$  centers may be coupled to optical resonators such as microdisks with sufficiently high quality factor<sup>147</sup> and light within these resonators may then be outcoupled via coupling with another waveguide<sup>148,149</sup> (see section III C). Despite the high refractive index of GaP, waveguiding in a GaP waveguide atop a diamond substrate can still be significantly lossy due to the reduced effective index of the guided mode and the moderately high refractive index of diamond. To enable waveguiding and to reduce losses due to mode leakage

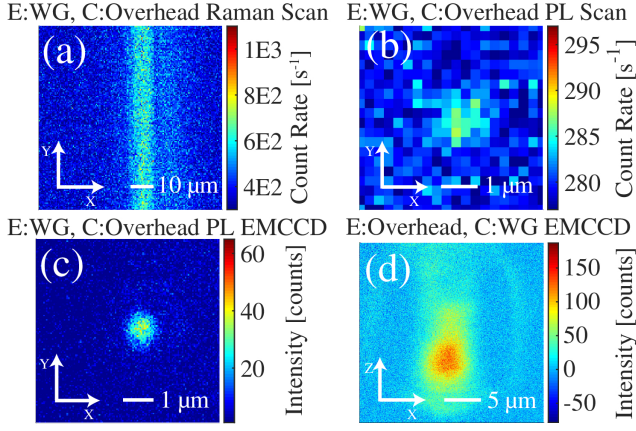


FIG. 8. Raman and NV fluorescence for various excitation (E)/collection (C) modes of an integrated laser written diamond waveguide and NV<sup>-</sup> center. (a) Raman scattered light collected above the waveguide after butt-coupled excitation of the waveguide, demonstrating waveguiding within the diamond. (b) Fluorescence of NV<sup>-</sup> above the waveguide after sending in excitation light from the end of the waveguide, demonstrating that the NV<sup>-</sup> is sufficiently close to the optical mode of the waveguide to interact with it. Fluorescence was measured using a home-built confocal microscope. (c) Same as in (b) but the fluorescence is measured using an electron multiplying charged coupled detector (EMCCD). (d) Fluorescence of the NV<sup>-</sup> measured at the end of the waveguide using an EMCCD after the NV<sup>-</sup> center was excited from above. Reprinted with permission from Ref. 144 © The Optical Society.

into the substrate, it is common to decrease the effective index of the substrate (from its bulk value) by etching it so as to create a diamond pedestal beneath the resonator<sup>128,147–150</sup>.

## B. Integration with resonators

### 1. Diamond ring resonators

One of the earliest demonstration of NV<sup>-</sup> integration with a resonator came in 2011 with the successful coupling of a NV<sup>-</sup> with a 4.8 μm outer diameter and 700 × 280 (width×height) nm diamond micro-ring resonator on top of a 300 nm high SiO<sub>2</sub> pedestal with mode volumes in the range of  $\approx 17 - 32 (\lambda/n)^3$ <sup>151</sup> (see Fig. 9). Photoluminescence measurements resolved roughly ten native NV<sup>-</sup> lines within the resonator. Characterization of the resonator was done at cryogenic temperatures (< 10 K) and xenon was flowed through the cryostat, which allowed tuning of the cavity's resonance as the xenon condensed on the cavity and altered its resonance wavelength<sup>152</sup>. A spontaneous emission enhancement of  $\approx 12$  was obtained on resonance with a FWHM of  $\approx 40$  GHz and a radiative lifetime of 8.3 ns. The broad linewidth has been attributed to strain within the

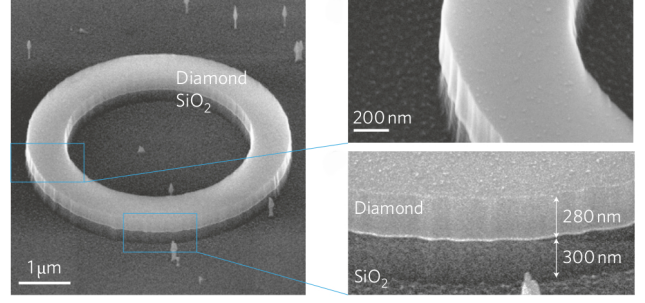


FIG. 9. A micro-ring resonator fabricated out of a single diamond crystal using EBL followed by RIE. Insets show the side wall roughness as well as how the SiO<sub>2</sub> substrate has been etched by 300 nm during the fabrication process. A NV<sup>-</sup> center coupled to the resonator was observed to have a spontaneous emission enhancement of  $\sim 12$ . Although theoretical  $Q$  values exceeded  $10^6$ , the achieved quality factors were only  $\sim 5000$  due to surface roughness of the ring. Reprinted with permission of Springer Nature Customer Service Center GmbH from Faraon, Barclay, Santori, Fu, and Beausoleil, “Resonant enhancement of the zero-phonon emission from a colour centre in a diamond cavity,” *Nature Photonics* **5**, 301-305 (2011), Copyright 2011.

diamond.

### 2. Diamond 2-D photonic crystal cavities

As discussed in section II B, although ring resonators are capable of achieving high  $Q$  factors, yet they tend to have large mode volumes and are therefore not as ideal in achieving Purcell factors. On the other hand, photonic crystal cavities provide a good compromise between having high quality factors and small mode volumes, which makes them particularly useful for enhancing a SPE's spontaneous emission rate. Accordingly, there has been various attempts at integrating NV<sup>-</sup> centers with PCCs. In Ref. 109, an all-diamond suspended L3 cavity with theoretical mode volume of  $\approx 0.88 (\lambda_{mode}/n)^3$  and  $Q = 6000$  was designed and fabricated to have a resonance close to the NV<sup>-</sup>'s ZPL (see Fig. 10). Confocal characterization of a native NV<sup>-</sup> center that was successfully coupled to the cavity gave a measured  $g^{(2)}(0)$  value of 0.38 and an on-resonant radiative lifetime of 4 ns. As in Ref. 151, the cavity's resonance wavelength was tuned by flowing xenon in a cryogenic environment. High resolution photoluminescence excitation measurements revealed two distinct peaks from the coupled NV<sup>-</sup> center, with the FWHM of the main peak at  $\approx 8$  GHz. Given that  $g^{(2)}(0)$  is 0.38, it's likely that the double peaks is due to strain-split branches of the same NV<sup>-</sup> and not to two spatially separated NV<sup>-</sup>.

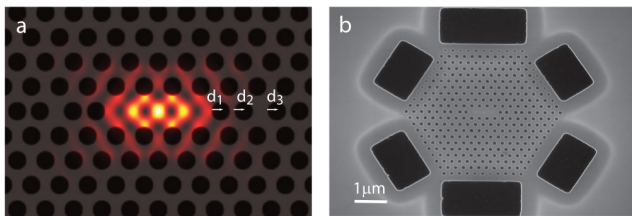


FIG. 10. (a) Simulated electric field energy density of a L3 cavity. (b) SEM image of a L3 cavity fabricated on a single crystal diamond membrane using EBL and RIE as described in the text. Reprinted figure with permission from Faraon, Santori, Huang, Acosta, and Beausoleil, “Coupling of Nitrogen-Vacancy Centers to Photonic Crystal Cavities in Monocrystalline Diamond,” *Phys. Rev. Lett.* **109**, 033604 (2012). Copyright 2012 by the American Physical Society.

### 3. Diamond 1-D photonic crystals cavities

Besides 2-D PCCs,  $NV^-$  centers have also been successfully integrated with 1-D PCCs. A relatively common 1-D PCC is a nanobeam that consists of a suspended diamond waveguide that contains periodic holes in it with some (optical) defects introduced near its center. Typically, the defect consists of either missing holes or holes with slightly different periodicity near the center. However, it is also possible to introduce a defect by increasing or decreasing the width of the waveguide in the middle<sup>153</sup>. In Ref. 123 1-D PCCs were created out of suspended 500 nm wide diamond waveguides that had 130 nm diameter air holes in it with a periodicity of 165 – 175 nm and a 400 nm tapered width in the middle (see Fig. 11). Photoluminescence excitation and white light transmission spectra give a spectrometer limited  $Q$  of above 6000 (simulated  $Q$  was  $\approx 5 \times 10^5$ ) and the mode volume is estimated to be  $1.8 (\lambda/n)^3$ . In this case, a two pronged strategy was employed to tune the cavity’s resonance to the ZPL of native  $NV^-$  centers within the nanobeams. First, a coarse tuning by means of controlled oxygen plasma etching was employed to blue shift the resonance, and then the device is later placed in a cryogenic environment (4 K) and xenon gas was introduced, as above, to red shift the resonance more precisely. A spontaneous emission enhancement of 7 was observed on resonance and  $g^{(2)}$  values of 0.2 can be obtained. However, we note that the FWHM of the plotted photoluminescence is rather large at  $\sim 490$  GHz.

In Ref. 137, 1-D nanobeams were also fabricated from a diamond membrane, albeit with a new Si mask transfer and RIE etch technique.  $NV^-$  centers were then created by  $^{15}N$  implantation and annealing. The cavities had a theoretical mode volume of  $1.05 (\lambda/n)^3$  and quality factors ranging in the 1000s. For a nanobeam with  $Q = 1700 \pm 300$ , a Purcell factor of 8 and 15 was achieved, for the  $E_x$  and  $E_y$  branch of a single  $NV^-$ ’s ZPL respectively. The measured  $g^{(2)}$  value was 0.28. As before, the enhancement was lower than expected from the  $Q/V$  ra-

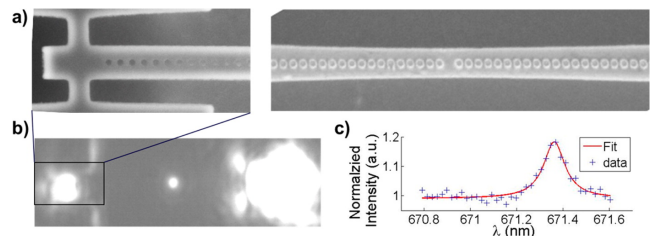


FIG. 11. (a) Left: SEM top view of the outcoupling region of a suspended diamond 1D nanobeam. Right: SEM top view of a suspended diamond 1D nanobeam. Note the tapering of the width in the middle. (b) Transmission measurement with a supercontinuum source coupled in from the right. Notice the localization of the mode in the center of the nanobeam. (c) Transmission spectrum indicating  $Q \sim 6000$ . Reprinted with permission from Hausmann, Shields, Quan, Chu, de Leon, Evans, Burek, Zibrov, Markham, Twitche, Park, Lukin, and Loncr, “Coupling of NV Centers to Photonic Crystal Nanobeams in Diamond,” *Nano Letters* **13**, 5791-5796 (2013). Copyright 2013 American Chemical Society. Permission for further reuse should be directed to ACS.

tio, but this is here attributed to a poor alignment of the NV axis and non-ideal spatial position in the cavity. In another nanobeam with  $Q$  factor of  $3300 \pm 50$ , a larger Purcell factor of 62 was achieved but in this case, there were multiple  $NV^-$  centers present (as judged by multiple spectrally distinct ZPL transitions). Interestingly however, the single  $NV^-$  center was observed to retain a long spin coherence time of  $\sim 230 \mu s$ , which is similar to the spin coherence time of  $NV^-$  centers in the parent unprocessed diamond. This indicates that the fabrication process using a Si mask did not adversely degrade the properties of the  $NV^-$  center and is promising for future applications requiring long spin coherence times in cavity coupled SPEs.

### C. Larger scale integration

Larger scale integration has also been achieved on an all-diamond platform consisting of micro-ring resonators coupled with waveguides and grating couplers<sup>154,155</sup>. The first demonstration<sup>154</sup> was characterized at room temperature with a confocal microscope that had two independent collection arms, with one of the collection arm also being used to excite the cavity. This allowed the structure to be excited at one location while emitted photons were collected at a different location. The micro-ring resonator had a outer diameter of 40  $\mu m$  and a  $1000 \times 410$  nm cross-section. Fluorescence collected from the output of both gratings gave a saturated count rate of  $(15 \pm 0.1) \times 10^3$  Hz with a saturated pump power of  $(100 \pm 4) \mu W$ . FDTD modeling suggests that the total collection efficiency is  $\sim 15\%$ , and therefore it appears that there remains room for significant improvement. In addition, coincidence counts of photons collected from the ring and each grating under simultaneous excitation

of the ring gave a  $g^{(2)}$  value of  $\sim 0.24$ , indicating that a single native  $NV^-$  center in the ring had successfully out-coupled to the gratings (see Fig. 12). Moreover, the fluorescence spectrum suggest a loaded  $Q$  of  $(3.2 \pm 0.4) \times 10^3$  at 665.9 nm. However, no attempt was made to determine if the ring had successfully enhanced the spontaneous emission rate of the coupled  $NV^-$  center.

This was accomplished in a slightly later demonstration of a very similar system consisting of a 4.5  $\mu\text{m}$  outer diameter micro-ring resonator, a ridge waveguide about  $\approx 100$  nm away, and grating couplers<sup>155</sup>. In this experiment, a spontaneous emission enhancement of  $\approx 12$  was reported after applying the same technique as in Ref. 151 to tune the cavity's resonance to native  $NV^-$  centers in the resonator. Transmission measurements of the mode used to enhance the  $NV^-$  center(s) ZPL line gave a coupled  $Q$  factor of 5500 and the mode volume is estimated to be  $\approx 15 (\lambda/n)^3$ . Excitation of native  $NV^-$  center(s) in the bulk material showed that when the cavity was on resonance, approximately 25 times more photons was collected from the grating than from the bulk. However, given that no  $g^{(2)}$  measurements were performed, it is not clear if only one  $NV^-$  center was excited in each case, and it is therefore difficult to make an unambiguous comparison.

Larger scale integration has also been achieved on a GaP-on-diamond hybrid architecture<sup>148,149</sup>. In Ref. 149, a 125 nm layer thick of GaP was transferred onto a diamond substrate, that had previously been implanted and annealed to produced  $NV^-$  centers approximately 15 nm below the surface. The GaP was then patterned using electron-beam lithography and etched through using a  $\text{Cl}_2/\text{N}_2/\text{Ar}$  RIE. To obtain better mode confinement, the diamond substrate was further etched using  $\text{O}_2$  RIE to get a  $\approx 600$  nm high diamond pedestal. GaP disk resonators, waveguides, directional couplers and grating couplers on a diamond pedestal were fabricated using this approach<sup>149</sup> (see Fig. 13). The coupled disk resonators were measured via transmission measurements to have loaded  $Q$  factors in the range of 2500 – 10000 and a full range of coupling ratios were obtained by varying the directional couplers' coupling region's length, which consisted of two 160 nm ridge waveguide spaced 80 nm apart (see Fig. 13b). Emission from  $NV^-$  below the ridge waveguide was successfully outcoupled by the grating couplers but unfortunately, no  $NV^-$  ZPL line was observed at the grating couplers when the coupled disk resonators were excited by 532 nm light due to a mismatch of the cavity's resonance (no attempt was made to tune the resonance here).

#### D. Deterministic integration

Most of the examples we have cited thus far relied on native  $NV^-$  centers that were randomly dispersed in the diamond membrane. Given that optimal placement of the  $NV^-$  center within the cavity is crucial to obtaining

ideal spontaneous emission enhancement, deterministic integration of  $NV^-$  centers is an important technological milestone. A 1-D deterministic integration of  $NV^-$  centers in the vertical dimension was first attempted by delta-doping<sup>156</sup> a high purity chemical vapor deposition (CVD) grown diamond membrane with a thin ( $\sim 6$  nm) layer of nitrogen impurities<sup>157</sup>. This produces a layer of  $NV^-$  centers that is well localized in the vertical dimension. Following this, 1-D suspended nanobeams are fabricated on the membrane with theoretical  $Q$  values of  $\sim 270,000$  and mode volumes of  $\sim 0.47 (\lambda/n)^3$ . However, measured photoluminescence spectra indicated that the highest  $Q$  obtained experimentally was  $\sim 24,000$ , which is generally attributed to imperfections in fabrication. A spontaneous emission enhancement of 27 was obtained by cooling the diamond to cryogenic temperatures (4.5 K) and flowing nitrogen into the cryostat to tune a cavity with mode of  $Q \sim 7000$  to the  $NV^-$ 's ZPL. An on-resonance life-time of  $10.43 \pm 0.5$  ns was also measured, which when combined with the off resonance life-time of  $22.34 \pm 1.1$  ns, and a Debye-Waller factor of 0.03, gives a similar Purcell factor of 22. It is worth noting that the enhancement is somewhat smaller than expected based on the structure's  $Q/V$  ratio. Compared to Ref. 123, the  $Q/V$  ratio is larger by a factor of 30 but the enhancement is only  $\sim 4$  times larger. Similarly, the  $Q/V$  ratio of this nanobeam is  $\sim 5$  times larger than the L-3 cavity in Ref. 109 but the enhancement is actually  $\sim 3$  times *smaller*. The surprisingly low enhancement in this case is attributed to the fact that there is likely to be several  $NV^-$  centers in the nanobeam and their linewidths has been estimated to be  $\sim 150 - 260$  GHz, which is, for comparison,  $\sim 4$  times larger than in Ref. 109. A consequence of this large linewidth is that the NVs' ZPL is poorly coupled to the cavity's resonance since the cavity mode is considerably narrower. The low enhancement could also plausibly be due to poor alignment of the NV axis (which affects the polarization of its emission) to the cavity.

Deterministic placement of  $NV^-$  in 2-D photonic crystals have also been attempted using ion implantation through a hole in an atomic force microscopy (AFM) tip<sup>158,159</sup>. In Ref. 158,  $NV^-$  centers were created at the center of 2D PCCs with measured  $Q$  of 150 – 1200 and estimated  $V_{mode} \approx 1(\lambda/n)^3$ . The created  $NV^-$ s had relatively large spectral diffusion limited FWHMs of  $\sim 250$  GHz at 10 K and were expected to have lateral spatial resolution of  $< 15$  nm and vertical spatial resolution of  $\approx 3$  nm. Unfortunately, the spatial resolution of the  $NV^-$  centers were only measured to be less than 1  $\mu\text{m}$  and it is not obvious if the expected resolution was actually obtained. Moreover, the  $NV^-$  creation yield was quite low at  $0.8 \pm 0.2$  %.

Higher deterministic single  $NV^-$  creation yield can be obtained by using hard Si masks for *both* implantation and diamond patterning where a single NV-cavity system yield of  $26 \pm 1$  % was obtained<sup>160</sup>. By having a high Si mask aspect ratio for the "implantation" holes, etching

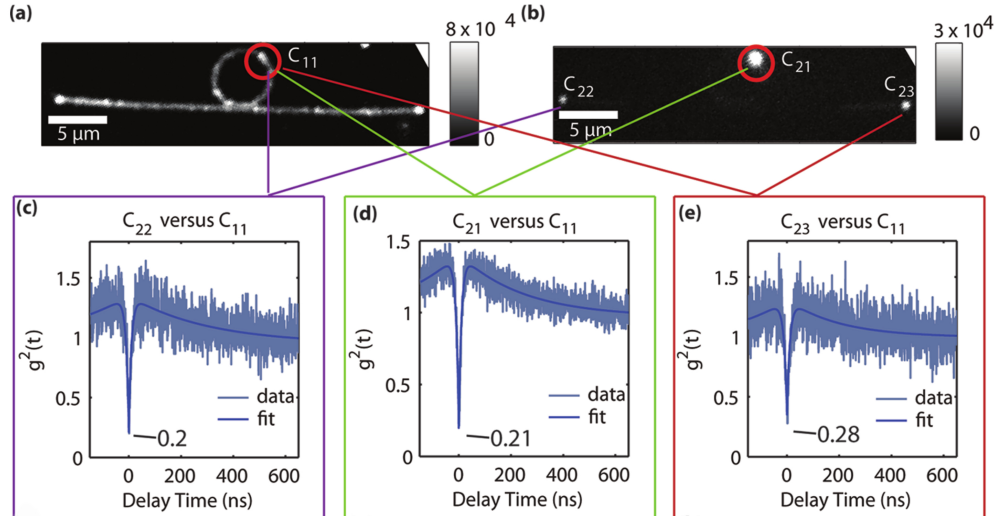


FIG. 12. (a), (b) Confocal images of the micro-ring resonator, waveguide and grating coupler. (c), (d), (e)  $g^{(2)}$  measurements made using correlation from light collected at  $C_{11}$ ,  $C_{21}$ ,  $C_{22}$  and  $C_{23}$  in (a), (b). Reprinted with permission from Hausmann, Shields, Quan, Maletinsky, McCutcheon, Choy, Babinec, Kubanek, Yacoby, Lukin, and Loncar, “Integrated Diamond Networks for Quantum Nanophotonics,” *Nano Letters* **12**, 1578-1582 (2012). Copyright 2012 American Chemical Society. Permission for further reuse should be directed to ACS.

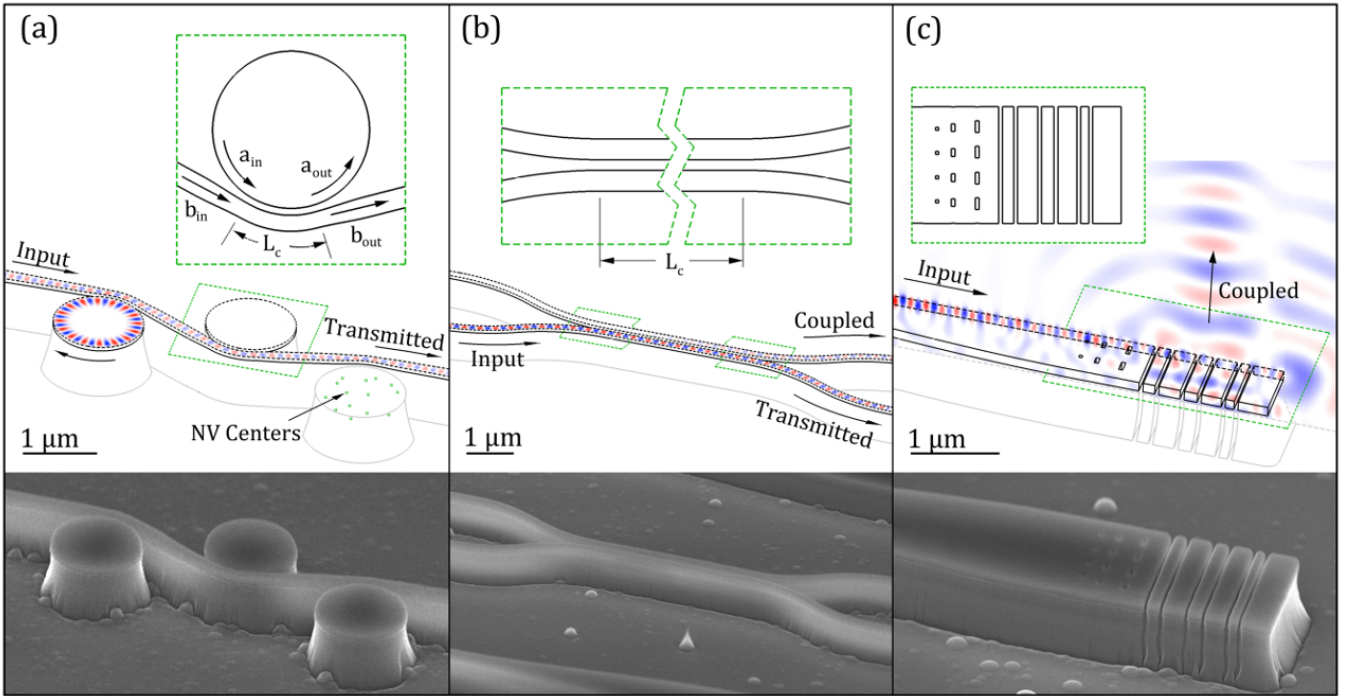


FIG. 13. Examples of integrated hybrid GaP-diamond systems where a thin 125 nm film of GaP was epitaxially grown and transferred onto a diamond substrate before being patterned with EBL and RIE. Above: schematic view overlaid with FDTD simulations, bottom: SEM images of integrated devices. (a) waveguide-coupled disk resonators, (b) directional coupler, (c) grating coupler. Reprinted with permission from Ref. 149 © The Optical Society.

rate for the underlying diamond substrate is negligible but N ions during implantation are still able to implant into the diamond due to different conditions for etching and implantation<sup>160</sup>. This allows for the use of a single mask for both diamond patterning and  $NV^-$  position-

ing, thereby eliminating any loss of accuracy due to realignment of separate masks. Unfortunately, there was no definite measurement of the overall spatial resolution obtained although a 1-D nanobeam with  $Q = 577$  and coupled single  $NV^-$  center was reported. Nevertheless,

considering that spatial positioning of  $NV^-$  to about  $\sim 10$  nm have been obtained using masks<sup>161,162</sup>, this scalable approach to deterministically position  $NV^-$  centers within photonic structures is promising.

## E. Outlook

Moving forward, we believe that there is still much room for improvement in deterministically integrating high quality single  $NV^-$  centers to complex photonic circuits using diverse strategies that have been developed over the years. Although most of the work discussed above which demonstrated coupling of  $NV^-$  centers to all-diamond photonic structures relied on randomly positioned native  $NV^-$  centers, we note that spatial positioning of  $NV^-$  centers to about  $\sim 10$  nm in all three dimensions<sup>161,162</sup> has already been separately demonstrated. In these demonstrations, delta doping of CVD grown diamond (see section [VII B 1](#)) is typically used together with a mask for accurately creating vacancies via irradiation that then lead to  $NV^-$  formation in the thin nitrogen doped layer after annealing. Previously, such mask consisted of spin-coated resist<sup>161</sup> and other additional layers<sup>162</sup> that can be difficult to coat with even thickness over a large area. However, the recent development of mask transfer techniques (see section [VIII D 2](#)) open up the possibility of using high quality Si masks that can be positioned with sub-micron or even nm scale accuracy on the diamond substrate and then later removed mechanically. It is therefore possible to imagine using a single mask to both create  $NV^-$ s and photonic structures at deterministic positions<sup>160</sup>. Successful  $NV^-$  integrated photonic structures, as characterized by optical measurements, can then be picked-and-placed (as in Ref. [129](#)) by a microprobe to integrate with other photonic structures of a potentially dissimilar material that will further unlock other functionalities. This allows  $NV^-$  centers to be created in high quality single crystal diamond (potentially with isotopically enriched  $^{12}C$ ) where they can have long optical and spin coherence times, while still being able to be efficiently routed and processed by other photonic elements on a chip.

## IV. COLOR CENTERS IN NANODIAMONDS

As discussed in the preceding section,  $NV$  centers are not the only defects in diamond that exhibit discrete energy levels with optical transitions although they are arguably the most studied defect. Recently, defect centers consisting of group-IV elements such as silicon vacancy ( $SiV$ )<sup>163,164</sup>, germanium-vacancy ( $GeV$ )<sup>165</sup> and tin-vacancy ( $SnV$ )<sup>166,167</sup> centers in diamond have been of particular interest due to symmetries in their configuration that leads to a higher Debye-Waller factor and narrower spectral lines that increases the indistinguishability of their emitted photons. Moreover, although

there has, as the preceding section shows, been a great deal of work in bulk diamond, there has also been considerable work in integrating color centers in nanodiamonds to hybrid photonic structures. We note however, that  $NV$  centers in nanodiamonds are less photo-stable and tend to have significantly larger inhomogeneously broadened ZPL linewidths as compared to their bulk counterparts. Although this makes them less suitable for many quantum computing/processing applications, nanodiamonds are more suited for bio-sensing/labeling applications<sup>168–170</sup>, and interestingly enough, the spontaneous emission rates of  $NV$  centers in nanodiamonds can also be enhanced by encasing them in phenol-ionic complexes<sup>171</sup>. Moreover, nanodiamonds with a high concentration of  $SiV$  centers can also be used as temperature sensors<sup>172</sup>. In this section, we give examples of other color centers in nanodiamonds that have been coupled to photonic structures.

### A. Fabrication

Nanodiamonds are synthesized by various techniques such as detonation, laser assisted synthesis, HPHT high energy ball milling of microcrystalline diamond, hydrothermal synthesis, CVD growth, ion bombardment on graphite, chlorination of carbides and ultrasonic cavitation<sup>173</sup>. In the laboratory, the detonation method and HPHT growth are commonly employed to synthesize  $NV$  containing nanodiamonds on a large scale<sup>174</sup>. CVD growth is another promising technique that has successfully synthesized single  $NV$  centers in nanodiamonds<sup>175</sup>. More recently, a new metal-catalyst free method to synthesize nanodiamonds with varying contents of  $NV$  and  $SiV$  centers produced high-quality color centers with almost lifetime-limited linewidths<sup>176,177</sup>.

In Ref. [178](#), the authors reported the first direct observation of  $NV$  centers in discrete 5 nm nanodiamonds at room temperature. Although the luminescence of those  $NV$  centers was intermittent (i.e. they undergo blinking), the authors were able to modify the surface of the nanodiamonds to mitigate the undesirable blinking. In another work, the authors showed the size reduction of nanodiamonds by air oxidation and its effect on the nitrogen-vacancy centers that they host<sup>179</sup>. The smallest nanodiamond in their samples that still hosted a  $NV$  center was about 8 nm in size.

$SiV$  centers in nanodiamonds have subsequently been investigated<sup>180–182</sup>. Ref. [180](#) describes the first ultra-bright single photon emission from  $SiV$  centers grown in nanodiamonds on iridium. The  $SiV$  centers were grown using microwave-plasma-assisted CVD and those single  $SiV^-$  defects achieved a photon count rate of about 4.8 Mcounts/s (at saturation). Bright luminescence in the 730-750 nm spectral range were observed using confocal microscopy. No blinking was observed but photobleaching occurred at high laser power. Enhanced stability might be gained by controlling the surface termination

of the nanodiamonds, as was shown for the case of NV centers<sup>50</sup>.

Residual silicon in CVD chambers often results in the formation of SiV<sup>-</sup> centers in most CVD-grown nanodiamonds<sup>177,180</sup>. Likewise, due to silicon-containing precursors, many HPHT-synthesized nanodiamonds also include SiV<sup>-</sup> centers<sup>183</sup>. In Ref. 182, the authors demonstrated optical coupling of single SiV<sup>-</sup> centers in nanodiamonds and were able to manipulate the nanodiamonds both translationally and rotationally with an AFM cantilever.

Fabrication of other color centers such as GeV centers in nanodiamond were also recently demonstrated. For example, single GeV centers in nanodiamonds were successfully fabricated by the authors in Ref. 184 after they introduced Ge during HPHT growth of the nanodiamonds. More generally, in Ref. 185, the authors studied a larger variety of group IV color centers in diamond, including SiV, GeV, SnV and PbV centers.

We note that it is possible to control the size and purity of the HPHT nanodiamonds down to 1 nm<sup>186</sup>. In other works, the size of nanodiamonds are typically tens of nanometers<sup>187–189</sup>, which make nano manipulation of them feasible. For example, emission from single NV centers hosted in uniformly-sized single-crystal nanodiamonds with size  $30.0 \pm 5.4$  nm have been reported<sup>189</sup>.

Although high count rates are in general achievable for NV and SiV color centers in nanodiamonds<sup>190</sup>, these high count rates were sometimes reported to be correlated to blinking<sup>191</sup>. Compared to SiV centers in the bulk, SiV centers in nanodiamonds have significantly less reproducible spectral features and can feature a broad range of ZPL emission wavelengths and linewidths<sup>192</sup>. More generally, the linewidths of SiV centers in nanodiamonds have been shown to depend on the strain of the diamond lattice<sup>192</sup>. Nevertheless it is sometimes possible to obtain nearly lifetime-broadened optical emission in SiV centers in nanodiamonds at cryogenic temperatures<sup>176,193</sup>, and indeed nearly lifetime limited zero-phonon linewidths have been obtained in both NV and SiV centers in nanodiamonds. For example, despite spectral diffusion and spin-nonconserving transitions, zero-phonon linewidths as small as 16 MHz has been reported for NV centers in type Ib nanodiamond at low temperature<sup>194</sup>.

For GeV centers in HPHT nanodiamond, the stability of its ZPL emission wavelength and linewidth has been attributed to the symmetry of its molecular configuration, although a large variation of lifetimes was also reported<sup>195</sup>. The authors there estimate a quantum efficiency of about 20% for GeV centers in HPHT nanodiamonds.

## B. Integration with photonic structures

As mentioned in section III above, a hybrid GaP-diamond platform is attractive for multiple reasons and there has been work involving not just bulk GaP-

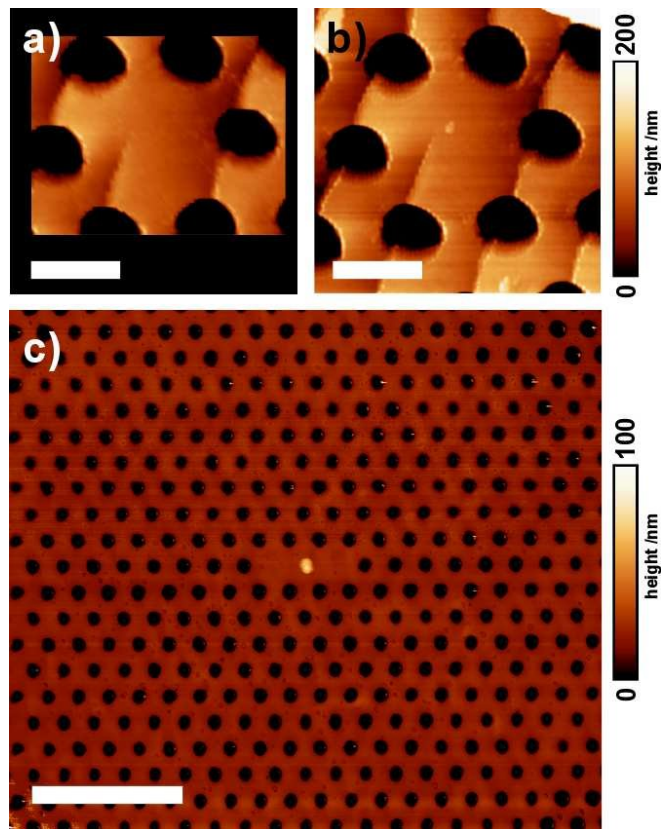


FIG. 14. (a) AFM image of the core of a photonic crystal fiber. (b) A pre-selected nanodiamond is then transferred to center of the photonic crystal fiber using a pick-and-place technique. (c) A nanodiamond in the center of a gallium phosphide photonic crystal membrane cavity. Reprinted from Schell, Kewes, Schröder, Wolters, Aichele, and Benson, “A scanning probe-based pick-and-place procedure for assembly of integrated quantum optical hybrid devices,” *Review of Scientific Instruments* **82**, 073709 (2011), with the permission of AIP Publishing.

diamond systems but also hybrid GaP-nanodiamond systems. For an extensive review, see Ref. 174. Purcell enhancement of the ZPL emission by a factor of 12.1 has been reported in a hybrid nanodiamond-GaP platform where the ZPL of an NV center is coupled to a single mode of a PCC<sup>196</sup>. In that work, both the nanodiamond and cavity are first pre-selected and the resonance of the cavity is then tuned to the ZPL of the NV center by locally oxidizing the GaP with a focused blue laser<sup>196</sup>. Finally, the pre-selected nanodiamond is then transferred to the GaP cavity using a pick-and-place technique<sup>197,198</sup> (see Fig. 14). Alternatively, a GaP PCC may be transferred using a micro-PDMS adhesive on a tungsten probe (briefly discussed and illustrated in section VIID 2 and Fig. 29) to a pre-selected nanodiamond containing a NV<sup>-</sup> center of desirable properties<sup>199</sup>.

Nanodiamonds were also integrated with silica micro-resonators to achieve cavity QED (cQED) effects. In one early attempt, diamond nanocrystals were attached to



silica micro-resonators by dipping silica micro-disks with diameters of  $20\ \mu\text{m}$  into an isopropanol solution containing suspended nanodiamonds with a mean diameter of  $70\ \text{nm}$ <sup>188</sup>. Initially, the micro-disks had a quality factor of  $Q = 40000$  at room temperature, but after deposition of the nanodiamonds, low temperature measurement showed that the quality factor decreased significantly to around  $2000 - 3000$ . By condensing nitrogen gas to tune the cavity modes, the authors observed that a single NV center could couple to two cavity modes simultaneously. However, there was no significant change in the spontaneous emission rate, which was probably due to, in addition to the emitters' large linewidth, the resonator's large mode volume and limited quality factor. In Ref. 200, a tapered fiber is used to both pick up and position NV containing nanodiamonds onto a high-Q  $\text{SiO}_2$  micro-disk cavity. The same tapered fiber could then also be used to characterize light transmission through the system. Coupling in the strong cQED regime has also been achieved between NV centers in nanodiamonds and silica micro-spheres resonators<sup>201</sup>.

Besides silica resonators, there has also been work on polystyrene micro-sphere resonators. Nanodiamonds with a mean diameter of  $25\ \text{nm}$  can be attached to polystyrene micro-spheres with diameters of  $\sim 5\ \mu\text{m}$  by first dispersing both on a cover slip and then using near-field scanning optical microscopy (NSOM) tips to bring the micro-spheres close to a pre-selected nanodiamond containing a single  $\text{NV}^-$  center<sup>187</sup>. Touching a nanodiamond with a micro-sphere then attaches the former to the latter. Using this technique, the authors demonstrated coupling of two single NV centers found in two different nanodiamonds to the same micro-sphere resonator<sup>187</sup>.

Silicon carbide is another material that can be integrated with diamond due to its similarity with diamond. For example, the authors in Ref. 174 developed a scalable hybrid photonics platform which integrates nanodiamonds with 3C-SiC micro-disk resonators fabricated on a silicon wafer. By condensing argon gas on the structure, the authors were able to continuously red shift the resonator's resonance and tune it to the color center's emission to observe an enhancement of the center's spontaneous emission.

It is also possible to enhance the spontaneous emission rate of a quantum emitter coupled to waveguiding structures like dielectric-loaded surface plasmon polariton waveguides (DLSPWs) where the significantly confined mode volume of the surface plasmon polariton can enable Purcell factors above unity (see Fig. 15). Experiments involving embedded nanodiamonds with NV centers in a DLSPW consisting of a hydrogen silsesquioxane (HSQ) waveguide on top of a silver film demonstrated a spontaneous emission enhancement of up to 42 times<sup>202,203</sup>. In a similar vein, a GeV center embedded within a similar DLSPW was successfully excited by  $532\ \text{nm}$  light propagating within the waveguide and achieved a three-fold enhancement in its spontaneous emission rate due to the small mode volume within the waveguide<sup>184</sup>.

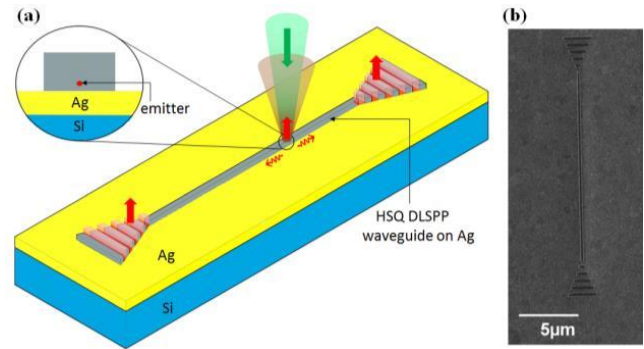


FIG. 15. (a) Dielectric-loaded surface plasmon polariton waveguide (DLSPW) circuits are built around nanodiamonds containing single photon emitter with enhanced emission rate. (b) Scanning electron micrograph of a hydrogen silsesquioxane (HSQ) waveguide fabricated on silver-coated silicon substrate. Reprinted with permission from Siampour, Kumar, and Bozhevolnyi, “Nanofabrication of Plasmonic Circuits Containing Single Photon Sources,” *ACS Photonics* 4, 1879-1884 (2017). Copyright 2017 American Chemical Society. Permission for further reuse should be directed to ACS.

Although likely to be less useful than coupling to DLSPWs due to higher losses, coupling of single NV centers in nanodiamonds to silver nanowires can enable interesting studies of surface plasmon polaritons (SPP) as in Ref. 204 where a wave-particle duality was demonstrated for SPPs excited by single photons from a nanodiamond.

The spontaneous emission rate of a quantum emitter can be significantly enhanced when coupled to a plasmonic nano-antenna. For example, enhancement factors of up to 90 times was observed for a NV center within a nanodiamond that was coupled to a nanopatch antenna<sup>205</sup>. Even higher enhancement of up to 300 times has been theoretically proposed by coupling SiV centers in a nanodiamond to a specific geometry of gold dimers<sup>206</sup>.

Besides static resonators such as micro-disks and micro-spheres, a fiber-based micro-cavity technique, where a tunable cavity is typically formed by the combination of a fiber and macroscopic mirror, can also be applied to NV and SiV centers in diamond to enhance their efficiency, brightness and single photon purity<sup>207-210</sup>. Lastly, it is also possible to directly couple the color centers in a nanodiamond to an optical fiber. For example, in Ref. 211 pre-selected NV containing nanodiamonds were placed directly on a fiber facet to create an alignment free single photon source. High coupling efficiency was also reported in a nanodiamond-tapered fiber system<sup>212-214</sup> (see Fig. 16), and in Ref. 215, NV containing nanodiamonds were successfully embedded in tellurite soft glass.

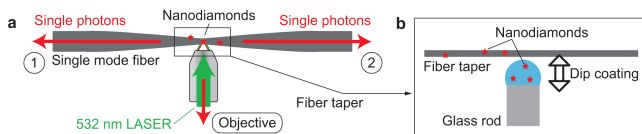


FIG. 16. (a) Nanodiamonds were attached to the fiber taper, and single photons emitted by the color centers were collected either through the objective or the fiber ends. (b) The tapered fiber was dipped into a small droplet of a nanodiamond solution on the facet of a thin glass rod. The nanodiamonds were attached to the fiber taper as it is moved through the droplet. Reprinted with permission from Ref. 212 © The Optical Society.

## V. QUANTUM DOTS

### A. Introduction to Quantum Dots

A quantum dot (QD) is a small nanometer-sized three-dimensional inclusion of a narrower bandgap material within a wider bandgap matrix. The 3D confinement potential of the QD leads to a discretization of energy levels and gives it localized, atom-like properties. By controlling and manipulating these properties, QDs can be utilized in many aspects of quantum technologies, such as SPEs or as qubit systems. QDs have also been studied extensively and developed for numerous optoelectronic applications, including light-emitting diodes (LEDs)<sup>216</sup>, photovoltaic devices<sup>217</sup>, and flexible displays<sup>218</sup>.

Compared to other atomic systems (e.g. trapped ions) used in early experimental realizations of quantum logic<sup>219</sup>, QDs are embedded within a solid-state medium and thus do not require bulky and complicated vacuum systems and optical trapping setups. Moreover, QD-based devices can take advantage of well-established growth techniques, e.g. molecular beam epitaxy (MBE)<sup>220–222</sup> or metalorganic vapor phase epitaxy (MOVPE)<sup>223–225</sup>, which allow for monolithic growth with monolayer precision. Coupled with the ability to electrically control these devices<sup>226–228</sup>, QDs have attracted extensive research efforts in developing and realizing QD photonic devices.

QDs used in integrated photonics applications are typically based on III-V materials, especially In(Ga)As in (Al, Ga)As matrices. The most common QD growth approach uses the Stranski-Krastanov mechanism<sup>229</sup>: as QD material is successively deposited and reaches a critical thickness, strain energy from mismatched lattice constants drive the formation of 3D nano-islands through a self-assembly process which allows for more efficient strain relaxation. The downside of self-assembly is that the QDs are randomly positioned, but site-controlled growth techniques have been developed to gain deterministic control over the QD positioning<sup>230,231</sup> and their coupling to nanophotonic structures<sup>232</sup>.

QD devices have numerous applications in quantum integrated photonics. They can serve as tunable, high-

quality single-photon sources that can be integrated into nanophotonic structures such as waveguides<sup>233</sup> and beamsplitters<sup>234</sup>. To complement this, photonic device components for photon manipulation, such as modulators<sup>235</sup>, frequency sorters<sup>236</sup>, and frequency converters<sup>237</sup>, have been developed. High-speed near-infrared (NIR) detectors<sup>238,239</sup> based on QDs have also been demonstrated in recent years. By controlling the QD spin, spin-photon interfaces can also be realised, allowing the QD to be used as a quantum memory, as well as a range of additional applications such as single-photon switching<sup>240</sup>.

In this work, we will focus more on examples and applications of QDs integrated on photonic platforms; a broad-spectrum overview can be found in another recent review<sup>241</sup>.

### B. As a Single-Photon Emitter

SPEs can be realized from QDs by utilizing the radiative recombination from an excitonic state of a single QD<sup>244,245</sup>. The first demonstrations of single-photon emission from QDs were performed under optical pumping<sup>244</sup>, and then by electrical pumping<sup>226</sup>. Beyond single-photon generation, multiphoton generation via demultiplexing of high-brightness integrated QDs has also achieved four-photon coincidence rates of  $>1$  Hz<sup>246</sup>. QD-based SPEs have been extensively studied, and in-depth discussions can be found in other review articles<sup>247,248</sup>.

The photon statistics of QD single-photon sources can be degraded by imperfections such as multi-photon emission from multi-exciton states, or if light is also collected from nearby QDs. As discussed in Section II A 3, we will use the  $g^{(2)}(0)$  value as a measure of the source's single-photon purity.

For non-resonant excitation, multi-photon emission can result from the QD capturing additional carriers after the first photon emission, which can subsequently recombine. Therefore, to obtain a low  $g^{(2)}(0)$ , relaxation into the QD and the radiative cascade causing recombination should occur on a longer timescale than the decay of the initial carriers<sup>249,250</sup>. With resonant, pulsed excitation,  $g^{(2)}(0)$  values close to zero have been demonstrated<sup>251–253</sup>, while the lowest reported  $g^{(2)}(0)$  values of below  $10^{-4}$  have been achieved with two-photon excitation<sup>254,255</sup>. However, we note that these lowest values were not obtained from QDs integrated with on-chip planar waveguides; demonstrations with integrated QDs have reported more modest  $g^{(2)}(0)$  values due to factors such as increased background emission from cavity modes<sup>256</sup> (see also Table I).

The radiative cascade of high-energy carriers also results in a temporal uncertainty (i.e. jitter) of photon emission<sup>249</sup>, which leads to decreased indistinguishability for higher excitation powers<sup>81</sup>. However, this can be overcome with strictly resonant pumping schemes<sup>251,257</sup>. Moreover, resonant pumping and adding a weak auxiliary

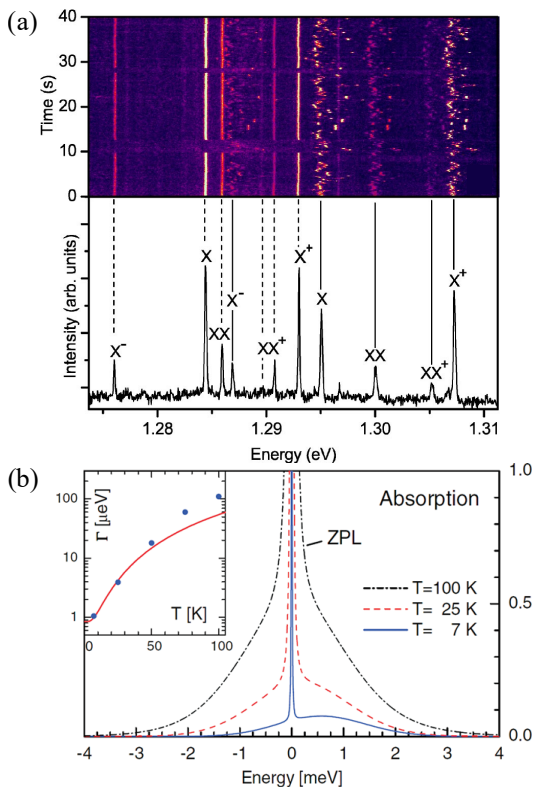


FIG. 17. (a) The bottom part shows a typical spectrum of multiple InAs/GaAs QDs. The top part shows the temporal evolution of the spectrum showing spectral wandering of the QD transitions. Reprinted figure with permission from Rodt, Schliwa, Pötschke, Guffarth, and Bimberg, “Correlation of structural and few-particle properties of self-organized InAsGaAs quantum dots,” *Phys. Rev. B* **71**, 155325 (2005). Copyright 2005 by the American Physical Society. (b) Calculated absorption spectra of an InAs QD. At lower temperatures, the broadband phonon interactions are suppressed, while the zero-phonon line (ZPL) is asymmetrically broadened. The inset compares the calculated broadening with experimental data (circles). Reprinted figure with permission from Muljarov and Zimmermann, “Dephasing in Quantum Dots: Quadratic Coupling to Acoustic Phonons,” *Phys. Rev. Lett.* **93**, 237401 (2004). Copyright 2004 by the American Physical Society.

continuous wave reference beam to the excitation beam of the QD can help to suppress charge fluctuations<sup>258</sup> that would otherwise lead to spectral diffusion.

To suppress the effects of phonon interactions, one can operate at cryogenic temperatures although we acknowledge that for InGaAs QDs at 4 K, PSB emissions can still represent  $\sim 10\%$  of emission (see Fig. 17a). Also, spectral filtering of the QD ZPL can yield high indistinguishability close to unity<sup>259</sup>, albeit at the expense of photon rates.

Since the first Hong-Ou-Mandel (HOM) two-photon interference experiment with QDs reported indistinguishabilities of  $\sim 70\%$ <sup>80</sup>, near-unity values have been consistently achieved<sup>257,260–262</sup> (e.g.  $0.995 \pm 0.007$ , Ref.

257). Recent reports have also reproduced high HOM visibility values QDs integrated with nanophotonic waveguides<sup>263–266</sup>.

### C. Spin-Photon Interfaces

By accessing and manipulating their spin, QDs can provide not only photonic qubits, but spin qubits as well. Various level structures can be exploited for qubit encoding, and rapid spin initialization, manipulation, and read-out can be achieved with short optical pulses (in the nanosecond range)<sup>267</sup>. Such spin-photon interfaces can enable many quantum information processing tasks, such as deterministic spin-photon entanglement and mediating strong photon-photon interactions.

The strong nonlinearity at a single-photon level has led to demonstrations of photon blockade<sup>268</sup> and tunable photon statistics via the Fano effect<sup>269</sup>. Single-photon switches and transistors have been realized via a QD spin<sup>108,270,271</sup> (see Fig. 18a). Coherent control of the QD spin has also been achieved, with Ref. 272 demonstrating Ramsey interference with a dephasing time  $T_2^* = 2.2 \pm 0.1$  ns (see Fig. 18b).

The strong light confinement in nanophotonic waveguides also opens up the possibilities of chiral, or propagation-direction-dependent, quantum optics<sup>273</sup>. This can be used to deterministically induce unidirectional photon emission from quantum dot spin states, i.e.  $\sigma_{\pm}$  transitions emit in different directions<sup>274,275</sup> (see Fig 18c). This can help to realize complex on-chip non-reciprocal devices such as single-photon optical circulators<sup>276</sup>. Although chirality has only been demonstrated to date using waveguides, recent theory papers have shown that chirality with significant Purcell enhancement should be possible using a ring resonator geometry<sup>276,277</sup>.

### D. Interfacing Multiple QDs

Hybrid quantum photonics platforms aim to integrate multiple quantum sources, including dissimilar quantum systems, onto the same device. Two-photon interference has been demonstrated between QDs and other quantum emitters, including atomic vapors<sup>282</sup>, a Poissonian laser<sup>283,284</sup>, parametric down-conversion source<sup>285,286</sup>, and frequency combs<sup>287</sup>. The rest of this section will focus on the interfacing of multiple QDs on the same photonics circuit.

To obtain high interference visibility, the emitted photons have to be identical, but it is experimentally challenging to find two QDs with almost identical emission energies, linewidths, and polarization. While much effort has been invested in fabricating highly reproducible QDs<sup>288</sup>, it is often necessary to employ tuning mechanisms, both for the QDs and the cavity structures they

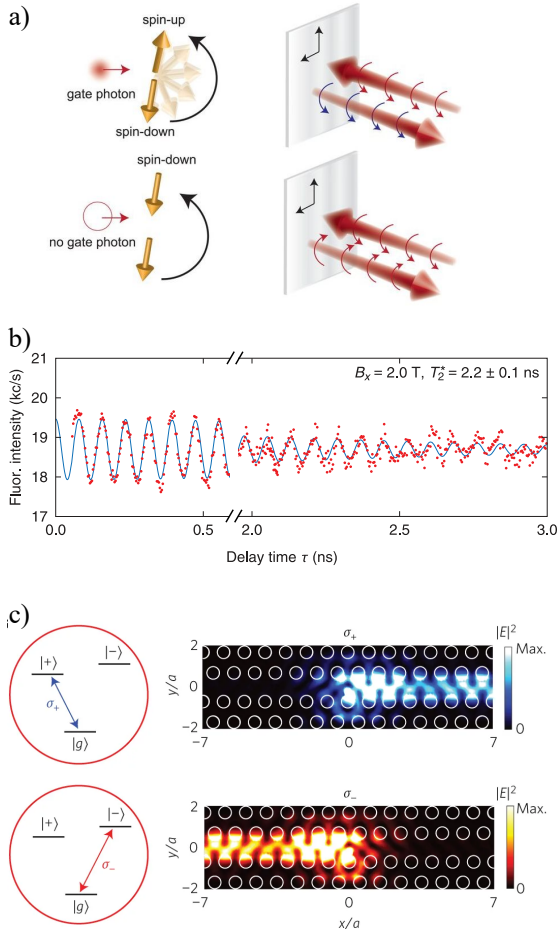


FIG. 18. (a) Schematic of the single-photon switch and transistor. A gate photon controls the state of the spin, and then the spin determines the polarization of the signal field. From Sun, Kim, Luo, Solomon, and Waks, “A single-photon switch and transistor enabled by a solid-state quantum memory,” *Science* **361**, 57–60 (2018). Reprinted with permission from AAAS. (b) Ramsey interference of a QD spin embedded in a nanobeam waveguide, with a dephasing time  $T_2^* = 2.2 \pm 0.1$  ns, and a contrast of 0.04 for the first period. Reprinted figure with permission from Ding, Appel, Javadi, Zhou, Löbl, Söllner, Schott, Papon, Pregolato, Midolo, Wieck, Ludwig, Warburton, Schröder, and Lodahl, “Coherent Optical Control of a Quantum-Dot Spin-Qubit in a Waveguide-Based Spin-Photon Interface,” *Phys. Rev. Applied* **11**, 031002 (2019). Copyright 2019 by the American Physical Society. (c) [Left] QD level scheme featuring two circularly polarized exciton transitions. [Right] Calculated directional emission patterns of  $\sigma_+$  and  $\sigma_-$  transitions. Reprinted with permission of Springer Nature Customer Service Center GmbH from Söllner, Mahmoodian, Hansen, Midolo, Javadi, Kirsanske, Pregolato, El-Ella, Lee, Song, Stobbe, and Lodahl, “Deterministic photon-emitter coupling in chiral photonic circuits,” *Nature Nanotechnology* **10**, 775–778 (2015), Copyright 2015.

are embedded in, to match the emission properties and ensure a high indistinguishability of the photons.

The photonics community has been actively developing multiple techniques for tuning on-chip resonators<sup>289–291</sup>. However, certain methods such as wet-chemical etching<sup>292</sup> and gas condensation<sup>152</sup> (unless used in conjunction with local heating) are not suited for tuning individual devices on a chip or array. We emphasize here that a scalable solution for fully integrated quantum photonics would require that the tuning can be applied locally and independently to individual emitter devices.

*a. Temperature* Temperature tuning can affect the bandgap structure, which strongly tunes the QD energy; it can also alter the refractive index and cause physical expansion, which would shift the resonances of a cavity device coupled to the QD. The simplest way to achieve this is to change the sample temperature in the cryostat, but this does not allow for the tuning of individual devices<sup>293,294</sup>. Instead, local temperature changes can be applied via electrical heaters or laser irradiation<sup>278,295,296</sup> (see Fig. 19a). A recent report has also employed temperature tuning of two QDs in a nanophotonic waveguide to achieve superradiant emission<sup>297</sup>.

*b. Strain* QD energy is sensitive to strain tuning, and strain sensors have been demonstrated by detecting energy shifts at the  $\mu\text{eV}$  level for InGaAs QDs embedded in a photonic crystal membrane<sup>298</sup>. However, to achieve larger tuning ranges, strain can be induced via piezoelectric crystals, and a tuning rate of  $\sim 1$  pm/V<sup>279</sup> has been achieved (see Fig. 19b). A difficulty with this approach is the relatively large fabrication overhead of integrating piezoelectric materials. However, another recent work has shown that strain tuning can be achieved via laser-induced local phase transitions of the crystal structure, which circumvents this issue<sup>299</sup>.

*c. Electric field* The application of electric fields across the QD can be used to control the energy of the QD excitonic lines via the quantum-confined Stark effect<sup>300–302</sup>. The application of a forward bias voltage leads to a blue-shift of the QD emission wavelength of several nm. This can be complemented by independently tuning the cavity mode of the photonic crystal structure, e.g. via electromechanical actuation<sup>280,303</sup> (see Fig. 19c). Beyond wavelength tuning, recent work has also shown that electrical control of QDs is crucial to obtain the best optical properties for integrated QDs<sup>228</sup>.

*d. Frequency conversion* An alternative strategy is to tune the emitted photons via on-chip quantum frequency conversion (QFC)<sup>237</sup>. Ref. 281 performs QFC separately on the output of two QDs to convert them from 904 nm to the telecom C-band, achieving a two-photon interference visibility of  $29 \pm 3\%$  (see Fig. 19d).

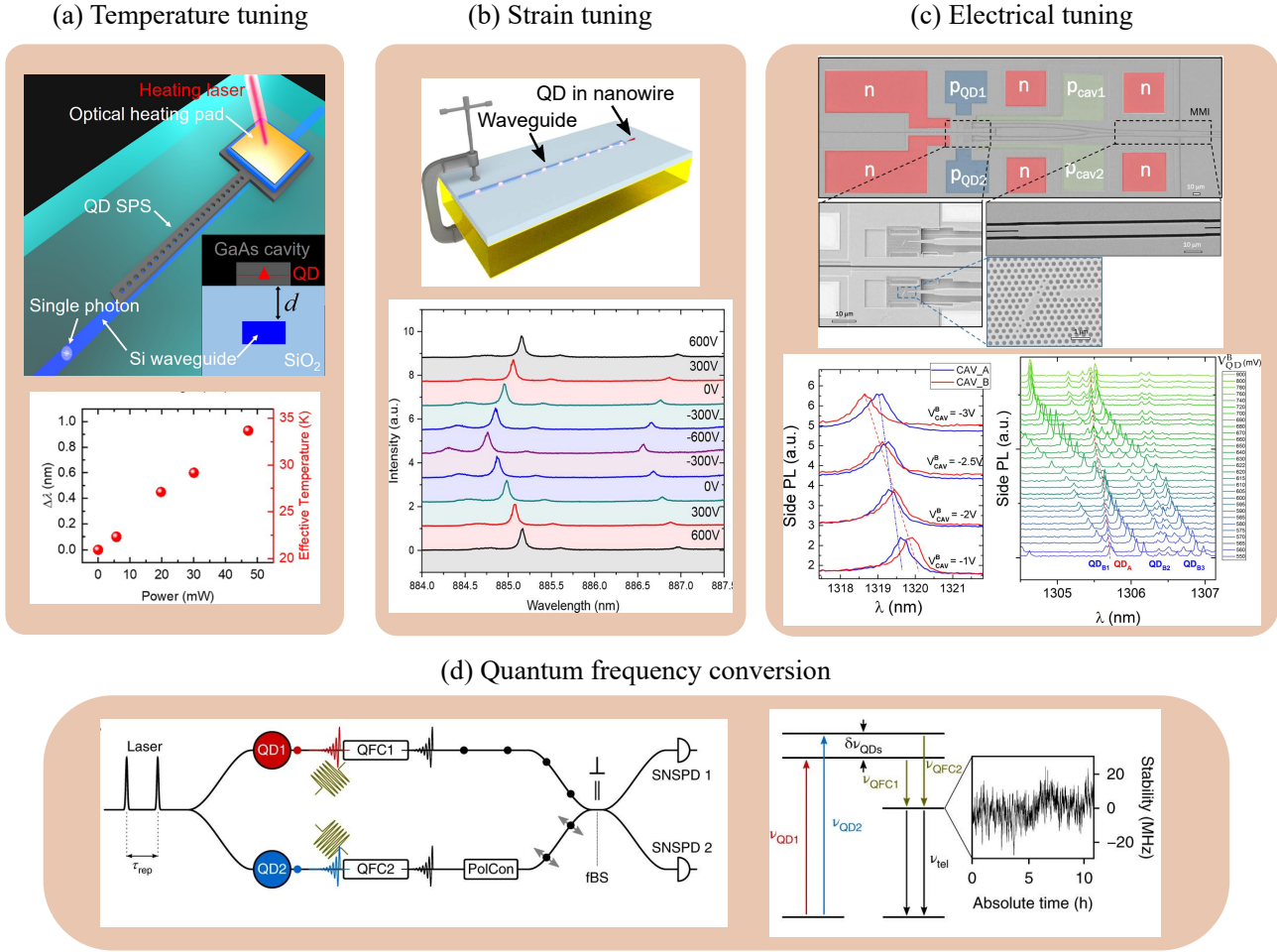


FIG. 19. (a) [Top] Schematic of a QD device temperature-tuned by laser irradiation on a heating pad. [Bottom] Dependence of the QD detuning on the heating laser power. Reprinted from [Katsumi, Ota, Osada, Tajiri, Yamaguchi, Kakuda, Iwamoto, Akiyama, and Arakawa](#), “In situ wavelength tuning of quantum-dot single-photon sources integrated on a CMOS-processed silicon waveguide,” *Applied Physics Letters* **116**, 041103 (2020), with the permission of AIP Publishing. (b) [Top] Artistic representation of a waveguide-coupled QD photon source fabricated on a strain-tunable substrate. [Bottom] Emission spectra of the nanowire QD as a function of the applied voltage to the piezoelectric substrate. Reprinted with permission from [Elshaari, Bykzer, Zadeh, Lettner, Zhao, Schll, Gyger, Reimer, Dalacu, Poole, Jns, and Zwiller](#), “Strain-Tunable Quantum Integrated Photonics,” *Nano Letters* **18**, 7969-7976 (2018). Copyright 2018 American Chemical Society. Permission for further reuse should be directed to ACS. (c) [Top] Annotated SEM picture of a device with two integrated QD devices. The QDs and cavities can be electrically tuned individually. [Bottom] Spectra showing the electromechanical tuning of the cavities (left) and the Stark tuning of the QDs (right). Reprinted from [Petruzzella, Birindelli, Pagliano, Pellegrino, Zobenica, Li, Linfield, and Fiore](#), “Quantum photonic integrated circuits based on tunable dots and tunable cavities,” *APL Photonics* **3**, 106103 (2018) under the [CC BY 4.0](#) license. (d) [Left] Schematic of a device where the emission of two QDs are individually tuned via quantum frequency conversion (QFC). [Right] Energy diagram depicting the QFC scheme. Reprinted with permission of Springer Nature Customer Service Center GmbH from [Weber, Kambs, Kettler, Kern, Maisch, Vural, Jetter, Portalupi, Becher, and Michler](#), “Two-photon interference in the telecom C-band after frequency conversion of photons from remote quantum emitters,” *Nature Nanotechnology* **14**, 23-26 (2019), Copyright 2019.

VI. 2-D MATERIALS

A. Introduction into 2D Materials

Single photon sources in 2D materials have unique advantages compared to other quantum emitters in 3-D bulk material. Confined in atomically thin material, they can potentially have high photon extraction efficiencies

and their emission properties can be controlled by a variety of effects including strain, temperature, pressure and applied electric and magnetic field. Indeed, single photon sources in monolayered 2D material can have almost unity out-coupling efficiency as none of the emitters are surrounded by high refractive index material and their emitted light are consequently not affected by Fresnel or total internal reflection<sup>304,305</sup>. In addition, 2D mate-

rials can be easily transferred and integrated with photonic structures or other 2D materials to form synergistic heterostructures that combine the advantages of various materials together in one unified structure<sup>306</sup>. In this review of single photon sources in 2D materials we restrict ourselves to transitional metal dichalcogenides (TMDC) and hexagonal boron nitride (hBN) although we acknowledge that there are other important examples of 2D materials including graphene, anisotropic black phosphorus and borophene<sup>307–309</sup>. An important feature of single photon emitters in these 2D materials is that similar to  $NV^-$  centers in diamonds and QDs, they can be used for efficient spin-photon quantum interfaces by tailoring the light-matter interactions due to the broken inversion symmetry<sup>310,311</sup>. The zero field splitting in TMDC materials can be up to  $\sim 0.7$  meV, which is about 50 times higher than InAs/GaAs self-assembled quantum dots, and it has a surprisingly large anomalous g-factor of  $\sim 8-10$  that can potentially allow for extremely fast coherent spin coupling<sup>312</sup>. On the other hand, hBN has a considerably smaller zero-field splitting of 0.00145 meV and a more modest g-factor of 2<sup>313</sup>.

### B. Single photon emitters in Transitional Metal Dichalcogenides (TMDC)

A monolayer of TMDC can be described as a  $MX_2$  sandwich structure with M being a transition metal atom (e.g., Mo, W) enclosed between two lattices of chalcogen atom X (e.g., S, Se, Te)<sup>315,316</sup>. Depending on the choice of elements and the number of layers present, TMDC materials can have widely varying electrical, optical, chemical, thermal and mechanical properties<sup>317–322</sup>. Although TMDCs have strong in-plane covalent bonds, they are only weakly bonded in between the layers by Van der Waals forces, which allows them to be easily exfoliated to form monolayer flakes. Alternatively, single layer TMDCs can be fabricated using CVD or MBE<sup>323,324</sup>. Despite the fact that multilayer TMDCs have indirect bandgaps, monolayer TMDCs are actually direct bandgap semiconductors, which enables them to have enhanced interactions with light<sup>317,325–327</sup>. There are two distinctive properties that are associated with monolayer TMDCs: strong excitonic effects and valley/spin-dependent properties. The latter can be attributed to the fact that there is no inversion center for a monolayer structure, which opens up a new degree of freedom for charge carriers, i.e. the  $k$ -valley index, that brings new valley-dependent optical and electrical properties into play<sup>321,328–330</sup>. In contrast, TMDC's strong excitonic effects is due to strong Coulomb interactions between charged particles (electrons and holes) and reduced dielectric screening, which result in the formation of excitons with large binding energies (0.2 to 0.8 eV), charged excitons (trions), and biexcitons<sup>331–335</sup>. These manifest themselves by broadband photoluminescence (tens of nanometers) in the visible and near-IR ranges

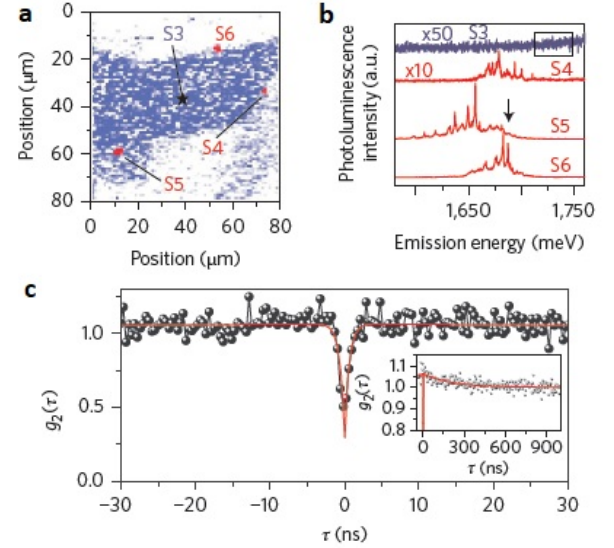


FIG. 20. Single photon emitters in TMDC materials: a) contour plot of photoluminescence scanning experiment for WSe<sub>2</sub> flake with emission spots at the edges of the flake; b) these spots possess narrow line emission spectra; c) measurement of  $g^2(0)$  for one of the narrow emission lines, the value below 0.5 clearly indicates the single photon properties of the emitter. Reprinted with permission of Springer Nature Customer Service Center GmbH from Koperski, Nogajewski, Arora, Cherkez, Mallet, Veuillen, Marcus, Kossacki, and Potemski, “Single photon emitters in exfoliated WSe<sub>2</sub> structures,” *Nature Nanotechnology* **10**, 503-506 (2015), Copyright 2015.

at room and cryogenic temperatures. At the same time, TMDCs can possess quantum-dot like defects, which exhibit themselves in the photoluminescence spectrum as a series of sharp peaks with peak intensities up to several hundred times larger than the excitonic photoluminescence with linewidths around 100  $\mu$ eV and excited state lifetime from 1 to several ns<sup>312,314,336,337</sup> (Fig. 20). For exfoliated samples these defects are usually associated with local strain and typically appear at cracks or edges of the flake while for grown samples they are mostly due to impurities and can appear everywhere. A number of works have shown that these defects emit in the single photon regime and can be controlled by induced strain, applied temperature, electric and magnetic fields<sup>312,337–340</sup>. However, a significant drawback is that the single photon emission quenches at temperatures above 20 K although some recent research have shown that special treatment of TMDC flakes can lead to a redistribution of the energy levels and enable emission at room temperature<sup>341,342</sup>.

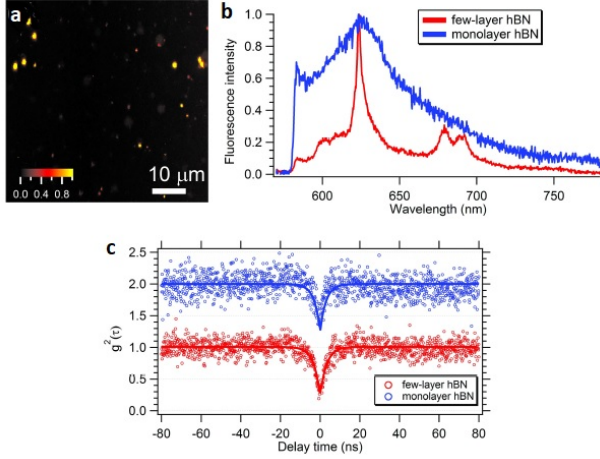


FIG. 21. Single photon emitters in hBN nanoflakes: a) scanning confocal map of hBN nanoflake with bright luminescent spots corresponding to single defects; b) room temperature emission spectrum for single defects in mono- and few-layer hBN nanoflakes; c) measurements of  $g^2(0)$  for single defects in mono- and few-layer hBN nanoflakes. The curves are shifted for clarity demonstrating  $g^2(0) < 0.5$ . Reprinted with permission of Springer Nature Customer Service Center GmbH from [Tran, Bray, Ford, Toth, and Aharonovich](#), “Quantum emission from hexagonal boron nitride monolayers,” *Nature Nanotechnology* **11**, 37-41 (2016), Copyright 2016.

### C. Single photon emitters in Hexagonal Boron Nitride (hBN)

hBN monolayers are structurally similar to TMDC but whereas single photon emitters (SPEs) in TMDCs are associated with localized excitons, SPEs in insulating hBN are, similar to color centers in diamond, attributed to atomic-like defects of the crystal structure<sup>343–345</sup>. These defects in hBN are some of the brightest single photon sources in the visible spectrum and have large Debye-Waller factors with good polarization contrasts. Like  $NV^-$  centers, their electronic levels are within the band gap ( $\sim 6$ eV), resulting in stable and extremely robust emitters at room temperature over a wide spectral bandwidth ranging from green to near infrared with most emitters emitting around the yellow-red region<sup>346</sup> (Fig. 21). These SPEs in hBN are generally characterized by short excited state lifetime (several ns), absolute photon stability, and high quantum efficiency<sup>343,344,346</sup>. Close to Fourier transform limited linewidths below 100 MHz have been recorded with resonant excitation at cryo and room temperatures<sup>347,348</sup>. Recent research indicates that various types of defects are responsible for the multiplicity of observed ZPL emissions, including nitrogen vacancy defects (NV), carbon substitutional (of a nitrogen atom) defects, and oxygen related defects<sup>345,349</sup>. Interestingly, the asymmetric linewidths of some of these ZPLs have been attributed to the existence of two independent electronic transitions<sup>350</sup>.

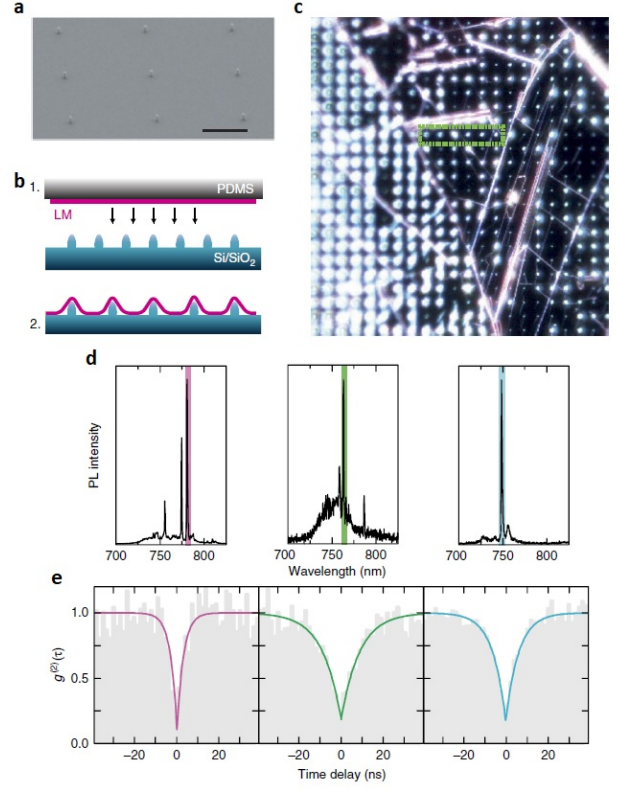


FIG. 22. Deterministic creation of single photon emitters by strain: a) SEM image of nanopillar substrate, fabricated using electron beam lithography, black scale bar corresponds to  $2 \mu\text{m}$ ; b) illustration of the fabrication method; c) dark-field optical image of mono-layer  $WSe_2$  flake on top of nanopillar array. Green rectangle indicates the 6 adjacent nanopillars where single photon emitters were measured; d) examples of measured spectras at different pillars demonstrating narrow emission lines; e) measurements of  $g^2(0)$  for the emission lines in (d). Reprinted from [Palacios-Berraquero, Kara, Montblanch, Barbone, Latawiec, Yoon, Ott, Loncar, Ferrari, and Atatüre](#), “Large-scale quantum-emitter arrays in atomically thin semiconductors,” *Nature Communications* **8**, 15093 (2017) under the [CC BY 4.0](#) license.

### D. Deterministic Creation and Control of Single Photon Emitters in 2D Materials

The random distribution of SPEs in 2D materials is a significant obstacle that prevents their integration with photonic structures. Deterministically creating SPEs in 2D materials is therefore an important technological goal. One way to do so is to induce SPEs by introducing strain to the material. This concept was successfully realized by several groups that transferred 2D materials onto the tops of metallic or dielectric nanopillar arrays<sup>339,340,351</sup> (Fig. 22). The SPE (as confirmed by measured  $g^2(0) < 0.1$ ) yield of this technique exceeds 90 % and the quality of these engineered SPEs was reported to be even higher than naturally occurring defects with 10 times less spectral diffusion ( $\sim 0.1$  meV)<sup>340</sup>. An

even simpler (but less scalable) way to create SPEs with strain was suggested by Rosenberger *et al.*: place a deformable polymer film below the 2D material of interest and apply mechanical force to the film using an atomic force microscopy (AFM) tip<sup>352</sup>. Although this approach is less scalable, it can enable one to tune the SPE's optical properties through careful strain engineering with the AFM tip.

Remarkably, emission from SPE in 2D material defects can be controlled through the application of a voltage<sup>337,338</sup>. For example, in Ref. 338, photo and electro-luminescence were observed from point defects in a 2D material ( $\text{WSe}_2$ ) sandwiched between hBN layers that served as tunnelling barriers between  $\text{WSe}_2$  and its graphene electrodes. Moreover, Schwarz *et al.* showed that it was possible to tune the emission wavelength of the SPE ( $\sim 0.4$  meV/V) by changing the applied bias voltage, which makes the platform amenable to a host of technological applications.

### E. Enhancement of Emission from 2D Materials by Coupling into Resonant Modes

Although the tunability and large oscillator strengths of SPEs in 2D materials make them attractive in photonic applications, their sub-nanometer thickness results in a small light-matter interaction length that limits their efficiency. However, as noted in section II B, this disadvantage may be mitigated by coupling them with resonant photonic structures where both their absorption and emission can potentially be enhanced<sup>354</sup>. Fortunately, the atomic thickness of 2D materials makes them especially amenable to integration with photonic structures such as planar photonic crystal cavities, ring resonators, and optical microcavities.

The first demonstration of this came from the coupling of photoluminescence from SPEs in TMDC materials to dielectric and plasmonic nanocavities<sup>353,356–358</sup> (Fig. 23, a - c). In Ref. 356, a coupling efficiency of over 80% was demonstrated and a spontaneous emission enhancement of over 70 times was reported. Intriguingly, the photoluminescence enhancement can be controlled via an optical spin orbit coupling, which depends on both the resonant nanoparticles' geometry as well as the incident laser's polarization and power<sup>353</sup> (Fig. 23, a, b). Subsequently, single photon emission from a single emitter in a hBN nanoflake was successfully coupled to both one and two resonant gold nanospheres<sup>355</sup> (Fig. 23, d - g). These nanospheres were brought into close proximity with a pre-characterized SPE (verified by measuring  $g^{(2)}(0) < 0.5$ ) by means of an AFM tip and the emitter was observed to have a photon flux of about 6 MHz that corresponded with a 3-fold Purcell enhancement<sup>355</sup>.

A natural structure for SPEs in 2D materials to couple to are noble metal nanopillars since they can kill two birds with one stone by first facilitating the deterministic creation of SPEs (as discussed in section VID above),

and then enhancing the created SPEs' spontaneous emission through the SPEs' coupling with surface plasmon resonances of the metallic nanopillars. This has been successfully implemented for both TMDCs and hBN at cryogenic and room temperatures where increased brightness, shorter lifetimes and enhanced spontaneous emission of the SPEs were all reported<sup>359–362</sup>. Coupling of the emitter to plasmonic modes results in linearly polarized emission that depends on the geometry of the nanopillars and the orientation of the optical dipole<sup>360</sup>. A record high Purcell enhancement of 551 times was achieved with metallic nanocubes<sup>361</sup>.

### F. Coupling and Transfer of Emission from 2D Materials into Photonic Structures

To fully integrate SPEs in 2D materials onto an on-chip photonic platform, it is also necessary to couple emission from SPEs into waveguiding photonic structures. To this end a few groups have successfully coupled emission from SPEs in 2D materials into the surface plasmon polariton modes of silver based waveguides. For example, localized SPEs formed from the intrinsic strain gradient formed along a  $\text{WSe}_2$  monolayer when it was deposited on top of a silver nanowire were efficiently coupled to the guided surface plasmon modes of the nanowire<sup>363</sup>. A coupling efficiency of 39% was measured for a single SPE by comparing the intensity of the laser excited SPE and the emission intensities at both ends of the silver nanowire<sup>363</sup>. Separately, S. Dutta *et al.* demonstrated the coupling of single emitters in  $\text{WSe}_2$  to propagating surface plasmon polaritons in silver-air-silver, Metal-Insulator-Metal (MIM) waveguides<sup>364</sup> (Fig. 24, a - d). The waveguides were fabricated using EBL, followed by metal deposition of Cr and Ag, and then a liftoff in acetone with subsequent protection by a 4 nm buffer layer of oxide. As before, strain gradients on the monolayer due to the waveguide generated sharp localized SPEs that were intrinsically close to the plasmonic mode. Due to the sub-wavelength confinement of the surface plasmon polariton modes, a 1.89 times enhancement of the SPE's radiative lifetime was observed under illumination at 532 nm at cryogenic (3.2 K) temperatures and bright narrow lines associated with the SPE's emission were measured.

Although surface plasmon polariton modes on silver waveguides may help to enhance the spontaneous emission of a SPE, the metal interface results in significantly lossy propagation that is undesirable. Such high propagation losses can be circumvented by using dielectric waveguides instead. In Ref. 365, integration of a monolayer  $\text{WSe}_2$  flake with a 700 nm wide  $\text{Si}_3\text{N}_4$  waveguide that was patterned using standard EBL techniques was achieved by carefully picking up and releasing a bulk exfoliated flake using a GelPak stamp (Fig. 24, e - g). Confocal scans of the  $\text{WSe}_2$  monolayer with a 532 nm excitation laser at cryogenic temperatures indicated that several SPEs were sufficiently close to the  $\text{Si}_3\text{N}_4$  waveguide



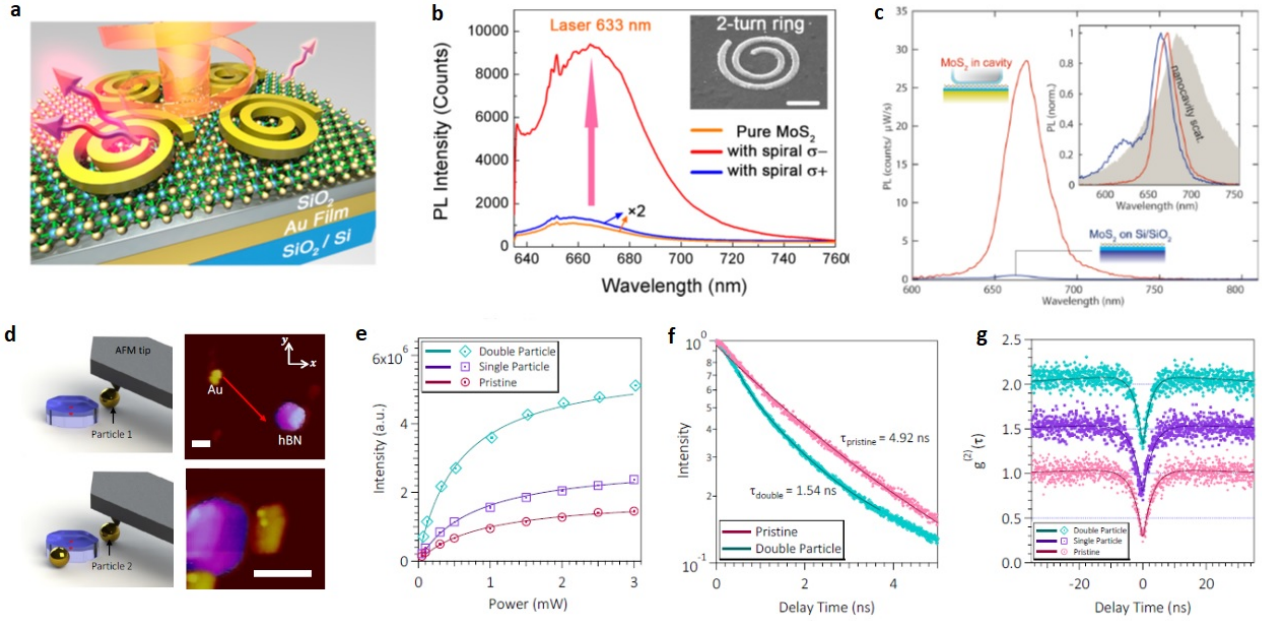


FIG. 23. Enhancement of spontaneous emission with nanocavities: (a) Schematic of spiral ring structure with circularly polarized light excitation. The photoluminescence intensity is enhanced when the MoS<sub>2</sub> monolayer couples with plasmonic spiral structures; (b) Spectra of MoS<sub>2</sub> monolayer with and without spiral structures, under the excitation of different circularly polarized light, inset shows the cross section view of a 2-turn spiral ring. The scale bar is 400 nm. Figures (a) and (b) are reprinted with permission from [Li, Li, Han, Wang, Yu, Tay, Liu, and Fang](#), “Tailoring MoS<sub>2</sub> ExcitonPlasmon Interaction by Optical SpinOrbit Coupling,” *ACS Nano* **11**, 1165-1171 (2017). Copyright 2017 American Chemical Society. Permission for further reuse should be directed to ACS. (c) Spectra of MoS<sub>2</sub> monolayer on a SiO<sub>2</sub>/Si substrate (blue) and in the nanocavity (red) obtained using a diffraction-limited excitation spot. The inset presents normalized spectra for the two cases along with the scattering spectrum for a typical nanocavity (gray). Reprinted with permission from [Akselrod, Ming, Argyropoulos, Hoang, Lin, Ling, Smith, Kong, and Mikkelsen](#), “Leveraging Nanocavity Harmonics for Control of Optical Processes in 2D Semiconductors,” *Nano Letters* **15**, 3578-3584 (2015). Copyright 2015 American Chemical Society. Permission for further reuse should be directed to ACS. (d) Deterministic positioning of gold nanospheres with hBN nanoflake by AFM tip, white scale bar is 250 nm. (e) A comparison between time-resolved measurements of pristine and double particle arrangement. (f) A comparison of fluorescence saturation curves between the pristine, single particle, and double particle arrangements. (g) Measurements of  $g^2(0)$  for pristine, single particle, and double particle arrangements. The curves are shifted for clarity. Figures (d) - (g) are republished with permission of the Royal Society of Chemistry from [Nguyen, Kim, Tran, Xu, Kianinia, Toth, and Aharonovich](#), “Nanoassembly of quantum emitters in hexagonal boron nitride and gold nanospheres,” *Nanoscale* **10**, 2267-2274 (2018); permission conveyed through Copyright Clearance Center, Inc.

to enable coupling to it. Although some luminescence was measured at the end of the waveguide, which provided proof of a non-zero coupling, the SPE’s coupling to the waveguide is strongly dependent on the orientation of its optical dipole and consequently, the photoluminescence spectra for a confocal scan can be significantly different from that obtained at the end of the waveguide. Brighter emission and saturation counts of up to 100 kHz can be obtained by exciting the SPE at close to the free exciton wavelength ( $\approx 702$  nm) with a tunable Ti:Sapphire laser. Besides enabling brighter emission, excitation at 702 nm also produces less background fluorescence. Measurements of the background subtracted  $g^{(2)}$  correlation function in confocal geometry revealed a anti-bunching dip with  $g^{(2)}(0) = 0.47$ , that suggest the existence of a SPE.

Finally, we note that there has been successful integration of SPEs in 2D materials to an on-chip beamsplitter

in the form of a lithium niobate directional coupler<sup>366</sup> (Fig. 24, h - i). Indeed, emission from an excited SPE in a strain engineered WSe<sub>2</sub> monolayer was coupled into one input port of the directional coupler and its photoluminescence, which consisted of strong emission lines corresponding to emission from the WSe<sub>2</sub> flake, was successfully measured at the other output port of the directional coupler (Fig. 24e), demonstrating the desired operation of the beam splitter and showing that an on-chip Hanbury Brown and Twiss measurement is possible.

## VII. INTEGRATION APPROACHES

Numerous techniques have been developed to directly integrate solid-state quantum emitters with on-chip nanophotonic structures. Doing so would allow for dense integration of these emitters on a large scale, and

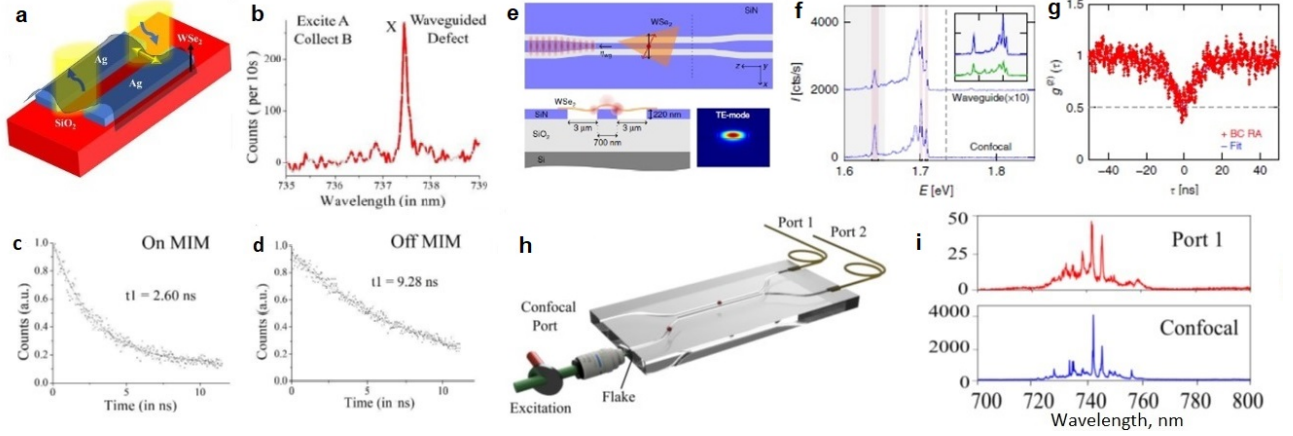


FIG. 24. Coupling and transport of single photon emission from 2D materials in photonic structures: (a) Scheme of an MIM waveguide covered by a  $\text{WSe}_2$  monolayer. The yellow dipole is a quantum emitter, the blue arrows denote the excitation and collection points; (b) The spectra of the defect with the excitation spot fixed at the location of the defect and collection spot moved to the far end of the waveguide; (c) and (d) Lifetime measurements for emitters located on the MIM waveguide and out of it. Figures (a) – (d) were reprinted from [Dutta, Cai, Buyukkaya, Barik, Aghaeimeibodi, and Waks, “Coupling quantum emitters in  \$\text{WSe}\_2\$  monolayers to a metal-insulator-metal waveguide,” Applied Physics Letters \*\*113\*\*, 191105 \(2018\)](#), with the permission of AIP Publishing. (e) Illustration of the  $\text{Si}_3\text{N}_4$  photonic device with a  $\text{WSe}_2$  flake integrated on top of a 220 nm thick single mode  $\text{Si}_3\text{N}_4$  waveguide, separated by 2 air trenches from the bulk  $\text{Si}_3\text{N}_4$ ; (f) Confocal and waveguide-coupled spectrum of the emitter excited by 702 nm pump. The waveguide spectrum is multiplied by 10 and offset by 2000 cts/sec for improved visualization. The inset shows confocal spectra obtained by either green excitation at 532 nm (green curve) or excitation at 702 nm (blue curve); (g) Background-corrected measurements of  $g^2(0)$  for the coupled emitter made in confocal geometry. Figures (e) – (g) were reprinted from [Peyskens, Chakraborty, Muneeb, Van Thourhout, and Englund, “Integration of single photon emitters in 2D layered materials with a silicon nitride photonic chip,” Nature Communications \*\*10\*\*, 4435 \(2019\)](#) under the [CC BY 4.0](#) license. (h) Scheme of Ti in diffused lithium niobate directional coupler with a  $\text{WSe}_2$  flake at the input facet. Emitters are excited in confocal geometry. Their emission is detected by a confocal microscope and through the two output ports (Port 1 and Port 2); (i) The spectra measured through the waveguide output port and confocally when the emitter is excited at the facet. Figure (h) and (i) were reprinted from [White, Branny, Chapman, Picard, Brotons-Gisbert, Boes, Peruzzo, Bonato, and Gerardot, “Atomically-thin quantum dots integrated with lithium niobate photonic chips \(Invited\),” Opt. Mater. Express \*\*9\*\*, 441–448 \(2019\)](#) under the [CC BY 4.0](#) license.

also provide potential benefits in coupling efficiencies, device stability, and ease of control.

In this section, we will provide an overview of hybrid integration approaches, and discuss their applicability to the solid-state emitters presented in this review. A detailed reference on integration methods for hybrid quantum photonics can be found in Ref. 6.

### A. Random Dispersion

A simple integration method is to forego deterministic positioning, and rely on the random placement of the quantum emitters. For QDs<sup>229,239</sup> and 2D materials<sup>312,314,336,337</sup>, the emitters may already be randomly distributed in their as-grown state.

In the case of  $\text{NV}^-$  centers, type Ib diamonds, which by definition have significant singly dispersed nitrogen impurities<sup>367–369</sup>, naturally host an ensemble of randomly positioned  $\text{NV}^-$  centers. Such diamonds can be found naturally or manufactured using a High-Pressure High-Temperature process<sup>367</sup>. Similarly, type IIa diamonds, which by definition have much lower concentra-

tions of nitrogen impurities compared to type Ib diamonds, also host a sparse ensemble of randomly positioned  $\text{NV}^-$  centers. Although rare in nature, type IIa diamonds can be grown using chemical vapor deposition<sup>370</sup>. Photonic structures fabricated on diamond membranes will therefore have randomly positioned NV centers, and indeed, although the yield for such structures is poor with sub-optimal coupling between the photonic structure and NV center, many early experiments relied on such a random dispersal technique. Other color centers in diamond do not form naturally and have to be integrated using more deterministic techniques.

Colloidal QDs and nanodiamonds containing color centers can also be randomly dispersed onto photonic structures via drop casting or spin coating<sup>371</sup>. Nanodiamonds have also been dip coated directly onto single mode optical fibers<sup>212</sup>. In this technique, the tapered fiber is dipped into a droplet of nanodiamond-containing solution on the tip of a glass rod. The tapered fiber is then pulled by a linear stage along the axis of the fiber. However, SPEs in the form of nanoparticles often have a large surface area, which may lead to optical instabilities such as blinking or bleaching. This is due to

the stronger influence of surface states and enhanced Auger recombination<sup>52</sup>. Moreover, random dispersion is not suitably scalable for quantum photonic applications where efficient, deterministic coupling between emitters and the photonic circuit is crucial.

To improve the positioning precision, and thus the coupling efficiency, a lithography-based masking method can be used to selectively deposit dispersed emitters on top of the photonic structures<sup>372</sup> (Fig. 28a). Despite its limitations, randomly positioning of emitters can still be a useful method to rapidly prototype hybrid quantum photonics platforms.

## B. Targeted Creation

### 1. Irradiation and annealing in diamond

Deterministic positioning of NV centers can be achieved by deliberately creating vacancies in type Ib diamonds with irradiation of either a focused ion<sup>373–375</sup>, proton<sup>376</sup> or electron<sup>373,377,378</sup> beam. Since vacancies in diamond can, with an activation energy of  $\approx 2.3$  eV migrate during annealing<sup>12,379,380</sup> at  $\gtrsim 600$  °C, the diamond is then typically annealed after irradiation to allow the vacancies to diffuse and be “captured” by an existing nitrogen impurity<sup>12,34,381</sup>. The spatial resolution of this technique is therefore not just dependent on the resolution of the focused ion or electron beam, but also on the concentration of nitrogen impurities in the diamond, which determines how far a vacancy has to diffuse before being captured by a nitrogen impurity. In fact, despite having a significantly larger concentration of nitrogen compared to type II diamonds, the spatial resolution of this technique in type Ib diamonds can still be limited by the concentration of nitrogen impurities<sup>373</sup>. The diffusion length  $l_D$  of the vacancies may be estimated using  $l_D \sim \sqrt{D\Delta t}$ , where  $D$  here is the diffusion coefficient and  $\Delta t$  is the anneal time.  $D$  may be obtained via the Arrhenius equation

$$D = D_0 \exp\left(-\frac{E_a}{k_B T}\right), \quad (22)$$

where  $E_a$  is the activation energy,  $k_B$  is the Boltzmann constant,  $T$  is the temperature, and  $D_0$  is the maximal diffusion constant calculated to be around  $3.7 \times 10^{-6}$  cm<sup>2</sup>/s for vacancies near the diamond surface<sup>382</sup>. For typical conditions, the diffusion length is likely to be  $\sim 100$  nm, and indeed, vacancies have been observed to diffuse by a few hundred nm in the vertical (along the irradiation axis) direction<sup>383</sup> and a vacancy diffusion limited transverse spot size of less than 180 nm was obtained using a focused Ga<sup>+</sup> ion beam<sup>373</sup>. Although there has been reports of vacancy transverse diffusion lengths that are in the tens of  $\mu\text{m}$  range<sup>384,385</sup> that seem to defy the simple  $l_d \sim \sqrt{D\Delta t}$  estimate, we note that this could potentially be explained by the scattering of

ions/electrons on masks<sup>386–389</sup> if they were used on the diamond’s surface<sup>390</sup>. Nevertheless, we note that if the mask is carefully designed, transverse spatial resolution in the tens of nanometers can be achieved using an implantation and annealing approach<sup>162</sup> (see Fig. 26 and section VII B 2). Furthermore, we note that the choice of radiation used can significantly affect the vertical distribution of vacancies. In general, the heavier ions deposit most of their energy within a narrow band and creates vacancies at a more well defined depth whereas the lighter electrons tend to create a more uniform depth profile of vacancies<sup>391</sup>.

An alternate pathway to creating NV<sup>-</sup> centers is to grow an isotopically pure <sup>12</sup>C (which has no nuclear spin) diamond layer on an existing substrate using plasma assisted CVD, and then introducing nitrogen gas during the last stages of the growth<sup>156,392,393</sup> (see Fig. 25). It is possible using this procedure to make single NV<sup>-</sup> centers with a long spin coherence time of  $T_2 \approx 1.7$  ms<sup>392</sup>. To achieve 3-D localization of NV<sup>-</sup> centers using such an approach, the depth of the nitrogen doped layer, which determines the depth of the NV centers, can first be carefully controlled by slowing the growth rate down to  $\sim 0.1$  nm/min<sup>156</sup>, which allows a depth precision of a few nm (delta doping). Transverse localization ( $\lesssim 450$  nm) of long coherence NV<sup>-</sup> centers with  $T_2 \approx 1$  ms can then be achieved by using a Transmission Electron Microscope (TEM) to create vacancies within the nitrogen doped layer followed by annealing<sup>394</sup>. The long coherence time of those NV centers are not limited by either <sup>13</sup>C nuclear spins or lattice damage induced by the electrons (which is thought to be small compared to ion implantation) but rather the presence of other nitrogen impurities that were not converted into NV centers<sup>394</sup>. A variation to using electron irradiation via a TEM is to use irradiation of <sup>12</sup>C<sup>161</sup> or He<sup>+</sup><sup>395</sup> ions to create vacancies. Compared to electron irradiation, using ions allows for a more localized layer of vacancies, which will reduce the unwanted creation of NV centers in the substrate of the CVD grown diamond. However, we note that using such an approach can possibly decrease the  $T_2$  of the NV centers due to increased lattice damage caused by the ions.

### 2. Implantation and annealing in diamond

A slightly different approach is to start with a type IIa diamond which does not contain significant amounts of nitrogen impurities and to introduce both the vacancy and nitrogen impurity at the same time by implanting N<sup>+</sup> (or N<sub>2</sub><sup>+</sup>) ions with a focused ion beam and then annealing at  $\gtrsim 600$  °C. Using this approach, it is possible to fabricate single NV<sup>-</sup> centers with transverse spatial resolution of tens of nm and a yield of  $\sim 50\%$  using 2 MeV N<sup>+</sup> ions with a beam diameter of 300 nm<sup>396</sup>. The NV<sup>-</sup> yield, which is defined as the ratio of active NV<sup>-</sup> centers to the number of implanted N<sup>+</sup> ions, is proportional to the ion beam’s energy with a particularly strong slope in

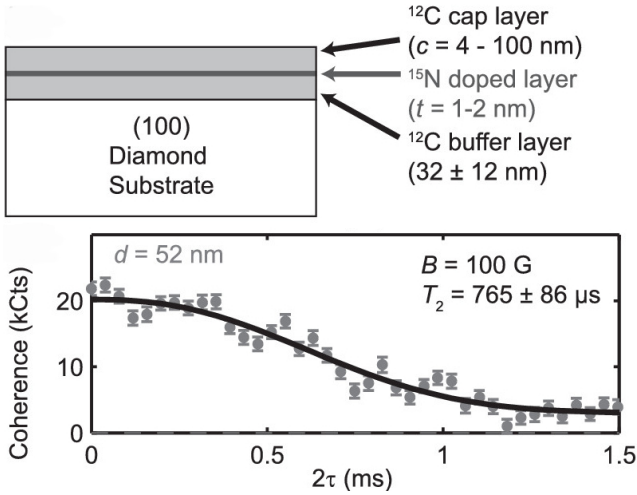


FIG. 25. Top:  $\text{NV}^-$  centers created by CVD growth and nitrogen delta doping of a bulk diamond substrate. Vacancies were created by electron irradiation at 2 MeV. Bottom:  $\text{NV}^-$  centers created in this way at a depth of 52 nm exhibited a Hahn-echo  $T_2$  coherence time of  $765 \mu\text{s}$  at room temperature. Using a similar procedure, Ref. 392 achieved a  $T_2$  of  $\approx 1.7$  ms in isotopically enriched  $^{12}\text{C}$  diamond. Reprinted from Ohno, Joseph Heremans, Bassett, Myers, Toyli, Bleszynski Jayich, Palmstrm, and Awschalom, “Engineering shallow spins in diamond with nitrogen delta-doping,” *Applied Physics Letters* **101**, 082413 (2012), with the permission of AIP Publishing.

the keV region<sup>397</sup>. This is most likely due to the fact that the number of vacancies an ion generates is also proportional to its energy and SRIM<sup>398</sup> calculations show that the  $\text{NV}^-$  yield show a very similar energy dependence<sup>397</sup>. A less energetic beam should therefore be used to decrease the  $\text{NV}^-$  yield (for single  $\text{NV}^-$  creation) but a less energetic beam also results in shallower  $\text{NV}^-$  centers within the diamond, which can be undesirable for some applications.

If a focused ion beam is not available, high spatial resolution can also be achieved by the appropriate use of a mask and (unfocused)  $\text{N}^+$  ion beam implantation. In Ref. 162,  $\text{NV}^-$  spatial resolution of  $\sim 10$  nm in all three directions were accomplished using  $\text{N}^+$  ion implantation with the mask shown in Figure 26.

### 3. Laser writing and annealing in diamond

While traditional irradiation or implantation of particles typically create a trail of vacancies following the implanted particle’s path (with increased straggling for lighter particles), irradiation of the diamond by focused femtosecond (fs) laser pulses can create vacancies at a more localized depth. Moreover, their transverse spatial resolution can be better than the diffraction limit due to the non-linear processes involved. In addition, fs laser pulses from the same optical system can also be used to fabricate other photonic structures on the same dia-

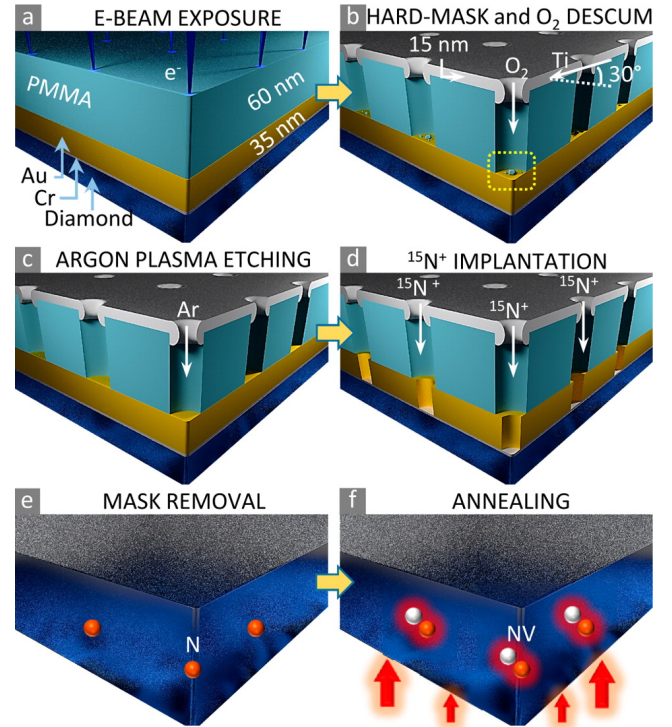


FIG. 26. Fabrication of  $\text{NV}^-$  center by implantation of  $^{15}\text{N}$  ions on a masked diamond substrate. (a) Electron beam lithography (EBL) is used to pattern a polymethyl methacrylate (PMMA) mask spin coated on top of an Au layer that sits on a 8 nm thick Cr adhesion layer. (b) After development of the PMMA resist, a hard Ti mask is deposited at  $30^\circ$  to reduce the aperture size and to protect the resist’s top surface from an  $\text{O}_2$  plasma reactive ion etch (RIE) that removes any resist residue from the bottom of the aperture. (c) The pattern is then transferred to the Au mask by Ar plasma etching. Note that the Cr layer is not etched. (d) 10 keV  $^{15}\text{N}^+$  ions were implanted to introduce nitrogen atoms at  $\approx 7.5$  nm below the surface. (e) Mask is removed by wet chemical treatment. (f) Sample was annealed at  $1000^\circ\text{C}$  to form  $\text{NV}^-$  center with spatial resolutions of  $\sim 13$  nm. Reprinted with permission from Scarabelli, Trusheim, Gaathon, Englund, and Wind, “Nanoscale Engineering of Closely-Spaced Electronic Spins in Diamond,” *Nano Letters* **16**, 4982-4990 (2016). Copyright 2016 American Chemical Society. Permission for further reuse should be directed to ACS.

mond, opening a convenient avenue of integrating photonic structures with NV centers on the same diamond.

Implementing fs laser machining in diamond is complicated by the fact that there is a significant mismatch between the refractive indices of diamond ( $\approx 2.4$  at 790 nm) and air or (more commonly) immersion oil ( $\approx 1.5$ ). This can result in considerable aberration of the focal point within diamond and cause a significant elongation of the focal volume (which reduces the peak field intensity and localization of vacancies) in the beam’s direction of propagation. Indeed, an early experiment attempting to create NV centers using fs lasers focused the beam above the diamond’s surface instead of within it and relied on

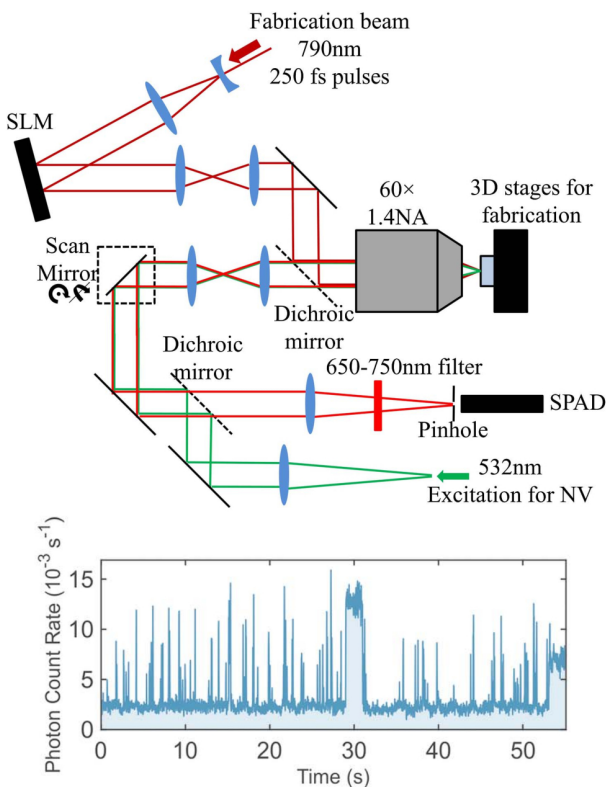


FIG. 27. Top: Optical setup enabling both vacancy creation and annealing using the same fs laser with a SLM to correct for aberrations. Vacancy creation uses a single 27 nJ pulse while annealing occurs with a 1 kHz pulse train consisting of 19 nJ pulses. Real time monitoring of photo luminescence is also possible by incorporating a separate optical arm consisting of both a 532 nm excitation laser and a single photon avalanche detector with a long-pass filter. Bottom: Fluorescence counts measured during the annealing pulses showing first the creation and destruction of a  $\text{NV}^-$  center ( $\approx 28$  to 30 ns) followed by the creation of a second  $\text{NV}^-$  center ( $\approx 52$  ns). Reprinted from [Chen, Griffiths, Weng, Nicley, Ishmael, Lekhai, Johnson, Stephen, Green, Morley, Newton, Booth, Salter, and Smith](#), “Laser writing of individual nitrogen-vacancy defects in diamond with near-unity yield,” *Optica* **6**, 662–667 (2019) under the [CC BY 4.0](#) license.

the ionization of  $\text{O}_2$  and  $\text{N}_2$  molecules in air to generate free electrons and ions that are subsequently accelerated by the light’s electric field into the diamond<sup>399</sup>.

Aberrations caused by refractive index mismatch between diamond and air (or immersion oil) may be corrected by using adaptive optics such as membrane deformable mirror (DM) and/or spatial light modulators (SLM) that modify the light’s wavefront to compensate for the refractive index mismatch. Indeed, NV centers have been successfully created using focused fs laser pulses with a SLM that had a transverse spatial resolution of  $\approx 200$  nm that was limited by the diamond’s nitrogen concentration<sup>403</sup>. More recently, it was demonstrated that the same fs laser system may be used to both create a vacancy *and* anneal the diamond (locally)

by careful control of the laser pulse energy<sup>400</sup>. Coupled together with real-time monitoring of the fluorescence, NV centers at a single site could be generated with near-unity yield and statistically selective generation of NV centers with a particular orientation is even possible by monitoring the polarization pattern of the fluorescence (which is correlated with the NV center’s orientation) and keeping the annealing pulse on until a desired polarization pattern is generated (NV centers with the “wrong orientation” can be destroyed after creation by keeping the annealing pulses on)<sup>400</sup> (see Fig. 27).

#### 4. In-situ Lithography

Photonic structures can be fabricated on adjacent layers to a QD sheet. However, in the absence of site-controlled growth<sup>232</sup>, the self-assembled QDs would be randomly located<sup>404</sup> and thus would not be optimally placed with respect to the photonic structures for efficient coupling. To circumvent this problem, the QDs can first be located and pre-selected, e.g. via cathode luminescence, and the waveguide structures can then be patterned and etched via an *in situ* lithography technique<sup>266</sup> (see Fig. 28b).

With this technique, very small systematic misalignments ( $< 10$  nm) have been achieved, as well as minimal fabrication-induced spectral shifts ( $\lesssim 1$  nm) which can be compensated via tuning of the QD<sup>405</sup>.

This approach has also been used for nanodiamonds, where DLSP waveguides were fabricated with deterministic positioning to include pre-characterized nanodiamonds with NV-centers<sup>202,203</sup>. The authors were able to control the in-plane position of the nanodiamond with the desired NV-center within about 30 nm.

#### C. Wafer Bonding

Quantum emitters embedded in a high-quality bulk crystalline material are able to produce stable single-photon emission with high purity and indistinguishability. Ideally, hybrid heterostructures of QDs and photonic components can be grown directly on a single wafer. However, growing such heterostructures directly often results in poor crystal quality due to the formation of antiphase boundaries and large mismatches in material lattice constants, thermal coefficients, and charge polarity<sup>6</sup>.

Wafer-to-wafer bonding is a method for integrating dissimilar material platforms<sup>406</sup>. Consider the transfer of a III-V material onto a silicon nitride photonics circuit: Each material is grown separately with optimized substrates and conditions, thus maintaining high crystal quality for both compounds. The III-V wafer is flipped and bonded onto the top surface of the photonic wafer; subsequent removal of the substrate of the transferred wafer leaves a thin membrane structure on top of the photonic circuit. Photonic structures are then patterned

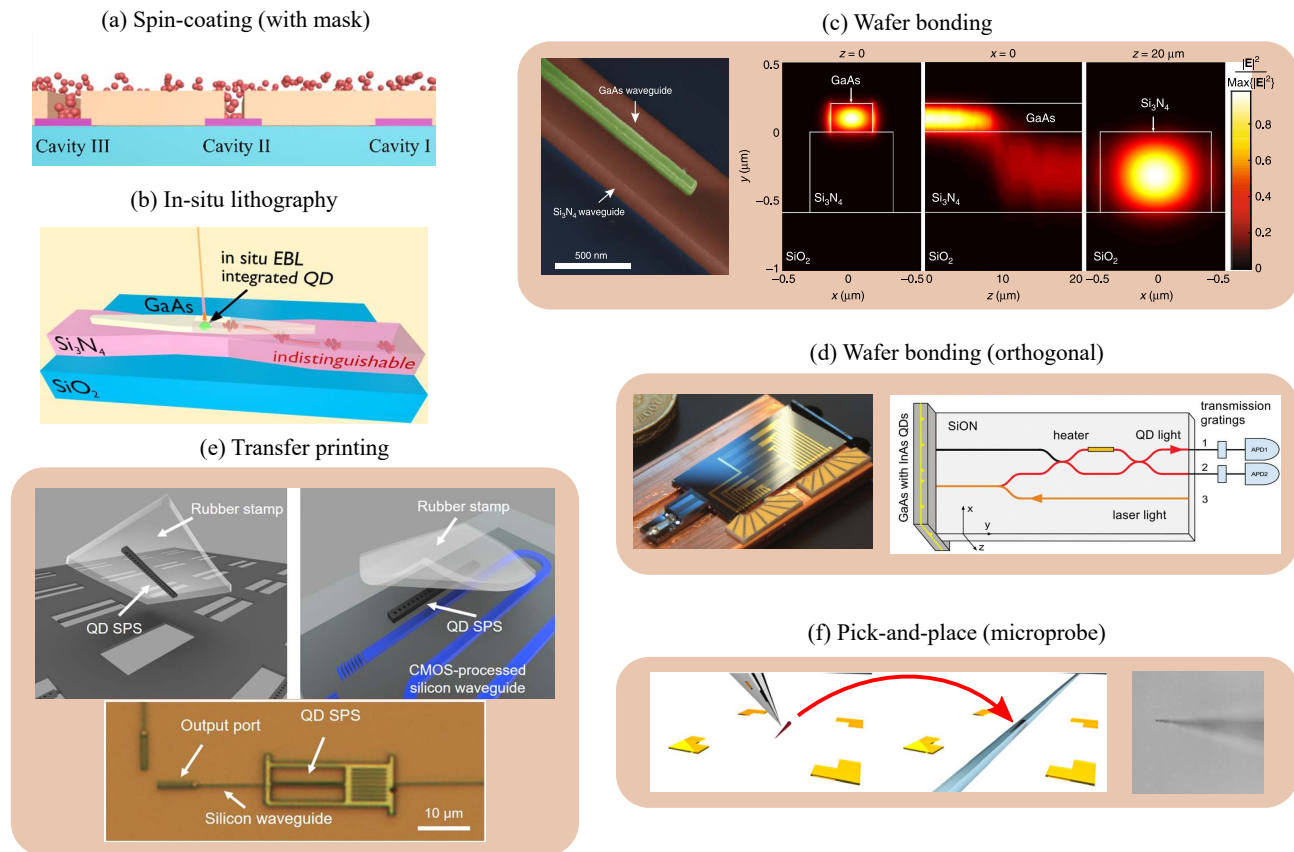


FIG. 28. Integration strategies for quantum dots (QDs) on photonic circuits. (a) Schematic of QDs deposited via spin-coating. A lithographic mask allows for deterministic positioning on top of photonic cavity devices. Reprinted with permission from [Chen, Ryou, Friedfeld, Fryett, Whitehead, Cossairt, and Majumdar](#), “Deterministic Positioning of Colloidal Quantum Dots on Silicon Nitride Nanobeam Cavities,” *Nano Letters* **18**, 6404-6410 (2018). Copyright 2018 American Chemical Society. Permission for further reuse should be directed to ACS. (b) Schematic of a photonic waveguide patterned via *in situ* electron beam lithography (EBL) around a pre-selected QD, ensuring optimal alignment between the QD and waveguide. Reprinted with permission from [Schnauber, Singh, Schall, Park, Song, Rodt, Srinivasan, Reitzenstein, and Davanco](#), “Indistinguishable Photons from Deterministically Integrated Single Quantum Dots in Heterogeneous GaAs/Si<sub>3</sub>N<sub>4</sub> Quantum Photonic Circuits,” *Nano Letters* **19**, 7164-7172 (2019). Copyright 2019 American Chemical Society. Permission for further reuse should be directed to ACS. (c) [Left] A GaAs nanobeam on a Si<sub>3</sub>N<sub>4</sub> waveguide fabricated via EBL from a wafer-bonded GaAs/Si<sub>3</sub>N<sub>4</sub> heterostructure. [Right] Simulation results showing the efficient coupling between the GaAs and Si<sub>3</sub>N<sub>4</sub> waveguides. Reprinted from [Davanco, Liu, Sapiezna, Zhang, De Miranda Cardoso, Verma, Mirin, Nam, Liu, and Srinivasan](#), “Heterogeneous integration for on-chip quantum photonic circuits with single quantum dot devices,” *Nature Communications* **8**, 889 (2017) under the [CC BY 4.0](#) license. (d) Optical image [left] and schematic [right] of InAs QDs integrated with a photonic chip via orthogonal wafer bonding. Reprinted from [Murray, Ellis, Meany, Floether, Lee, Griffiths, Jones, Farrer, Ritchie, Bennett, and Shields](#), “Quantum photonics hybrid integration platform,” *Applied Physics Letters* **107**, 171108 (2015), with the permission of AIP Publishing. (e) [Top] Schematic of the transfer printing technique using a transparent rubber stamp. [Bottom] Optical image of a transfer-printed QD device on top of a silicon waveguide. Reprinted from [Katsumi, Ota, Osada, Yamaguchi, Tajiri, Kakuda, Iwamoto, Akiyama, and Arakawa](#), “Quantum-dot single-photon source on a CMOS silicon photonic chip integrated using transfer printing,” *APL Photonics* **4**, 036105 (2019) under the [CC BY 4.0](#) license. (f) [Left] Schematic of pick-and-place positioning of QD devices using a sharp microprobe. [Right] Electron microscope image of a nanowire QD attached to a microprobe. Reprinted from [Elshaari, Zadeh, Fognini, Reimer, Dalacu, Poole, Zwiller, and Jöns](#), “On-chip single photon filtering and multiplexing in hybrid quantum photonic circuits,” *Nature Communications* **8**, 379 (2017) under the [CC BY 4.0](#) license.

using lithographic techniques; for example, the coupling of the emission from InAs QDs in a GaAs waveguide cavity structure into an underlying silicon nitride waveguide has been observed, with an overall coupling efficiency of  $\sim 0.2$ <sup>256</sup> (Fig. 28c). Similar techniques can be employed to integrate diamond with other material platforms. For

example, numerous GaP-on-diamond platforms<sup>146,148,149</sup> have been realized by bonding a thin epitaxial film of GaP to a diamond substrate via Van der Waals bonding.

However, random positioning of SPEs with respect to the photonic structures in such wafers will result in non-optimal coupling, leading to a low yield of efficiently cou-

pled devices across the wafer. This can be improved via *in situ* lithography (see section VII B 4) around pre-identified SPEs after the wafer bonding step<sup>266</sup>.

The wafer bonding can also be performed orthogonally (Fig. 28d) for optimized SPE out-of-plane emission (e.g. with distributed Bragg reflector cavities<sup>401,407</sup>) to be efficiently coupled into photonic waveguides. However, since only devices at the wafer edge can be integrated (as opposed to across the entire wafer for non-orthogonal bonding), this approach appears to be less scalable.

#### D. Pick-and-place

Another approach that allows for precise positioning of emitters on the photonic circuit is to pick-and-place individual emitters (or the nanostructures they are embedded in) instead of having a single wafer-scale integration step. Emitters can be pre-characterized and pre-selected, and then selectively integrated at desired positions on the photonic circuit. For example, they can be either placed on top of existing waveguides<sup>129,233,236</sup>, or at specific points relative to a marker for subsequent waveguide encapsulation, i.e. waveguide material is deposited and patterned over the emitter<sup>408</sup>. Besides ensuring optimal coupling of the emitters to the photonic circuit, this method also allows for a greater flexibility in the choice of emitter host material and device geometry.

There are two common techniques for performing the pick-and-place transfer: transfer printing via an adhesive stamp, and using a sharp microprobe.

##### 1. Transfer Printing

The transfer printing method typically uses a stamp made of an adhesive and transparent material, such as polydimethylsiloxane (PDMS) or Gelfilm from Gelpak, which allows for precise alignment of the structures under an optical microscope during the transfer. This has been successfully demonstrated for exfoliable layered crystals<sup>409</sup> and QDs<sup>278,402,410</sup> (Fig. 28e). In the case of 2D flakes, using a dry viscoelastic stamp is advantageous compared to wet processes<sup>411–413</sup>, since there are no capillary forces involved which could potentially collapse suspended material.

First, the emitter (e.g. QD nanowire or exfoliated 2D flake) is attached to the stamp. Next, the emitter is brought to the sample surface using XYZ micromanipulators. To release the emitter, the stamp is pressed against the surface and then peeled off slowly. Due to the stamp's viscoelasticity, it behaves as an elastic solid at short timescales while slowly flowing at longer timescales. Consequently, the viscoelastic material can detach from the emitter by slowly peeling the stamp off the surface. Different strategies to control the adhesion of the stamp are detailed in a separate review paper<sup>414</sup>.

There are several challenges in using the transfer printing technique. The stamping process induces a force over a large sample area and may damage parts of the fragile photonic circuit, although this may be mitigated by using a sufficiently small stamp not much larger than the transferred material<sup>415</sup>. Moreover, it is difficult to re-position the emitters as the adhesion between the integrated structures is typically much stronger than their adhesion to the stamp.

Nevertheless, this method provides close to 100% success rate for transfer onto atomically flat materials, though for rougher surfaces the yield is lower due to reduced adhesion forces. With the aid of additional alignment markers, positioning accuracies better than 100 nm have been achieved<sup>410</sup>.

##### 2. Microprobe

An alternative is to perform the pick-up and transfer using a sharp microprobe (Fig. 28f). A small amount of adhesive (e.g. PDMS) can be added to the probe tip to aid the transfer, analogous to a micro-stamp<sup>416</sup>. Although this technique requires precise control of the microprobe, it is able to transfer small, fragile structures such as single nanowires with high accuracy and controllability when aided by an optical microscope<sup>236,279,408</sup>, and especially so when using an electron microscope<sup>234</sup>. Currently, the manual transfer of individual devices one by one can be very time-consuming, but there is great potential in automating the process and allowing for scalable fabrication of many integrated devices.

Besides picking up single nanowires, a microprobe enabled pick-and-place technique allows for the mechanical transfer and removal of Si masks onto diamond substrates (see Fig. 29). This allows for the fabrication of high quality Si masks due to existing mature Si processing technology, which when combined with a negligible Si etch rate during O<sub>2</sub> RIE etching of the diamond membrane, allows for tight fabrication tolerances of the diamond membrane. Moreover, such a mask can be reused multiple times due to the negligible Si etch rate. One significant advantage of this mask transfer technique is that the diamond membrane is never exposed to damaging irradiation that can adversely affect the NV<sup>-</sup> centers' properties. Indeed, using such a fabrication procedure, spin coherence lifetimes of  $\sim 200 \mu\text{s}$  were measured for NV<sup>-</sup> centers coupled to suspended 1-D photonic crystal defects, which are similar to lifetimes measured in their parent CVD crystals<sup>137</sup>. Masks positioned in this way can be placed with sub-micron or even nm scale accuracy if integrated with an electron microscope<sup>416,417</sup>.

Another commonly used microprobe is the tip of an atomic force microscope (AFM). Combined with a confocal microscope, nanoparticles such as nanodiamonds containing desired color centers can be picked up and integrated with the optical devices such as photonic crystal cavity<sup>197</sup>. Scanning the AFM tip in intermittent

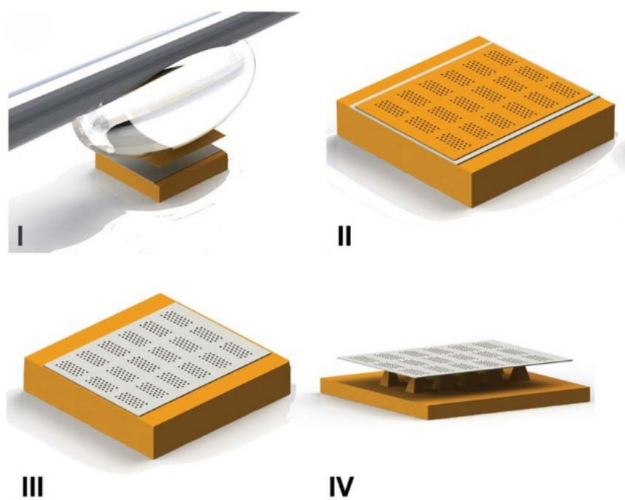


FIG. 29. Schematic of mask transfer technique. (I) A micro-PDMS adhesive on a tungsten probe tip is used to transfer a Si mask (orange) onto a diamond membrane (grey) on top of a Si substrate. (II) The Si mask serves as an etch mask for  $O_2$  plasma RIE. (III) Pattern on Si mask is transferred to the diamond membrane after etching and removal of the Si mask. (IV) An isotropic  $SF_6$  dry etch can then be used to undercut the Si substrate to create a suspended diamond photonic structure if desired. Reprinted from [Li, Bayn, Lu, Nam, Schröder, Stein, Harris, and Englund](#), “Nanofabrication on unconventional substrates using transferred hard masks,” *Scientific Reports* **5**, 7802 (2015) under the [CC BY-NC-ND 4.0](#) license.

contact mode over the focus of the confocal microscope allows identification of the pre-characterized nanodiamonds. The tip is then pressed on the center of the nanodiamond. A force is applied and surface adhesion allows the nanodiamond to be attached to the tip. After successful picking up, which could take over 50 trials, the tip is pressed over the new desired place to allow the nanodiamond to be integrated with the photonic structure. However, there is only limited success rate for the placing stage<sup>197</sup>.

## VIII. CONCLUSION AND OUTLOOK

In this paper we have reviewed a variety of SPEs that are conveniently embedded within a solid. These emitters have promising properties and can be used to form the building blocks of future quantum networks. As discussed in section II A, there are various important metrics to evaluate a SPE in terms of its suitability for various applications. For the sake of easy comparison, Table I lists a selected range of integrated SPE, along with some of the metrics introduced in section II A. Similarly, Table II tabulates various resonators that have been integrated with SPEs and characterizes them based on a few relevant properties.

As tables I and II show, there are a few ways of integrating SPEs with on-chip optical structures and thus realizing functional quantum devices. Indeed, these interfaces enhance the light-matter interaction and allow efficient interaction and entanglement between the distant emitters. However, translation from proof-of-concept laboratory demonstrations of individual components to full-scale quantum devices is still quite immature. Considerable efforts are required to overcome issues associated with the material incompatibility of quantum emitters, photonic circuits and other required components on the same chip. Furthermore there are still challenges in developing high-throughput and reliable integration techniques. We propose the following four critical steps to address these challenges:

First, quantum photonic devices should be thoroughly designed, fabricated and tested since quantum information processing imposes stringent demands on loss and fabrication accuracy. These demands, which are at the limits of conventional silicon photonic technology, might require fabrication for quantum applications to be achieved at the expense of scalable fabrication by, for example, using time-consuming electron beam lithography instead of photolithography.

Second, the coupling between quantum systems and resonant photonic cavities should be optimized through the accurate positioning of the emitter in the cavity. This calls for further improvements in the reliability and throughput of methods such as AFM manipulation, nano-patterning, and various transfer techniques that have been employed for accurate positioning of these quantum emitters.

Third, full scalability implies integration with on-chip single-photon sensitive detectors and lasers on-chip. The development of on-chip active devices would eliminate the need for using bulk optics and allow a significantly smaller footprint for the photonic platform. Design, fabrication, and characterization of on-chip photodetectors and lasers operating at desired performance levels is a challenging task since it involves multiple fabrication steps involving various materials that require state-of-the-art clean room facilities and a comprehensive strategy for heat management and integrating associated optoelectronics.

Fourth, a crucial building block for quantum networks is the realization of quantum-mechanical interaction and entanglement between two separate quantum nodes on the same optical chip. Photons emitted by two independent nodes should be able to coherently interfere on a beamsplitter and produce an interference signal. This task requires demanding control of quantum emitters and photonic elements but demonstration of such an interaction would lead to more complicated schemes of quantum networking, including the interaction of a large number of quantum emitters on the same chip.

Clearly, a consolidation of new technologies is required to address these challenges and to demonstrate a platform for quantum networking that is scalable and



SPE	Platform	$\lambda$ (nm)	$g^{(2)}(0)$	$R_{\text{count}}$	$T_1$ (ns)	$\Gamma^\dagger/2\pi$ (GHz)	$\xi^\dagger$	$V$	Ref
InAs QD	GaAs WG on SiN WG	1130	0.0(1)	-	1.014(4)	-	-	-	256
InAs QD	GaAs RR on SiN WG	1110	0.52(8)	-	0.263(7)	-	-	-	256
InAsP QD	InP NW on SiN WG	988	0.03	22.4 MHz	1.3	14.5	0.008	-	233
InAs QD	GaAs WG on SiN WG	916	0.11(4)	-	1.39(4)	2.20(19)	0.052(6)	$0.89^{+0.11}_{-0.29}$	266
InAs QD	InP NB on Si WG/GC	1300	0.33	2.1 MHz	1.25	-	-	-	234
InAs QD	GaAs NB/GC	921	-	-	0.182(1)	0.96(7)	0.91(7)	-	418
InAs QD	GaAs NB/GC	927	0.05	2.9 MHz	1.4	-	-	-	246
InGaAs QD	GaAs NB	921	0.006	-	0.185	1.12(3)	0.77(2)	0.94(1)	264
InAs QD	GaAs PCW/GC	944-950	-	-	0.346(2)	0.54	0.852(4)	-	228
InAs QD	GaAs PCW/GC	895	0.02(2)	-	0.70(3)	0.22(3)	1.0(2)	0.80(3)	263
InAs QD	GaAs PCW to fiber	931	0.20(8)	8.2(1.7) MHz	0.885	-	-	-	419
InGaAs QD	GaAs WG	941	0.009(2)	-	0.50(1)	-	-	0.975(5)	265
NV <sup>-</sup>	Diamond RR	637	-	-	8.3	40	0.0005	-	151
NV <sup>-</sup>	Diamond RR/WG/GC	638	-	325 Hz	8	51	0.0004	-	155
NV <sup>-</sup>	Diamond RR/WG/GC	637	0.24	15 kHz	-	-	-	-	154
NV <sup>-</sup>	Diamond L3 PCC	637	0.38	13.2 kHz	4	10	0.004	-	109
NV <sup>-</sup>	Diamond NB	638	0.2	-	-	491	-	-	123
NV <sup>-</sup>	Diamond NB	637	0.28	60 kHz	-	15	-	-	137
NV <sup>-</sup>	Diamond WG	637	0.07	1.45 MHz	-	0.323	-	-	129
NV <sup>-</sup> in ND	GaP PCC	643	< 0.5	1 MHz	12.7	-	-	-	199
NV <sup>-</sup> in ND	HSQ WG/GC	650-700	< 0.5	-	6	-	-	-	202
NV <sup>-</sup> in ND	HSQ Cavity/WG/GC	700-750	< 0.5	-	3	-	-	-	203
NV <sup>-</sup> in ND	Ag Nanopatch antennas	650	0.41	56.3 MHz	0.36	-	-	-	205
SiV in ND	Optical Microcavity to fiber	737-759	< 0.5	0.106 - 1.78 MHz	0.46-1.97	21	-	-	210
GeV in ND	HSQ WG/GC	602	< 0.5	-	3.8	-	-	-	184
2D nanoflake	WSe <sub>2</sub> on silver NW	736.74	-	30 kHz	2.4	44.2	0.0015	-	363
2D nanoflake	WSe <sub>2</sub> on MIM WG	737.1	-	300 Hz	3.2(1.1)	55.2	0.0009	-	364
2D nanoflake	WSe <sub>2</sub> on LiNbO <sub>3</sub> BS	720-760	-	4 kHz	-	-	-	-	366
2D nanoflake	WSe <sub>2</sub> on Si <sub>3</sub> N <sub>4</sub> WG	730-750	0.47	100 kHz	7.99	725	$27.5 \times 10^{-6}$	-	365

TABLE I. Comparison of selected integrated SPEs.  $\lambda$  is the SPE's emission wavelength,  $R_{\text{count}}$  gives the count rate and  $V$  is the HOM visibility.  $g^{(2)}(0)$  and  $T_1$  are as defined in equations (4) and (1) respectively.  $\Gamma^\dagger$  is the experimentally measured FWHM of the optical transition that may or may not be homogeneously broadened.  $\xi^\dagger$  is computed using Eq. (1) with  $\Gamma \rightarrow \Gamma^\dagger$ . We note that although  $\xi^\dagger \in [0, 1]$  no longer predicts the size of a HOM dip (since  $\Gamma^\dagger \neq \Gamma$  for an inhomogeneously broadened line), it still serves as a measure of indistinguishability, with  $\xi^\dagger = 1$  indicating perfect indistinguishability. We have made the following abbreviations for the sake of brevity: WG - waveguide, RR - ring resonator, NW - nanowire, NB - nanobeam, PCW - photonic crystal waveguide, PCC - photonic crystal cavity, GC - grating coupler, and BS - beamsplitter. Measurement uncertainties are given in brackets.

amenable to mass manufacturing. This program should leverage on a broad collaboration between experts in quantum physics, integrated photonics, material science, and electronics.

#### DATA AVAILABILITY STATEMENT

Data sharing is not applicable to this article as no new data were created or analyzed in this study.

#### ACKNOWLEDGMENTS

This work was supported by NRF-CRP14-2014-04, "Engineering of a Scalable Photonics Platform for Quantum Enabled Technologies" and the Quantum Technologies for Engineering program of A\*STAR. The authors also acknowledge support from the Quantum Technologies for Engineering (QTE) program of A\*STAR project # A1685b0005.

Type	Material	$Q_{the}$	$Q_{exp}$	$V_{mode} (\lambda/n)^3$	$\lambda$ (nm)	$F_{exp}$	Ref
Ring resonator	Diamond	-	5500	15	638	12	155
L3 PCC	Diamond	6000	3000	0.88	637	70	109
Ring resonator	Diamond	$> 10^6$	$\sim 4000$	17 - 32	637	12	151
1D nanobeam	Diamond	$10^4$	1635	3.7	638	7	123
Ring resonator + WG	Diamond	-	$(3.2 \pm 0.4) \times 10^3$	-	665.9	-	154
1D nanobeam	Diamond	-	7000	0.47	637	22	157
1D nanobeam	Diamond	-	3300	-	637	62	137
Disk resonator	GaP	-	2500 – 10,000	-	637	-	149
L3 PCC	ND+GaP	1000	603	0.75	639.5	12.1	196
L3 PCC	ND+GaP	6000	610	0.74	643	7.0	199
Microdisk cavity	ND+SiO <sub>2</sub>	340000	170000	82	637	-	200
Optical microcavity	ND+Planar mirror + SM optical fiber	-	19000	3.4	737 – 759	9.2	210
Microdisk resonator	ND+3C-SiC	150000	2700	5.5	737	2 – 5	174

TABLE II. Comparison of various integrated resonators.  $Q_{the}$  and  $Q_{exp}$  are the theoretical and experimental quality factors respectively.  $V_{mode}$ ,  $\lambda$  and  $F_{exp}$  are the mode volume, resonance wavelength and experimental Purcell factor respectively.

## REFERENCES

- <sup>1</sup>H. J. Kimble, “The quantum internet,” *Nature* **453**, 1023–1030 (2008).
- <sup>2</sup>N. Sangouard, C. Simon, H. de Riedmatten, and N. Gisin, “Quantum repeaters based on atomic ensembles and linear optics,” *Rev. Mod. Phys.* **83**, 33–80 (2011).
- <sup>3</sup>J. R. Maze, P. L. Stanwix, J. S. Hodges, S. Hong, J. M. Taylor, P. Cappellaro, L. Jiang, M. V. G. Dutt, E. Togan, A. S. Zibrov, A. Yacoby, R. L. Walsworth, and M. D. Lukin, “Nanoscale magnetic sensing with an individual electronic spin in diamond,” *Nature* **455**, 644–647 (2008).
- <sup>4</sup>G. Balasubramanian, I. Y. Chan, R. Kolesov, M. Al-Hmoud, J. Tisler, C. Shin, C. Kim, A. Wojcik, P. R. Hemmer, A. Krueger, T. Hanke, A. Leitenstorfer, R. Bratschitsch, F. Jelezko, and J. Wrachtrup, “Nanoscale imaging magnetometry with diamond spins under ambient conditions,” *Nature* **455**, 648–651 (2008).
- <sup>5</sup>A. W. Elshaari, W. Pernice, K. Srinivasan, O. Benson, and V. Zwiller, “Hybrid integrated quantum photonic circuits,” *Nature Photonics* **14**, 285–298 (2020).
- <sup>6</sup>J.-H. Kim, S. Aghaieimobodi, J. Carolan, D. Englund, and E. Waks, “Hybrid integration methods for on-chip quantum photonics,” *Optica* **7**, 291–308 (2020).
- <sup>7</sup>I. Aharonovich, D. Englund, and M. Toth, “Solid-state single-photon emitters,” *Nature Photonics* **10**, 631–641 (2016).
- <sup>8</sup>Ádám Gali, “Ab initio theory of the nitrogen-vacancy center in diamond,” *Nanophotonics* **8**, 1907 – 1943 (2019).
- <sup>9</sup>A. M. Edmonds, U. F. S. D’Haenens-Johansson, R. J. Crundace, M. E. Newton, K.-M. C. Fu, C. Santori, R. G. Beausoleil, D. J. Twitchen, and M. L. Markham, “Production of oriented nitrogen-vacancy color centers in synthetic diamond,” *Phys. Rev. B* **86**, 035201 (2012).
- <sup>10</sup>L. M. Pham, N. Bar-Gill, D. Le Sage, C. Belthangady, A. Stacey, M. Markham, D. J. Twitchen, M. D. Lukin, and R. L. Walsworth, “Enhanced metrology using preferential orientation of nitrogen-vacancy centers in diamond,” *Phys. Rev. B* **86**, 121202 (2012).
- <sup>11</sup>T. Fukui, Y. Doi, T. Miyazaki, Y. Miyamoto, H. Kato, T. Matsumoto, T. Makino, S. Yamasaki, R. Morimoto, N. Tokuda, M. Hatano, Y. Sakagawa, H. Morishita, T. Tashima, S. Miwa, Y. Suzuki, and N. Mizuochi, “Perfect selective alignment of nitrogen-vacancy centers in diamond,” *Applied Physics Express* **7**, 055201 (2014).
- <sup>12</sup>G. Davies, S. C. Lawson, A. T. Collins, A. Mainwood, and S. J. Sharp, “Vacancy-related centers in diamond,” *Phys. Rev. B* **46**, 13157–13170 (1992).
- <sup>13</sup>F. Jelezko, T. Gaebel, I. Popa, M. Domhan, A. Gruber, and J. Wrachtrup, “Observation of Coherent Oscillation of a Single Nuclear Spin and Realization of a Two-Qubit Conditional Quantum Gate,” *Phys. Rev. Lett.* **93**, 130501 (2004).
- <sup>14</sup>B. Hensen, H. Bernien, A. E. Dréau, A. Reiserer, N. Kalb, M. S. Blok, J. Ruitenber, R. F. L. Vermeulen, R. N. Schouten, C. Abellán, W. Amaya, V. Pruneri, M. W. Mitchell, M. Markham, D. J. Twitchen, D. Elkouss, S. Wehner, T. H. Taminiau, and R. Hanson, “Loophole-free Bell inequality violation using electron spins separated by 1.3 kilometres,” *Nature* **526**, 682–686 (2015).
- <sup>15</sup>J. M. Taylor, P. Cappellaro, L. Childress, L. Jiang, D. Budker, P. R. Hemmer, A. Yacoby, R. Walsworth, and M. D. Lukin, “High-sensitivity diamond magnetometer with nanoscale resolution,” *Nature Physics* **4**, 810–816 (2008).
- <sup>16</sup>F. Dolde, H. Fedder, M. W. Doherty, T. Nöbauer, F. Rempp, G. Balasubramanian, T. Wolf, F. Reinhard, L. C. L. Hollenberg, F. Jelezko, and J. Wrachtrup, “Electric-field sensing using single diamond spins,” *Nature Physics* **7**, 459–463 (2011).
- <sup>17</sup>P. Kehayias, M. J. Turner, R. Trubko, J. M. Schloss, C. A. Hart, M. Wesson, D. R. Glenn, and R. L. Walsworth, “Imaging crystal stress in diamond using ensembles of nitrogen-vacancy centers,” *Phys. Rev. B* **100**, 174103 (2019).
- <sup>18</sup>A. Ajoy and P. Cappellaro, “Stable three-axis nuclear-spin gyroscope in diamond,” *Phys. Rev. A* **86**, 062104 (2012).
- <sup>19</sup>P. Neumann, I. Jakobi, F. Dolde, C. Burk, R. Reuter, G. Waldherr, J. Honert, T. Wolf, A. Brunner, J. H. Shim, D. Suter, H. Sumiya, J. Isoya, and J. Wrachtrup, “High-Precision Nanoscale Temperature Sensing Using Single Defects in Diamond,” *Nano Letters* **13**, 2738–2742 (2013).
- <sup>20</sup>M. W. Doherty, N. B. Manson, P. Delaney, and L. C. L. Hollenberg, “The negatively charged nitrogen-vacancy centre in diamond: the electronic solution,” *New Journal of Physics* **13**, 025019 (2011).
- <sup>21</sup>A. Lenef and S. C. Rand, “Electronic structure of the N-V center in diamond: Theory,” *Phys. Rev. B* **53**, 13441–13455 (1996).
- <sup>22</sup>M. W. Doherty, N. B. Manson, P. Delaney, F. Jelezko, J. Wrachtrup, and L. C. Hollenberg, “The nitrogen-vacancy colour centre in diamond,” *Physics Reports* **528**, 1 – 45 (2013).

- <sup>23</sup>D. A. Redman, S. Brown, R. H. Sands, and S. C. Rand, "Spin dynamics and electronic states of N-V centers in diamond by EPR and four-wave-mixing spectroscopy," *Phys. Rev. Lett.* **67**, 3420–3423 (1991).
- <sup>24</sup>N. Reddy, N. Manson, and E. Krausz, "Two-laser spectral hole burning in a colour centre in diamond," *Journal of Luminescence* **38**, 46 – 47 (1987).
- <sup>25</sup>E. van Oort, N. B. Manson, and M. Glasbeek, "Optically detected spin coherence of the diamond N-V centre in its triplet ground state," *Journal of Physics C: Solid State Physics* **21**, 4385–4391 (1988).
- <sup>26</sup>J. Brossel and F. Bitter, "A New "Double Resonance" Method for Investigating Atomic Energy Levels. Application to  $\text{Hg}^3P_1$ ," *Phys. Rev.* **86**, 308–316 (1952).
- <sup>27</sup>N. B. Manson, X.-F. He, and P. T. H. Fisk, "Raman heterodyne detected electron-nuclear-double-resonance measurements of the nitrogen-vacancy center in diamond," *Opt. Lett.* **15**, 1094–1096 (1990).
- <sup>28</sup>J. H. N. Loubser and J. A. van Wyk, "Electron spin resonance in the study of diamond," *Reports on Progress in Physics* **41**, 1201–1248 (1978).
- <sup>29</sup>J. Martin, "Fine structure of excited  $^3E$  state in nitrogen-vacancy centre of diamond," *Journal of Luminescence* **81**, 237 – 247 (1999).
- <sup>30</sup>N. B. Manson, J. P. Harrison, and M. J. Sellars, "Nitrogen-vacancy center in diamond: Model of the electronic structure and associated dynamics," *Phys. Rev. B* **74**, 104303 (2006).
- <sup>31</sup>G. D. Fuchs, V. V. Dobrovitski, R. Hanson, A. Batra, C. D. Weis, T. Schenkel, and D. D. Awschalom, "Excited-State Spectroscopy Using Single Spin Manipulation in Diamond," *Phys. Rev. Lett.* **101**, 117601 (2008).
- <sup>32</sup>P. Neumann, R. Kolesov, V. Jacques, J. Beck, J. Tisler, A. Batalov, L. Rogers, N. B. Manson, G. Balasubramanian, F. Jelezko, and J. Wrachtrup, "Excited-state spectroscopy of single NV defects in diamond using optically detected magnetic resonance," *New Journal of Physics* **11**, 013017 (2009).
- <sup>33</sup>P. Tamarat, N. B. Manson, J. P. Harrison, R. L. McMurry, A. Nizovtsev, C. Santori, R. G. Beausoleil, P. Neumann, T. Gaebel, F. Jelezko, P. Hemmer, and J. Wrachtrup, "Spin-flip and spin-conserving optical transitions of the nitrogen-vacancy centre in diamond," *New Journal of Physics* **10**, 045004 (2008).
- <sup>34</sup>G. Davies and M. F. Hamer, "Optical studies of the 1.945 eV vibronic band in diamond," *Proceedings of the Royal Society of London. A. Mathematical and Physical Sciences* **348**, 285–298 (1976).
- <sup>35</sup>K.-M. C. Fu, C. Santori, P. E. Barclay, L. J. Rogers, N. B. Manson, and R. G. Beausoleil, "Observation of the Dynamic Jahn-Teller Effect in the Excited States of Nitrogen-Vacancy Centers in Diamond," *Phys. Rev. Lett.* **103**, 256404 (2009).
- <sup>36</sup>A. P. Demchenko, "Photobleaching of organic fluorophores: quantitative characterization, mechanisms, protection," *Methods and Applications in Fluorescence* **8**, 022001 (2020).
- <sup>37</sup>T. Plakhotnik and R. Chapman, "Nitrogen-vacancy centers in nano-diamond reversibly decrease the luminescence quantum yield under strong pulsed-laser irradiation," *New Journal of Physics* **13**, 045001 (2011).
- <sup>38</sup>R. Chapman and T. Plakhotnik, "Anomalous saturation effects due to optical spin depolarization in nitrogen-vacancy centers in diamond nanocrystals," *Phys. Rev. B* **86**, 045204 (2012).
- <sup>39</sup>N. D. Lai, O. Faklaris, D. Zheng, V. Jacques, H.-C. Chang, J.-F. Roch, and F. Treussart, "Quenching nitrogen-vacancy center photoluminescence with an infrared pulsed laser," *New Journal of Physics* **15**, 033030 (2013).
- <sup>40</sup>Y. Dumeige, F. Treussart, R. Allalume, T. Gacoin, J.-F. Roch, and P. Grangier, "Photo-induced creation of nitrogen-related color centers in diamond nanocrystals under femtosecond illumination," *Journal of Luminescence* **109**, 61 – 67 (2004).
- <sup>41</sup>R. P. Roberts, M. L. Juan, and G. Molina-Terriza, "Spin-dependent charge state interconversion of nitrogen vacancy centers in nanodiamonds," *Phys. Rev. B* **99**, 174307 (2019).
- <sup>42</sup>K. Beha, A. Batalov, N. B. Manson, R. Bratschitsch, and A. Leitenstorfer, "Optimum Photoluminescence Excitation and Recharging Cycle of Single Nitrogen-Vacancy Centers in Ultra-pure Diamond," *Phys. Rev. Lett.* **109**, 097404 (2012).
- <sup>43</sup>G. Waldherr, J. Beck, M. Steiner, P. Neumann, A. Gali, T. Frauenheim, F. Jelezko, and J. Wrachtrup, "Dark States of Single Nitrogen-Vacancy Centers in Diamond Unraveled by Single Shot NMR," *Phys. Rev. Lett.* **106**, 157601 (2011).
- <sup>44</sup>B. Naydenov, F. Reinhard, A. Lmmle, V. Richter, R. Kalish, U. F. S. DHaenens-Johansson, M. Newton, F. Jelezko, and J. Wrachtrup, "Increasing the coherence time of single electron spins in diamond by high temperature annealing," *Applied Physics Letters* **97**, 242511 (2010).
- <sup>45</sup>J. O. Orwa, C. Santori, K. M. C. Fu, B. Gibson, D. Simpson, I. Aharonovich, A. Stacey, A. Cimmino, P. Balog, M. Markham, D. Twitchen, A. D. Greentree, R. G. Beausoleil, and S. Prawer, "Engineering of nitrogen-vacancy color centers in high purity diamond by ion implantation and annealing," *Journal of Applied Physics* **109**, 083530 (2011).
- <sup>46</sup>A. Wotherspoon, J. Steeds, B. Catmull, and J. Butler, "Photoluminescence and positron annihilation measurements of nitrogen doped CVD diamond," *Diamond and Related Materials* **12**, 652 – 657 (2003).
- <sup>47</sup>Y. Mita, "Change of absorption spectra in type-Ib diamond with heavy neutron irradiation," *Phys. Rev. B* **53**, 11360–11364 (1996).
- <sup>48</sup>A. T. Collins, "The Fermi level in diamond," *Journal of Physics: Condensed Matter* **14**, 3743–3750 (2002).
- <sup>49</sup>B. T. Webber, M. C. Per, D. W. Drumm, L. C. L. Hollenberg, and S. P. Russo, "Ab initio thermodynamics calculation of the relative concentration of  $\text{NV}^-$  and  $\text{NV}^0$  defects in diamond," *Phys. Rev. B* **85**, 014102 (2012).
- <sup>50</sup>K.-M. C. Fu, C. Santori, P. E. Barclay, and R. G. Beausoleil, "Conversion of neutral nitrogen-vacancy centers to negatively charged nitrogen-vacancy centers through selective oxidation," *Applied Physics Letters* **96**, 121907 (2010).
- <sup>51</sup>M. V. Hauf, B. Grotz, B. Naydenov, M. Dankerl, S. Pezzagna, J. Meijer, F. Jelezko, J. Wrachtrup, M. Stutzmann, F. Reinhard, and J. A. Garrido, "Chemical control of the charge state of nitrogen-vacancy centers in diamond," *Phys. Rev. B* **83**, 081304 (2011).
- <sup>52</sup>A. L. Efros and D. J. Nesbitt, "Origin and control of blinking in quantum dots," *Nature Nanotechnology* **11**, 661–671 (2016).
- <sup>53</sup>G. Yuan, D. E. Gmez, N. Kirkwood, K. Boldt, and P. Mulvaney, "Two Mechanisms Determine Quantum Dot Blinking," *ACS Nano* **12**, 3397–3405 (2018).
- <sup>54</sup>A. Brenneis, L. Gaudreau, M. Seifert, H. Karl, M. S. Brandt, H. Huebl, J. A. Garrido, F. H. L. Koppens, and A. W. Holleitner, "Ultrafast electronic readout of diamond nitrogen-vacancy centres coupled to graphene," *Nature Nanotechnology* **10**, 135–139 (2015).
- <sup>55</sup>Y. L. Lim, A. Beige, and L. C. Kwek, "Repeat-Until-Success Linear Optics Distributed Quantum Computing," *Phys. Rev. Lett.* **95**, 030505 (2005).
- <sup>56</sup>Y. L. Lim, S. D. Barrett, A. Beige, P. Kok, and L. C. Kwek, "Repeat-until-success quantum computing using stationary and flying qubits," *Phys. Rev. A* **73**, 012304 (2006).
- <sup>57</sup>D. E. Bruschi, T. M. Barlow, M. Razavi, and A. Beige, "Repeat-until-success quantum repeaters," *Phys. Rev. A* **90**, 032306 (2014).
- <sup>58</sup>I. Aharonovich, S. Castelletto, D. A. Simpson, C.-H. Su, A. D. Greentree, and S. Prawer, "Diamond-based single-photon emitters," *Reports on Progress in Physics* **74**, 076501 (2011).
- <sup>59</sup>H.-Q. Zhao, M. Fujiwara, and S. Takeuchi, "Suppression of fluorescence phonon sideband from nitrogen vacancy centers in diamond nanocrystals by substrate effect," *Opt. Express* **20**, 15628–15635 (2012).
- <sup>60</sup>S. Choi, M. Jain, and S. G. Louie, "Mechanism for optical initialization of spin in  $\text{NV}^-$  center in diamond," *Phys. Rev. B* **86**, 041202 (2012).

- <sup>61</sup>L. Robledo, H. Bernien, T. van der Sar, and R. Hanson, “Spin dynamics in the optical cycle of single nitrogen-vacancy centres in diamond,” *New Journal of Physics* **13**, 025013 (2011).
- <sup>62</sup>G. D. Fuchs, V. V. Dobrovitski, D. M. Toyli, F. J. Heremans, C. D. Weis, T. Schenkel, and D. D. Awschalom, “Excited-state spin coherence of a single nitrogen-vacancy centre in diamond,” *Nature Physics* **6**, 668–672 (2010).
- <sup>63</sup>A. Gupta, L. Hacquebard, and L. Childress, “Efficient signal processing for time-resolved fluorescence detection of nitrogen-vacancy spins in diamond,” *J. Opt. Soc. Am. B* **33**, B28–B34 (2016).
- <sup>64</sup>P. Kok, W. J. Munro, K. Nemoto, T. C. Ralph, J. P. Dowling, and G. J. Milburn, “Linear optical quantum computing with photonic qubits,” *Rev. Mod. Phys.* **79**, 135–174 (2007).
- <sup>65</sup>C. H. Bennett, G. Brassard, C. Crépeau, R. Jozsa, A. Peres, and W. K. Wootters, “Teleporting an unknown quantum state via dual classical and Einstein-Podolsky-Rosen channels,” *Phys. Rev. Lett.* **70**, 1895–1899 (1993).
- <sup>66</sup>D. Bouwmeester, J.-W. Pan, K. Mattle, M. Eibl, H. Weinfurter, and A. Zeilinger, “Experimental quantum teleportation,” *Nature* **390**, 575–579 (1997).
- <sup>67</sup>F. De Martini, V. Buzek, F. Sciarrino, and C. Sias, “Experimental realization of the quantum universal NOT gate,” *Nature* **419**, 815–818 (2002).
- <sup>68</sup>M. Żukowski, A. Zeilinger, M. A. Horne, and A. K. Ekert, “Event-ready-detectors” Bell experiment via entanglement swapping,” *Phys. Rev. Lett.* **71**, 4287–4290 (1993).
- <sup>69</sup>J.-W. Pan, D. Bouwmeester, H. Weinfurter, and A. Zeilinger, “Experimental Entanglement Swapping: Entangling Photons That Never Interacted,” *Phys. Rev. Lett.* **80**, 3891–3894 (1998).
- <sup>70</sup>A. V. Kuhlmann, J. Houel, A. Ludwig, L. Greuter, D. Reuter, A. D. Wieck, M. Poggio, and R. J. Warburton, “Charge noise and spin noise in a semiconductor quantum device,” *Nature Physics* **9**, 570–575 (2013).
- <sup>71</sup>A. Berthelot, I. Faverro, G. Cassabois, C. Voisin, C. Delalande, P. Roussignol, R. Ferreira, and J. M. Gérard, “Unconventional motional narrowing in the optical spectrum of a semiconductor quantum dot,” *Nature Physics* **2**, 759–764 (2006).
- <sup>72</sup>A. Kiraz, M. Atatüre, and A. Imamoglu, “Quantum-dot single-photon sources: Prospects for applications in linear optics quantum-information processing,” *Phys. Rev. A* **69**, 032305 (2004).
- <sup>73</sup>L. C. Bassett, F. J. Heremans, C. G. Yale, B. B. Buckley, and D. D. Awschalom, “Electrical tuning of single nitrogen-vacancy center optical transitions enhanced by photoinduced fields,” *Phys. Rev. Lett.* **107**, 266403 (2011).
- <sup>74</sup>P. Siyushev, H. Pinto, M. Vörös, A. Gali, F. Jelezko, and J. Wrachtrup, “Optically controlled switching of the charge state of a single nitrogen-vacancy center in diamond at cryogenic temperatures,” *Phys. Rev. Lett.* **110**, 167402 (2013).
- <sup>75</sup>J. Bylander, I. Robert-Philip, and I. Abram, “Interference and correlation of two independent photons,” *The European Physical Journal D - Atomic, Molecular, Optical and Plasma Physics* **22**, 295–301 (2003).
- <sup>76</sup>C. K. Hong, Z. Y. Ou, and L. Mandel, “Measurement of subpicosecond time intervals between two photons by interference,” *Phys. Rev. Lett.* **59**, 2044–2046 (1987).
- <sup>77</sup>A. Sipahigil, M. L. Goldman, E. Togan, Y. Chu, M. Markham, D. J. Twitchen, A. S. Zibrov, A. Kubanek, and M. D. Lukin, “Quantum interference of single photons from remote nitrogen-vacancy centers in diamond,” *Phys. Rev. Lett.* **108**, 143601 (2012).
- <sup>78</sup>H. Bernien, L. Childress, L. Robledo, M. Markham, D. Twitchen, and R. Hanson, “Two-Photon Quantum Interference from Separate Nitrogen Vacancy Centers in Diamond,” *Phys. Rev. Lett.* **108**, 043604 (2012).
- <sup>79</sup>A. Sipahigil, K. D. Jahnke, L. J. Rogers, T. Teraji, J. Isoya, A. S. Zibrov, F. Jelezko, and M. D. Lukin, “Indistinguishable photons from separated silicon-vacancy centers in diamond,” *Phys. Rev. Lett.* **113**, 113602 (2014).
- <sup>80</sup>C. Santori, D. Fattal, J. Vuckovic, G. S. Solomon, and Y. Yamamoto, “Indistinguishable photons from a single-photon device,” *Nature* **419**, 594–597 (2002).
- <sup>81</sup>O. Gazzano, S. Michaelis de Vasconcellos, C. Arnold, A. Nowak, E. Galopin, I. Sagnes, L. Lanco, A. Lemaître, and P. Senellart, “Bright solid-state sources of indistinguishable single photons,” *Nature Communications* **4**, 1425 (2013).
- <sup>82</sup>T. M. Sweeney, S. G. Carter, A. S. Bracker, M. Kim, C. S. Kim, L. Yang, P. M. Vora, P. G. Brereton, E. R. Cleveland, and D. Gammon, “Cavity-stimulated raman emission from a single quantum dot spin,” *Nature Photonics* **8**, 442–447 (2014).
- <sup>83</sup>Y. Chu, N. de Leon, B. Shields, B. Hausmann, R. Evans, E. Togan, M. J. Burek, M. Markham, A. Stacey, A. Zibrov, A. Yacoby, D. Twitchen, M. Loncar, H. Park, P. Maletinsky, and M. Lukin, “Coherent Optical Transitions in Implanted Nitrogen Vacancy Centers,” *Nano Letters* **14**, 1982–1986 (2014).
- <sup>84</sup>V. M. Acosta, C. Santori, A. Faraon, Z. Huang, K.-M. C. Fu, A. Stacey, D. A. Simpson, K. Ganesan, S. Tomljenovic-Hanic, A. D. Greentree, S. Praver, and R. G. Beausoleil, “Dynamic Stabilization of the Optical Resonances of Single Nitrogen-Vacancy Centers in Diamond,” *Phys. Rev. Lett.* **108**, 206401 (2012).
- <sup>85</sup>G. Brassard, N. Lütkenhaus, T. Mor, and B. C. Sanders, “Limitations on Practical Quantum Cryptography,” *Phys. Rev. Lett.* **85**, 1330–1333 (2000).
- <sup>86</sup>N. Lütkenhaus, “Security against individual attacks for realistic quantum key distribution,” *Phys. Rev. A* **61**, 052304 (2000).
- <sup>87</sup>R. J. Glauber, “The Quantum Theory of Optical Coherence,” *Phys. Rev.* **130**, 2529–2539 (1963).
- <sup>88</sup>H. J. Kimble, M. Dagenais, and L. Mandel, “Photon Antibunching in Resonance Fluorescence,” *Phys. Rev. Lett.* **39**, 691–695 (1977).
- <sup>89</sup>L. Novotny and B. Hecht, *Principles of Nano-Optics* (Cambridge University Press, 2006).
- <sup>90</sup>W. L. Barnes, S. A. R. Horsley, and W. L. Vos, “Classical antennae, quantum emitters, and densities of optical states,” *Journal of Optics* (2020).
- <sup>91</sup>A. Taflove and S. C. Hagness, *Computational Electrodynamics: The Finite-Difference Time-Domain Method*, 2nd ed. (Artech House, 2000).
- <sup>92</sup>R.-C. Ge and S. Hughes, “Design of an efficient single photon source from a metallic nanorod dimer: a quasi-normal mode finite-difference time-domain approach,” *Opt. Lett.* **39**, 4235–4238 (2014).
- <sup>93</sup>P. T. Kristensen and S. Hughes, “Modes and Mode Volumes of Leaky Optical Cavities and Plasmonic Nanoresonators,” *ACS Photonics* **1**, 2–10 (2014).
- <sup>94</sup>P. T. Leung, S. Y. Liu, and K. Young, “Completeness and orthogonality of quasinormal modes in leaky optical cavities,” *Phys. Rev. A* **49**, 3057–3067 (1994).
- <sup>95</sup>E. A. Muljarov and W. Langbein, “Exact mode volume and Purcell factor of open optical systems,” *Phys. Rev. B* **94**, 235438 (2016).
- <sup>96</sup>C. Sauvan, J. P. Hugonin, I. S. Maksymov, and P. Lalanne, “Theory of the Spontaneous Optical Emission of Nanosize Photonic and Plasmon Resonators,” *Phys. Rev. Lett.* **110**, 237401 (2013).
- <sup>97</sup>R. Coccioli, M. Boroditsky, K. W. Kim, Y. Rahmat-Samii, and E. Yablonovitch, “Smallest possible electromagnetic mode volume in a dielectric cavity,” *IEEE Proceedings - Optoelectronics* **145**, 391–397 (1998).
- <sup>98</sup>E. Neu, P. Appel, M. Ganzhorn, J. Miguel-Sánchez, M. Lesik, V. Mille, V. Jacques, A. Tallaire, J. Achard, and P. Maletinsky, “Photonic nano-structures on (111)-oriented diamond,” *Applied Physics Letters* **104**, 153108 (2014).
- <sup>99</sup>K. Srinivasan and O. Painter, “Linear and nonlinear optical spectroscopy of a strongly coupled microdisk-quantum dot system,” *Nature* **450**, 862–865 (2007).
- <sup>100</sup>B. Khanaliloo, M. Mitchell, A. C. Hryciw, and P. E. Barclay, “High-Q/V Monolithic Diamond Microdisks Fabricated with

- Quasi-isotropic Etching,” *Nano Letters* **15**, 5131–5136 (2015).
- <sup>101</sup>H.-Z. Song, W. Zhang, L.-B. Yu, and Z. M. Wang, “Micropillar Cavity Design for 1.55- $\mu\text{m}$  Quantum-Dot Single-Photon Sources,” *Journal of Electronic Science and Technology* **17**, 221–230 (2019).
- <sup>102</sup>G. Alagappan, L. A. Krivitsky, and C. E. Png, “Diamond in a Nanopocket: A New Route to a Strong Purcell Effect,” *ACS Omega* **3**, 4733–4742 (2018).
- <sup>103</sup>G. Alagappan, L. A. Krivitsky, and C. E. Png, “Purcell enhancement of light emission in nanodiamond using a trenced nanobeam cavity,” *Journal of Optics* **22**, 025401 (2020).
- <sup>104</sup>J. E. Frch, S. Kim, C. Stewart, X. Xu, Z. Du, M. Lockrey, M. Toth, and I. Aharonovich, “Photonic Nanobeam Cavities with Nanopockets for Efficient Integration of Fluorescent Nanoparticles,” *Nano Letters* **In print**, null (2020).
- <sup>105</sup>W. Fan, Z. Hao, E. Stock, J. Kang, Y. Luo, and D. Bimberg, “Comparison between two types of photonic-crystal cavities for single-photon emitters,” *Semiconductor Science and Technology* **26**, 014014 (2010).
- <sup>106</sup>T. M. Babinec, B. J. M. Hausmann, M. Khan, Y. Zhang, J. R. Maze, P. R. Hemmer, and M. Loncar, “A diamond nanowire single-photon source,” *Nature Nanotechnology* **5**, 195–199 (2010).
- <sup>107</sup>K. G. Lagoudakis, K. Fischer, T. Sarmiento, A. Majumdar, A. Rundquist, J. Lu, M. Bajcsy, and J. Vučković, “Deterministically charged quantum dots in photonic crystal nanoresonators for efficient spin–photon interfaces,” *New Journal of Physics* **15**, 113056 (2013).
- <sup>108</sup>Z. Luo, S. Sun, A. Karasahin, A. S. Bracker, S. G. Carter, M. K. Yakes, D. Gammon, and E. Waks, “A Spin-Photon Interface Using Charge-Tunable Quantum Dots Strongly Coupled to a Cavity,” *Nano Letters* **19**, 7072–7077 (2019).
- <sup>109</sup>A. Faraon, C. Santori, Z. Huang, V. M. Acosta, and R. G. Beausoleil, “Coupling of Nitrogen-Vacancy Centers to Photonic Crystal Cavities in Monocrystalline Diamond,” *Phys. Rev. Lett.* **109**, 033604 (2012).
- <sup>110</sup>F. Liu, A. J. Brash, J. O’Hara, L. M. P. P. Martins, C. L. Phillips, R. J. Coles, B. Royall, E. Clarke, C. Bentham, N. Prtljaga, I. E. Itskevich, L. R. Wilson, M. S. Skolnick, and A. M. Fox, “High purcell factor generation of indistinguishable on-chip single photons,” *Nature Nanotechnology* **13**, 835–840 (2018).
- <sup>111</sup>M. Jamali, I. Gerhardt, M. Rezai, K. Frenner, H. Fedder, and J. Wrachtrup, “Microscopic diamond solid-immersion-lenses fabricated around single defect centers by focused ion beam milling,” *Review of Scientific Instruments* **85**, 123703 (2014).
- <sup>112</sup>C. Hepp, T. Müller, V. Waselowski, J. N. Becker, B. Pingault, H. Sternschulte, D. Steinmüller-Nethl, A. Gali, J. R. Maze, M. Atatüre, and C. Becher, “Electronic Structure of the Silicon Vacancy Color Center in Diamond,” *Phys. Rev. Lett.* **112**, 036405 (2014).
- <sup>113</sup>E. Neu, M. Fischer, S. Gsell, M. Schreck, and C. Becher, “Fluorescence and polarization spectroscopy of single silicon vacancy centers in heteroepitaxial nanodiamonds on iridium,” *Phys. Rev. B* **84**, 205211 (2011).
- <sup>114</sup>B. J. Shields, Q. P. Unterreithmeier, N. P. de Leon, H. Park, and M. D. Lukin, “Efficient Readout of a Single Spin State in Diamond via Spin-to-Charge Conversion,” *Phys. Rev. Lett.* **114**, 136402 (2015).
- <sup>115</sup>D. A. Hopper, R. R. Grote, A. L. Exarhos, and L. C. Bassett, “Near-infrared-assisted charge control and spin readout of the nitrogen-vacancy center in diamond,” *Phys. Rev. B* **94**, 241201 (2016).
- <sup>116</sup>E. Bourgeois, A. Jarmola, P. Siyushev, M. Gulka, J. Hruby, F. Jelezko, D. Budker, and M. Nesladek, “Photoelectric detection of electron spin resonance of nitrogen-vacancy centres in diamond,” *Nature Communications* **6**, 8577 (2015).
- <sup>117</sup>K. Jensen, N. Leefer, A. Jarmola, Y. Dumeige, V. M. Acosta, P. Kehayias, B. Patton, and D. Budker, “Cavity-Enhanced Room-Temperature Magnetometry Using Absorption by Nitrogen-Vacancy Centers in Diamond,” *Phys. Rev. Lett.* **112**, 160802 (2014).
- <sup>118</sup>Y. Dumeige, M. Chipaux, V. Jacques, F. Treussart, J.-F. Roch, T. Debuisschert, V. M. Acosta, A. Jarmola, K. Jensen, P. Kehayias, and D. Budker, “Magnetometry with nitrogen-vacancy ensembles in diamond based on infrared absorption in a doubly resonant optical cavity,” *Phys. Rev. B* **87**, 155202 (2013).
- <sup>119</sup>C. F. Wang, Y.-S. Choi, J. C. Lee, E. L. Hu, J. Yang, and J. E. Butler, “Observation of whispering gallery modes in nanocrystalline diamond microdisks,” *Applied Physics Letters* **90**, 081110 (2007).
- <sup>120</sup>C. F. Wang, R. Hanson, D. D. Awschalom, E. L. Hu, T. Feygelson, J. Yang, and J. E. Butler, “Fabrication and characterization of two-dimensional photonic crystal microcavities in nanocrystalline diamond,” *Applied Physics Letters* **91**, 201112 (2007).
- <sup>121</sup>L. Li, M. Trusheim, O. Gaathon, K. Kisslinger, C.-J. Cheng, M. Lu, D. Su, X. Yao, H.-C. Huang, I. Bayn, A. Wolcott, R. M. Osgood, and D. Englund, “Reactive ion etching: Optimized diamond membrane fabrication for transmission electron microscopy,” *Journal of Vacuum Science & Technology B* **31**, 06FF01 (2013).
- <sup>122</sup>J. S. Hodges, L. Li, M. Lu, E. H. Chen, M. E. Trusheim, S. Allegri, X. Yao, O. Gaathon, H. Bakhr, and D. Englund, “Long-lived NV-spin coherence in high-purity diamond membranes,” *New Journal of Physics* **14**, 093004 (2012).
- <sup>123</sup>B. J. M. Hausmann, B. J. Shields, Q. Quan, Y. Chu, N. P. de Leon, R. Evans, M. J. Burek, A. S. Zibrov, M. Markham, D. J. Twitchen, H. Park, M. D. Lukin, and M. Loncar, “Coupling of NV Centers to Photonic Crystal Nanobeams in Diamond,” *Nano Letters* **13**, 5791–5796 (2013).
- <sup>124</sup>M. J. Burek, N. P. de Leon, B. J. Shields, B. J. M. Hausmann, Y. Chu, Q. Quan, A. S. Zibrov, H. Park, M. D. Lukin, and M. Loncar, “Free-Standing Mechanical and Photonic Nanostructures in Single-Crystal Diamond,” *Nano Letters* **12**, 6084–6089 (2012).
- <sup>125</sup>M. J. Burek, Y. Chu, M. S. Z. Liddy, P. Patel, J. Rochman, S. Meesala, W. Hong, Q. Quan, M. D. Lukin, and M. Loncar, “High quality-factor optical nanocavities in bulk single-crystal diamond,” *Nature Communications* **5**, 5718 (2014).
- <sup>126</sup>B. Khanaliloo, H. Jayakumar, A. C. Hryciw, D. P. Lake, H. Kaviani, and P. E. Barclay, “Single-Crystal Diamond Nanobeam Waveguide Optomechanics,” *Phys. Rev. X* **5**, 041051 (2015).
- <sup>127</sup>S. Mouradian, N. H. Wan, T. Schrder, and D. Englund, “Rectangular photonic crystal nanobeam cavities in bulk diamond,” *Applied Physics Letters* **111**, 021103 (2017).
- <sup>128</sup>P. E. Barclay, K.-M. Fu, C. Santori, and R. G. Beausoleil, “Hybrid photonic crystal cavity and waveguide for coupling to diamond NV-centers,” *Opt. Express* **17**, 9588–9601 (2009).
- <sup>129</sup>S. L. Mouradian, T. Schröder, C. B. Poitras, L. Li, J. Goldstein, E. H. Chen, M. Walsh, J. Cardenas, M. L. Markham, D. J. Twitchen, M. Lipson, and D. Englund, “Scalable integration of long-lived quantum memories into a photonic circuit,” *Phys. Rev. X* **5**, 031009 (2015).
- <sup>130</sup>B. J. M. Hausmann, I. Bulu, V. Venkataraman, P. Deotare, and M. Loncar, “Diamond nonlinear photonics,” *Nature Photonics* **8**, 369–374 (2014).
- <sup>131</sup>K. Rivoire, Z. Lin, F. Hatami, W. T. Masselink, and J. Vučković, “Second harmonic generation in gallium phosphide photonic crystal nanocavities with ultralow continuous wave pump power,” *Opt. Express* **17**, 22609–22615 (2009).
- <sup>132</sup>E. Anastassakis and E. Burstein, “Second-Order Electro-Optic Effect in Diamond,” *J. Opt. Soc. Am.* **61**, 1618–1621 (1971).
- <sup>133</sup>D. F. Nelson and E. H. Turner, “Electrooptic and Piezoelectric Coefficients and Refractive Index of Gallium Phosphide,” *Journal of Applied Physics* **39**, 3337–3343 (1968).
- <sup>134</sup>C. Xiong, W. H. P. Pernice, X. Sun, C. Schuck, K. Y. Fong, and H. X. Tang, “Aluminum nitride as a new material for chip-scale optomechanics and nonlinear optics,” *New Journal of Physics* **14**, 095014 (2012).

- <sup>135</sup>C. Xiong, W. H. P. Pernice, and H. X. Tang, “Low-Loss, Silicon Integrated, Aluminum Nitride Photonic Circuits and Their Use for Electro-Optic Signal Processing,” *Nano Letters* **12**, 3562–3568 (2012).
- <sup>136</sup>J. P. Sprengers, A. Gaggero, D. Sahin, S. Jahanmirinejad, G. Frucci, F. Mattioli, R. Leoni, J. Beetz, M. Lermer, M. Kamp, S. Hfling, R. Sanjines, and A. Fiore, “Waveguide superconducting single-photon detectors for integrated quantum photonic circuits,” *Applied Physics Letters* **99**, 181110 (2011).
- <sup>137</sup>L. Li, T. Schröder, E. H. Chen, M. Walsh, I. Bayn, J. Goldstein, O. Gaathon, M. E. Trusheim, M. Lu, J. Mower, M. Cotlet, M. L. Markham, D. J. Twitchen, and D. Englund, “Coherent spin control of a nanocavity-enhanced qubit in diamond,” *Nature Communications* **6**, 6173 (2015).
- <sup>138</sup>G. Balasubramanian, P. Neumann, D. Twitchen, M. Markham, R. Kolesov, N. Mizuochi, J. Isoya, J. Achard, J. Beck, J. Tissler, V. Jacques, P. R. Hemmer, F. Jelezko, and J. Wrachtrup, “Ultralong spin coherence time in isotopically engineered diamond,” *Nature Materials* **8**, 383–387 (2009).
- <sup>139</sup>J. Burghoff, C. Grebing, S. Nolte, and A. Tünnermann, “Efficient frequency doubling in femtosecond laser-written waveguides in lithium niobate,” *Applied Physics Letters* **89**, 081108 (2006).
- <sup>140</sup>J. Burghoff, S. Nolte, and A. Tünnermann, “Origins of waveguiding in femtosecond laser-structured LiNbO<sub>3</sub>,” *Applied Physics A* **89**, 127–132 (2007).
- <sup>141</sup>A. Benayas, D. Jaque, B. McMillen, and K. P. Chen, “Thermal stability of microstructural and optical modifications induced in sapphire by ultrafast laser filamentation,” *Journal of Applied Physics* **107**, 033522 (2010).
- <sup>142</sup>B. Sotillo, A. Chiappini, V. Bharadwaj, J. P. Hadden, F. Bosia, P. Olivero, M. Ferrari, R. Ramponi, P. E. Barclay, and S. M. Eaton, “Polarized micro-Raman studies of femtosecond laser written stress-induced optical waveguides in diamond,” *Applied Physics Letters* **112**, 031109 (2018).
- <sup>143</sup>B. Sotillo, V. Bharadwaj, J. P. Hadden, S. Rampini, A. Chiappini, T. T. Fernandez, C. Armellini, A. Serpengzel, M. Ferrari, P. E. Barclay, R. Ramponi, and S. M. Eaton, “Visible to Infrared Diamond Photonics Enabled by Focused Femtosecond Laser Pulses,” *Micromachines* **8** (2017), 10.3390/mi8020060.
- <sup>144</sup>J. P. Hadden, V. Bharadwaj, B. Sotillo, S. Rampini, R. Oselame, J. D. Witmer, H. Jayakumar, T. T. Fernandez, A. Chiappini, C. Armellini, M. Ferrari, R. Ramponi, P. E. Barclay, and S. M. Eaton, “Integrated waveguides and deterministically positioned nitrogen vacancy centers in diamond created by femtosecond laser writing,” *Opt. Lett.* **43**, 3586–3589 (2018).
- <sup>145</sup>E. Yablonovitch, D. M. Hwang, T. J. Gmitter, L. T. Florez, and J. P. Harbison, “Van der Waals bonding of GaAs epitaxial lift-off films onto arbitrary substrates,” *Applied Physics Letters* **56**, 2419–2421 (1990).
- <sup>146</sup>K.-M. C. Fu, C. Santori, P. E. Barclay, I. Aharonovich, S. Praver, N. Meyer, A. M. Holm, and R. G. Beausoleil, “Coupling of nitrogen-vacancy centers in diamond to a GaP waveguide,” *Applied Physics Letters* **93**, 234107 (2008).
- <sup>147</sup>P. E. Barclay, K.-M. C. Fu, C. Santori, and R. G. Beausoleil, “Chip-based microcavities coupled to nitrogen-vacancy centers in single crystal diamond,” *Applied Physics Letters* **95**, 191115 (2009).
- <sup>148</sup>N. Thomas, R. J. Barbour, Y. Song, M. L. Lee, and K.-M. C. Fu, “Waveguide-integrated single-crystalline GaP resonators on diamond,” *Opt. Express* **22**, 13555–13564 (2014).
- <sup>149</sup>M. Gould, S. Chakravarthi, I. R. Christen, N. Thomas, S. Dadgostar, Y. Song, M. L. Lee, F. Hatami, and K.-M. C. Fu, “Large-scale GaP-on-diamond integrated photonics platform for NV center-based quantum information,” *J. Opt. Soc. Am. B* **33**, B35–B42 (2016).
- <sup>150</sup>P. E. Barclay, K.-M. C. Fu, C. Santori, A. Faraon, and R. G. Beausoleil, “Hybrid Nanocavity Resonant Enhancement of Color Center Emission in Diamond,” *Phys. Rev. X* **1**, 011007 (2011).
- <sup>151</sup>A. Faraon, P. E. Barclay, C. Santori, K.-M. C. Fu, and R. G. Beausoleil, “Resonant enhancement of the zero-phonon emission from a colour centre in a diamond cavity,” *Nature Photonics* **5**, 301–305 (2011).
- <sup>152</sup>S. Mosor, J. Hendrickson, B. C. Richards, J. Sweet, G. Khitrova, H. M. Gibbs, T. Yoshie, A. Scherer, O. B. Shchekin, and D. G. Deppe, “Scanning a photonic crystal slab nanocavity by condensation of xenon,” *Applied Physics Letters* **87**, 141105 (2005).
- <sup>153</sup>Q. Quan and M. Loncar, “Deterministic design of wavelength scale, ultra-high Q photonic crystal nanobeam cavities,” *Opt. Express* **19**, 18529–18542 (2011).
- <sup>154</sup>B. J. M. Hausmann, B. Shields, Q. Quan, P. Maletinsky, M. McCutcheon, J. T. Choy, T. M. Babinec, A. Kubanek, A. Yacoby, M. D. Lukin, and M. Loncar, “Integrated Diamond Networks for Quantum Nanophotonics,” *Nano Letters* **12**, 1578–1582 (2012).
- <sup>155</sup>A. Faraon, C. Santori, Z. Huang, K.-M. C. Fu, V. M. Acosta, D. Fattal, and R. G. Beausoleil, “Quantum photonic devices in single-crystal diamond,” *New Journal of Physics* **15**, 025010 (2013).
- <sup>156</sup>K. Ohno, F. Joseph Heremans, L. C. Bassett, B. A. Myers, D. M. Toyli, A. C. Bleszynski Jayich, C. J. Palmstrom, and D. D. Awschalom, “Engineering shallow spins in diamond with nitrogen delta-doping,” *Applied Physics Letters* **101**, 082413 (2012).
- <sup>157</sup>J. C. Lee, D. O. Bracher, S. Cui, K. Ohno, C. A. McLellan, X. Zhang, P. Andrich, B. Alemn, K. J. Russell, A. P. Magyar, I. Aharonovich, A. Bleszynski Jayich, D. Awschalom, and E. L. Hu, “Deterministic coupling of delta-doped nitrogen vacancy centers to a nanobeam photonic crystal cavity,” *Applied Physics Letters* **105**, 261101 (2014).
- <sup>158</sup>J. Riedrich-Miller, S. Pezzagna, J. Meijer, C. Pauly, F. Mcklich, M. Markham, A. M. Edmonds, and C. Becher, “Nanoimplantation and Purcell enhancement of single nitrogen-vacancy centers in photonic crystal cavities in diamond,” *Applied Physics Letters* **106**, 221103 (2015).
- <sup>159</sup>T. Jung, J. Grlitz, B. Kambs, C. Pauly, N. Raatz, R. Nelz, E. Neu, A. M. Edmonds, M. Markham, F. Mcklich, J. Meijer, and C. Becher, “Spin measurements of NV centers coupled to a photonic crystal cavity,” *APL Photonics* **4**, 120803 (2019).
- <sup>160</sup>M. Schukraft, J. Zheng, T. Schröder, S. L. Mouradian, M. Walsh, M. E. Trusheim, H. Bakhru, and D. R. Englund, “Invited Article: Precision nanoimplantation of nitrogen vacancy centers into diamond photonic crystal cavities and waveguides,” *APL Photonics* **1**, 020801 (2016).
- <sup>161</sup>K. Ohno, F. Joseph Heremans, C. F. de las Casas, B. A. Myers, B. J. Alemn, A. C. Bleszynski Jayich, and D. D. Awschalom, “Three-dimensional localization of spins in diamond using 12C implantation,” *Applied Physics Letters* **105**, 052406 (2014).
- <sup>162</sup>D. Scarabelli, M. Trusheim, O. Gaathon, D. Englund, and S. J. Wind, “Nanoscale Engineering of Closely-Spaced Electronic Spins in Diamond,” *Nano Letters* **16**, 4982–4990 (2016).
- <sup>163</sup>A. Sipahigil, R. E. Evans, D. D. Sukachev, M. J. Burek, J. Borregaard, M. K. Bhaskar, C. T. Nguyen, J. L. Pacheco, H. A. Atikian, C. Meuwly, R. M. Camacho, F. Jelezko, E. Bielejec, H. Park, M. Lončar, and M. D. Lukin, “An integrated diamond nanophotonics platform for quantum-optical networks,” *Science* **354**, 847–850 (2016).
- <sup>164</sup>S. Kumar, V. A. Davydov, V. N. Agafonov, and S. I. Bozhevolnyi, “Excitation of nanowire surface plasmons by silicon vacancy centers in nanodiamonds,” *Opt. Mater. Express* **7**, 2586–2596 (2017).
- <sup>165</sup>M. K. Bhaskar, D. D. Sukachev, A. Sipahigil, R. E. Evans, M. J. Burek, C. T. Nguyen, L. J. Rogers, P. Siyushev, M. H. Metsch, H. Park, F. Jelezko, M. Lončar, and M. D. Lukin, “Quantum Nonlinear Optics with a Germanium-Vacancy Color Center in a Nanoscale Diamond Waveguide,” *Phys. Rev. Lett.* **118**, 223603 (2017).
- <sup>166</sup>S. D. Tchernij, T. Herzig, J. Forneris, J. Kpper, S. Pezzagna, P. Traina, E. Moreva, I. P. Degiovanni, G. Brida, N. Skukan, M. Genovese, M. Jaki, J. Meijer, and P. Olivero, “Single-

- Photon-Emitting Optical Centers in Diamond Fabricated upon Sn Implantation,” *ACS Photonics* **4**, 2580–2586 (2017).
- <sup>167</sup>T. Iwasaki, Y. Miyamoto, T. Taniguchi, P. Siyushev, M. H. Metsch, F. Jelezko, and M. Hatano, “Tin-Vacancy Quantum Emitters in Diamond,” *Phys. Rev. Lett.* **119**, 253601 (2017).
- <sup>168</sup>A. Hegyi and E. Yablonovitch, “Molecular Imaging by Optically Detected Electron Spin Resonance of Nitrogen-Vacancies in Nanodiamonds,” *Nano Letters* **13**, 1173–1178 (2013).
- <sup>169</sup>R. Schirhagl, K. Chang, M. Loretz, and C. L. Degen, “Nitrogen-Vacancy Centers in Diamond: Nanoscale Sensors for Physics and Biology,” *Annual Review of Physical Chemistry* **65**, 83–105 (2014).
- <sup>170</sup>L. Childress, R. Walsworth, and M. Lukin, *Physics Today* **67**, 38 (2014).
- <sup>171</sup>K. Bray, R. Previdi, B. C. Gibson, O. Shimon, and I. Aharonovich, “Enhanced photoluminescence from single nitrogen-vacancy defects in nanodiamonds coated with phenolic complexes,” *Nanoscale* **7**, 4869–4874 (2015).
- <sup>172</sup>S. Choi, V. N. Agafonov, V. A. Davydov, and T. Plakhotnik, “Ultrasensitive All-Optical Thermometry Using Nanodiamonds with a High Concentration of Silicon-Vacancy Centers and Multiparametric Data Analysis,” *ACS Photonics* **6**, 1387–1392 (2019).
- <sup>173</sup>Z. H. Khan, ed., *Nanomaterials and Their Applications*, 1st ed. (Springer Singapore, 2018).
- <sup>174</sup>M. Radulaski, J. L. Zhang, Y.-K. Tzeng, K. G. Lagoudakis, H. Ishiwata, C. Dory, K. A. Fischer, Y. A. Kelaita, S. Sun, P. C. Maurer, K. Allassaad, G. Ferro, Z.-X. Shen, N. A. Melosh, S. Chu, and J. Vukovi, “Nanodiamond Integration with Photonic Devices,” *Laser & Photonics Reviews* **13**, 1800316 (2019).
- <sup>175</sup>J. R. Rabeau, A. Stacey, A. Rabeau, S. Praver, F. Jelezko, I. Mirza, and J. Wrachtrup, “Single Nitrogen Vacancy Centers in Chemical Vapor Deposited Diamond Nanocrystals,” *Nano Letters* **7**, 3433–3437 (2007).
- <sup>176</sup>U. Jantzen, A. B. Kurz, D. S. Rudnicki, C. Schfermeier, K. D. Jahnke, U. L. Andersen, V. A. Davydov, V. N. Agafonov, A. Kubanek, L. J. Rogers, and F. Jelezko, “Nanodiamonds carrying silicon-vacancy quantum emitters with almost lifetime-limited linewidths,” *New Journal of Physics* **18**, 073036 (2016).
- <sup>177</sup>T. T. Tran, M. Kianinia, K. Bray, S. Kim, Z.-Q. Xu, A. Gentle, B. Sontheimer, C. Bradac, and I. Aharonovich, “Nanodiamonds with photostable, sub-gigahertz linewidth quantum emitters,” *APL Photonics* **2**, 116103 (2017).
- <sup>178</sup>C. Bradac, T. Gaebel, N. Naidoo, M. J. Sellars, J. Twamley, L. J. Brown, A. S. Barnard, T. Plakhotnik, A. V. Zvyagin, and J. R. Rabeau, “Observation and control of blinking nitrogen-vacancy centres in discrete nanodiamonds,” *Nature Nanotechnology* **5**, 345–349 (2010).
- <sup>179</sup>T. Gaebel, C. Bradac, J. Chen, J. Say, L. Brown, P. Hemmer, and J. Rabeau, “Size-reduction of nanodiamonds via air oxidation,” *Diamond and Related Materials* **21**, 28 – 32 (2012).
- <sup>180</sup>E. Neu, D. Steinmetz, J. Riedrich-Müller, S. Gsell, M. Fischer, M. Schreck, and C. Becher, “Single photon emission from silicon-vacancy colour centres in chemical vapour deposition nano-diamonds on iridium,” *New Journal of Physics* **13**, 025012 (2011).
- <sup>181</sup>T. Müller, C. Hepp, B. Pingault, E. Neu, S. Gsell, M. Schreck, H. Sternschulte, D. Steinmüller-Nethl, C. Becher, and M. Atatüre, “Optical signatures of silicon-vacancy spins in diamond,” *Nature Communications* **5**, 3328 (2014).
- <sup>182</sup>S. Hufler, L. Hartung, K. G. Fehler, L. Antoniuk, L. F. Kulikova, V. A. Davydov, V. N. Agafonov, F. Jelezko, and A. Kubanek, “Preparing single SiV- center in nanodiamonds for external, optical coupling with access to all degrees of freedom,” *New Journal of Physics* **21**, 103047 (2019).
- <sup>183</sup>M. J. Crane, A. Petrone, R. A. Beck, M. B. Lim, X. Zhou, X. Li, R. M. Stroud, and P. J. Pauzauskie, “High-pressure, high-temperature molecular doping of nanodiamond,” *Science Advances* **5** (2019), 10.1126/sciadv.aau6073.
- <sup>184</sup>H. Siampour, S. Kumar, V. A. Davydov, L. F. Kulikova, V. N. Agafonov, and S. I. Bozhevolnyi, “On-chip excitation of single germanium vacancies in nanodiamonds embedded in plasmonic waveguides,” *Light: Science & Applications* **7**, 61 (2018).
- <sup>185</sup>C. Bradac, W. Gao, J. Forneris, M. E. Trusheim, and I. Aharonovich, “Quantum nanophotonics with group IV defects in diamond,” *Nature Communications* **10**, 5625 (2019).
- <sup>186</sup>S. Stehlik, M. Varga, M. Ledinsky, V. Jirasek, A. Artemenko, H. Kozak, L. Ondic, V. Skakalova, G. Argentero, T. Pennycook, J. C. Meyer, A. Fejfar, A. Kromka, and B. Rezek, “Size and Purity Control of HPHT Nanodiamonds down to 1 nm,” *The Journal of Physical Chemistry C* **119**, 27708–27720 (2015).
- <sup>187</sup>S. Schietinger, T. Schrder, and O. Benson, “One-by-one coupling of single defect centers in nanodiamonds to high-q modes of an optical microresonator,” *Nano Letters* **8**, 3911–3915 (2008).
- <sup>188</sup>C. Santori, P. E. Barclay, K.-M. C. Fu, R. G. Beausoleil, S. Spillane, and M. Fisch, “Nanophotonics for quantum optics using nitrogen-vacancy centers in diamond,” *Nanotechnology* **21**, 274008 (2010).
- <sup>189</sup>J. Zheng, B. Lienhard, G. Doerk, M. Cotlet, E. Bersin, H. S. Kim, Y.-C. Byun, C.-Y. Nam, J. Kim, C. T. Black, and D. Englund, “Top-down fabrication of high-uniformity nanodiamonds by self-assembled block copolymer masks,” *Scientific Reports* **9**, 6914 (2019).
- <sup>190</sup>I. Aharonovich, S. Castelletto, D. A. Simpson, A. Stacey, J. McCallum, A. D. Greentree, and S. Praver, “Two-Level Ultra-bright Single Photon Emission from Diamond Nanocrystals,” *Nano Letters* **9**, 3191–3195 (2009).
- <sup>191</sup>T. Schrder, F. Gdeke, M. J. Banholzer, and O. Benson, “Ultra-bright and efficient single-photon generation based on nitrogen-vacancy centres in nanodiamonds on a solid immersion lens,” *New Journal of Physics* **13**, 055017 (2011).
- <sup>192</sup>S. Lindner, A. Bommer, A. Muzha, A. Krueger, L. Gines, S. Mandal, O. Williams, E. Londero, A. Gali, and C. Becher, “Strongly inhomogeneous distribution of spectral properties of silicon-vacancy color centers in nanodiamonds,” *New Journal of Physics* **20**, 115002 (2018).
- <sup>193</sup>K. Li, Y. Zhou, A. Rasmita, I. Aharonovich, and W. B. Gao, “Nonblinking Emitters with Nearly Lifetime-Limited Linewidths in CVD Nanodiamonds,” *Phys. Rev. Applied* **6**, 024010 (2016).
- <sup>194</sup>Y. Shen, T. M. Sweeney, and H. Wang, “Zero-phonon linewidth of single nitrogen vacancy centers in diamond nanocrystals,” *Phys. Rev. B* **77**, 033201 (2008).
- <sup>195</sup>M. Nguyen, N. Nikolay, C. Bradac, M. Kianinia, E. A. Ekimov, N. Mendelson, O. Benson, and I. Aharonovich, “Photodynamics and quantum efficiency of germanium vacancy color centers in diamond,” *Advanced Photonics* **1**, 1 – 7 (2019).
- <sup>196</sup>J. Wolters, A. W. Schell, G. Kewes, N. Nsse, M. Schoengen, H. Dscher, T. Hannappel, B. Lchel, M. Barth, and O. Benson, “Enhancement of the zero phonon line emission from a single nitrogen vacancy center in a nanodiamond via coupling to a photonic crystal cavity,” *Applied Physics Letters* **97**, 141108 (2010).
- <sup>197</sup>A. W. Schell, G. Kewes, T. Schrder, J. Wolters, T. Aichele, and O. Benson, “A scanning probe-based pick-and-place procedure for assembly of integrated quantum optical hybrid devices,” *Review of Scientific Instruments* **82**, 073709 (2011).
- <sup>198</sup>O. Benson, “Assembly of hybrid photonic architectures from nanophotonic constituents,” *Nature* **480**, 193–199 (2011).
- <sup>199</sup>D. Englund, B. Shields, K. Rivoire, F. Hatami, J. Vukovi, H. Park, and M. D. Lukin, “Deterministic Coupling of a Single Nitrogen Vacancy Center to a Photonic Crystal Cavity,” *Nano Letters* **10**, 3922–3926 (2010).
- <sup>200</sup>P. E. Barclay, C. Santori, K.-M. Fu, R. G. Beausoleil, and O. Painter, “Coherent interference effects in a nano-assembled diamond NV center cavity-QED system,” *Opt. Express* **17**, 8081–8197 (2009).

- <sup>201</sup>Y.-S. Park, A. K. Cook, and H. Wang, "Cavity QED with Diamond Nanocrystals and Silica Microspheres," *Nano Letters* **6**, 2075–2079 (2006).
- <sup>202</sup>H. Siampour, S. Kumar, and S. I. Bozhevolnyi, "Nanofabrication of Plasmonic Circuits Containing Single Photon Sources," *ACS Photonics* **4**, 1879–1884 (2017).
- <sup>203</sup>H. Siampour, S. Kumar, and S. I. Bozhevolnyi, "Chip-integrated plasmonic cavity-enhanced single nitrogen-vacancy center emission," *Nanoscale* **9**, 17902–17908 (2017).
- <sup>204</sup>R. Kolesov, B. Grotz, G. Balasubramanian, R. J. Stöhr, A. A. L. Nicolet, P. R. Hemmer, F. Jelezko, and J. Wrachtrup, "Wave-particle duality of single surface plasmon polaritons," *Nature Physics* **5**, 470–474 (2009).
- <sup>205</sup>S. I. Bogdanov, M. Y. Shalaginov, A. S. Lagutchev, C.-C. Chiang, D. Shah, A. S. Baburin, I. A. Ryzhikov, I. A. Rodionov, A. V. Kildishev, A. Boltasseva, and V. M. Shalaev, "Ultra-bright Room-Temperature Sub-Nanosecond Emission from Single Nitrogen-Vacancy Centers Coupled to Nanopatch Antennas," *Nano Letters* **18**, 4837–4844 (2018).
- <sup>206</sup>X. Meng, S. Liu, J. I. Dadap, and R. M. Osgood, "Plasmonic enhancement of a silicon-vacancy center in a nanodiamond crystal," *Phys. Rev. Materials* **1**, 015202 (2017).
- <sup>207</sup>H. Kaupp, C. Deutsch, H.-C. Chang, J. Reichel, T. W. Hänsch, and D. Hunger, "Scaling laws of the cavity enhancement for nitrogen-vacancy centers in diamond," *Phys. Rev. A* **88**, 053812 (2013).
- <sup>208</sup>R. Albrecht, A. Bommer, C. Deutsch, J. Reichel, and C. Becher, "Coupling of a Single Nitrogen-Vacancy Center in Diamond to a Fiber-Based Microcavity," *Phys. Rev. Lett.* **110**, 243602 (2013).
- <sup>209</sup>H. Kaupp, T. Hümmer, M. Mader, B. Schleder, J. Benedikter, P. Haeusser, H.-C. Chang, H. Fedder, T. W. Hänsch, and D. Hunger, "Purcell-Enhanced Single-Photon Emission from Nitrogen-Vacancy Centers Coupled to a Tunable Microcavity," *Phys. Rev. Applied* **6**, 054010 (2016).
- <sup>210</sup>J. Benedikter, H. Kaupp, T. Hümmer, Y. Liang, A. Bommer, C. Becher, A. Krueger, J. M. Smith, T. W. Hänsch, and D. Hunger, "Cavity-Enhanced Single-Photon Source Based on the Silicon-Vacancy Center in Diamond," *Phys. Rev. Applied* **7**, 024031 (2017).
- <sup>211</sup>T. Schröder, A. W. Schell, G. Kewes, T. Aichele, and O. Benson, "Fiber-integrated diamond-based single photon source," *Nano Letters* **11**, 198–202 (2011).
- <sup>212</sup>T. Schröder, M. Fujiwara, T. Noda, H.-Q. Zhao, O. Benson, and S. Takeuchi, "A nanodiamond-tapered fiber system with high single-mode coupling efficiency," *Opt. Express* **20**, 10490–10497 (2012).
- <sup>213</sup>L. Liebermeister, F. Petersen, A. v. Mnchow, D. Burchardt, J. Hermelbracht, T. Tashima, A. W. Schell, O. Benson, T. Meinhardt, A. Krueger, A. Stiebeiner, A. Rauschenbeutel, H. Weinfurter, and M. Weber, "Tapered fiber coupling of single photons emitted by a deterministically positioned single nitrogen vacancy center," *Applied Physics Letters* **104**, 031101 (2014).
- <sup>214</sup>V. V. Vorobyov, V. V. Soshenko, S. V. Bolshedvorskii, J. Javadzade, N. Lebedev, A. N. Smolyaninov, V. N. Sorokin, and A. V. Akimov, "Coupling of single NV center to adiabatically tapered optical single mode fiber," *The European Physical Journal D* **70**, 269 (2016).
- <sup>215</sup>M. R. Henderson, B. C. Gibson, H. Ebendorff-Heidepriem, K. Kuan, S. Afshar V., J. O. Orwa, I. Aharonovich, S. Tomljenovic-Hanic, A. D. Greentree, S. Prawer, and T. M. Monro, "Diamond in Tellurite Glass: a New Medium for Quantum Information," *Advanced Materials* **23**, 2806–2810 (2011).
- <sup>216</sup>V. Wood and V. Bulovi, "Colloidal quantum dot light-emitting devices," *Nano Reviews* **1**, 5202 (2010).
- <sup>217</sup>E. H. Sargent, "Colloidal quantum dot solar cells," *Nature Photonics* **6**, 133–135 (2012).
- <sup>218</sup>M. K. Choi, J. Yang, T. Hyeon, and D.-H. Kim, "Flexible quantum dot light-emitting diodes for next-generation displays," *npj Flexible Electronics* **2**, 10 (2018).
- <sup>219</sup>C. Monroe, D. M. Meekhof, B. E. King, W. M. Itano, and D. J. Wineland, "Demonstration of a Fundamental Quantum Logic Gate," *Phys. Rev. Lett.* **75**, 4714–4717 (1995).
- <sup>220</sup>C. W. Snyder, B. G. Orr, D. Kessler, and L. M. Sander, "Effect of strain on surface morphology in highly strained InGaAs films," *Phys. Rev. Lett.* **66**, 3032–3035 (1991).
- <sup>221</sup>S. H. Xin, P. D. Wang, A. Yin, C. Kim, M. Dobrowolska, J. L. Merz, and J. K. Furdyna, "Formation of self-assembling CdSe quantum dots on ZnSe by molecular beam epitaxy," *Applied Physics Letters* **69**, 3884–3886 (1996).
- <sup>222</sup>S. Fafard, Z. Wasilewski, J. McCaffrey, S. Raymond, and S. Charbonneau, "InAs self-assembled quantum dots on InP by molecular beam epitaxy," *Applied Physics Letters* **68**, 991–993 (1996).
- <sup>223</sup>J. Oshinowo, M. Nishioka, S. Ishida, and Y. Arakawa, "Highly uniform InGaAs/GaAs quantum dots (15 nm) by metalorganic chemical vapor deposition," *Applied Physics Letters* **65**, 1421–1423 (1994).
- <sup>224</sup>F. Heinrichsdorff, M.-H. Mao, N. Kirstaedter, A. Krost, D. Bimberg, A. O. Kosogov, and P. Werner, "Room-temperature continuous-wave lasing from stacked InAs/GaAs quantum dots grown by metalorganic chemical vapor deposition," *Applied Physics Letters* **71**, 22–24 (1997).
- <sup>225</sup>S.-W. Kim, S. Fujita, and S. Fujita, "Self-organized ZnO quantum dots on SiO<sub>2</sub>/Si substrates by metalorganic chemical vapor deposition," *Applied Physics Letters* **81**, 5036–5038 (2002).
- <sup>226</sup>Z. Yuan, B. E. Kardynal, R. M. Stevenson, A. J. Shields, C. J. Lobo, K. Cooper, N. S. Beattie, D. A. Ritchie, and M. Pepper, "Electrically Driven Single-Photon Source," *Science* **295**, 102–105 (2002).
- <sup>227</sup>J. Yu, S. Shendre, W.-k. Koh, B. Liu, M. Li, S. Hou, C. Hettiarachchi, S. Delikanli, P. Hernández-Martínez, M. D. Birowosuto, H. Wang, T. Sum, H. V. Demir, and C. Dang, "Electrically control amplified spontaneous emission in colloidal quantum dots," *Science Advances* **5** (2019), 10.1126/sciadv.aav3140.
- <sup>228</sup>F. T. Pedersen, Y. Wang, C. T. Olesen, S. Scholz, A. D. Wieck, A. Ludwig, M. C. Löbl, R. J. Warburton, L. Midolo, R. Uppu, *et al.*, "Near transform-limited quantum dot linewidths in a broadband photonic crystal waveguide," *arXiv preprint arXiv:2005.03943* (2020).
- <sup>229</sup>R. P. Mirin, J. P. Ibbetson, K. Nishi, A. C. Gossard, and J. E. Bowers, "1.3  $\mu\text{m}$  photoluminescence from InGaAs quantum dots on GaAs," *Applied Physics Letters* **67**, 3795–3797 (1995).
- <sup>230</sup>A. Surrente, M. Felici, P. Gallo, A. Rudra, B. Dwir, and E. Kapon, "Dense arrays of site-controlled quantum dots with tailored emission wavelength: Growth mechanisms and optical properties," *Applied Physics Letters* **111**, 221102 (2017).
- <sup>231</sup>M. Strauß, A. Kaganskiy, R. Voigt, P. Schnauber, J.-H. Schulze, S. Rodt, A. Strittmatter, and S. Reitzenstein, "Resonance fluorescence of a site-controlled quantum dot realized by the buried-stressor growth technique," *Applied Physics Letters* **110**, 111101 (2017).
- <sup>232</sup>B. Rigal, B. Dwir, A. Rudra, I. Kulkova, A. Lyasota, and E. Kapon, "Single photon extraction and propagation in photonic crystal waveguides incorporating site-controlled quantum dots," *Applied Physics Letters* **112**, 051105 (2018).
- <sup>233</sup>K. Mnaymneh, D. Dalacu, J. McKee, J. Lapointe, S. Haffouz, J. F. Weber, D. B. Northeast, P. C. Poole, G. C. Aers, and R. L. Williams, "On-Chip Integration of Single Photon Sources via Evanescent Coupling of Tapered Nanowires to SiN Waveguides," *Advanced Quantum Technologies* **3**, 1900021 (2020).
- <sup>234</sup>J.-H. Kim, S. Aghaieimebodi, C. J. K. Richardson, R. P. Leavitt, D. Englund, and E. Waks, "Hybrid Integration of Solid-State Quantum Emitters on a Silicon Photonic Chip," *Nano Letters* **17**, 7394–7400 (2017).
- <sup>235</sup>P. Bhasker, J. Norman, J. Bowers, and N. Dagli, "Intensity and phase modulators at 1.55  $\mu\text{m}$  with InAs/InGaAs quantum dots epitaxially grown on silicon," in *Conference on Lasers and Electro-Optics/Pacific Rim* (Optical Society of America, 2018)



- pp. Th2J-3.
- <sup>236</sup>A. W. Elshaari, I. E. Zadeh, A. Fognini, M. E. Reimer, D. Dalacu, P. J. Poole, V. Zwiller, and K. D. Jöns, “On-chip single photon filtering and multiplexing in hybrid quantum photonic circuits,” *Nature Communications* **8**, 379 (2017).
- <sup>237</sup>A. Singh, Q. Li, S. Liu, Y. Yu, X. Lu, C. Schneider, S. Höfling, J. Lawall, V. Verma, R. Mirin, S. W. Nam, J. Liu, and K. Srinivasan, “Quantum frequency conversion of a quantum dot single-photon source on a nanophotonic chip,” *Optica* **6**, 563–569 (2019).
- <sup>238</sup>T. Umezawa, K. Akahane, A. Kanno, and T. Kawanishi, “Investigation of a 1.5- $\mu\text{m}$ -wavelength InAs-quantum-dot absorption layer for high-speed photodetector,” *Applied Physics Express* **7**, 032201 (2014).
- <sup>239</sup>Y. Wan, Z. Zhang, R. Chao, J. Norman, D. Jung, C. Shang, Q. Li, M. Kennedy, D. Liang, C. Zhang, J.-W. Shi, A. C. Gossard, K. M. Lau, and J. E. Bowers, “Monolithically integrated InAs/InGaAs quantum dot photodetectors on silicon substrates,” *Opt. Express* **25**, 27715–27723 (2017).
- <sup>240</sup>P. Lodahl, “Quantum-dot based photonic quantum networks,” *Quantum Science and Technology* **3**, 013001 (2017).
- <sup>241</sup>Y. Arakawa and M. J. Holmes, “Progress in quantum-dot single photon sources for quantum information technologies: A broad spectrum overview,” *Applied Physics Reviews* **7**, 021309 (2020).
- <sup>242</sup>S. Rodt, A. Schliwa, K. Pötschke, F. Guffarth, and D. Bimberg, “Correlation of structural and few-particle properties of self-organized InAsGaAs quantum dots,” *Phys. Rev. B* **71**, 155325 (2005).
- <sup>243</sup>E. A. Muljarov and R. Zimmermann, “Dephasing in Quantum Dots: Quadratic Coupling to Acoustic Phonons,” *Phys. Rev. Lett.* **93**, 237401 (2004).
- <sup>244</sup>P. Michler, A. Kiraz, C. Becher, W. V. Schoenfeld, P. M. Petroff, L. Zhang, E. Hu, and A. Imamoglu, “A Quantum Dot Single-Photon Turnstile Device,” *Science* **290**, 2282–2285 (2000).
- <sup>245</sup>C. P. Dietrich, A. Fiore, M. G. Thompson, M. Kamp, and S. Höfling, “GaAs integrated quantum photonics: Towards compact and multi-functional quantum photonic integrated circuits,” *Laser & Photonics Reviews* **10**, 870–894 (2016).
- <sup>246</sup>T. Hummel, C. Ouellet-Plamondon, E. Ugur, I. Kulkova, T. Lund-Hansen, M. A. Broome, R. Uppu, and P. Lodahl, “Efficient demultiplexed single-photon source with a quantum dot coupled to a nanophotonic waveguide,” *Applied Physics Letters* **115**, 021102 (2019).
- <sup>247</sup>A. J. Shields, “Semiconductor quantum light sources,” *Nature Photonics* **1**, 215–223 (2007).
- <sup>248</sup>P. Senellart, G. Solomon, and A. White, “High-performance semiconductor quantum-dot single-photon sources,” *Nature Nanotechnology* **12**, 1026–1039 (2017).
- <sup>249</sup>E. B. Flagg, S. V. Polyakov, T. Thomay, and G. S. Solomon, “Dynamics of Nonclassical Light from a Single Solid-State Quantum Emitter,” *Phys. Rev. Lett.* **109**, 163601 (2012).
- <sup>250</sup>V. Giesz, O. Gazzano, A. K. Nowak, S. L. Portalupi, A. Lemaitre, I. Sagnes, L. Lanco, and P. Senellart, “Influence of the Purcell effect on the purity of bright single photon sources,” *Applied Physics Letters* **103**, 033113 (2013).
- <sup>251</sup>Y.-M. He, Y. He, Y.-J. Wei, D. Wu, M. Atatüre, C. Schneider, S. Höfling, M. Kamp, C.-Y. Lu, and J.-W. Pan, “On-demand semiconductor single-photon source with near-unity indistinguishability,” *Nature Nanotechnology* **8**, 213–217 (2013).
- <sup>252</sup>X. Ding, Y. He, Z.-C. Duan, N. Gregersen, M.-C. Chen, S. Unsleber, S. Maier, C. Schneider, M. Kamp, S. Höfling, C.-Y. Lu, and J.-W. Pan, “On-Demand Single Photons with High Extraction Efficiency and Near-Unity Indistinguishability from a Resonantly Driven Quantum Dot in a Micropillar,” *Phys. Rev. Lett.* **116**, 020401 (2016).
- <sup>253</sup>N. Somaschi, V. Giesz, L. De Santis, J. C. Loredo, M. P. Almeida, G. Hornecker, S. L. Portalupi, T. Grange, C. Antón, J. Demory, C. Gómez, I. Sagnes, N. D. Lanzillotti-Kimura, A. Lemaitre, A. Aufferes, A. G. White, L. Lanco, and P. Senellart, “Near-optimal single-photon sources in the solid state,” *Nature Photonics* **10**, 340–345 (2016).
- <sup>254</sup>L. Schweickert, K. D. Jöns, K. D. Zeuner, S. F. Covre da Silva, H. Huang, T. Lettner, M. Reindl, J. Zichi, R. Trotta, A. Rastelli, *et al.*, “On-demand generation of background-free single photons from a solid-state source,” *Applied Physics Letters* **112**, 093106 (2018).
- <sup>255</sup>L. Hanschke, K. A. Fischer, S. Appel, D. Lukin, J. Wierzbowski, S. Sun, R. Trivedi, J. Vučković, J. J. Finley, and K. Müller, “Quantum dot single-photon sources with ultra-low multiphoton probability,” *npj Quantum Information* **4**, 1–6 (2018).
- <sup>256</sup>M. Davanco, J. Liu, L. Sapienza, C.-Z. Zhang, J. V. De Miranda Cardoso, V. Verma, R. Mirin, S. W. Nam, L. Liu, and K. Srinivasan, “Heterogeneous integration for on-chip quantum photonic circuits with single quantum dot devices,” *Nature Communications* **8**, 889 (2017).
- <sup>257</sup>Y.-J. Wei, Y.-M. He, M.-C. Chen, Y.-N. Hu, Y. He, D. Wu, C. Schneider, M. Kamp, S. Höfling, C.-Y. Lu, and J.-W. Pan, “Deterministic and Robust Generation of Single Photons from a Single Quantum Dot with 99.5% Indistinguishability Using Adiabatic Rapid Passage,” *Nano Letters* **14**, 6515–6519 (2014).
- <sup>258</sup>K. Konthasinghe, J. Walker, M. Peiris, C. K. Shih, Y. Yu, M. F. Li, J. F. He, L. J. Wang, H. Q. Ni, Z. C. Niu, and A. Müller, “Coherent versus incoherent light scattering from a quantum dot,” *Phys. Rev. B* **85**, 235315 (2012).
- <sup>259</sup>A. Thoma, P. Schnauber, M. Gschrey, M. Seifried, J. Wolters, J.-H. Schulze, A. Strittmatter, S. Rodt, A. Carmele, A. Knorr, T. Heindel, and S. Reitzenstein, “Exploring Dephasing of a Solid-State Quantum Emitter via Time- and Temperature-Dependent Hong-Ou-Mandel Experiments,” *Phys. Rev. Lett.* **116**, 033601 (2016).
- <sup>260</sup>H. Wang, Z.-C. Duan, Y.-H. Li, S. Chen, J.-P. Li, Y.-M. He, M.-C. Chen, Y. He, X. Ding, C.-Z. Peng, C. Schneider, M. Kamp, S. Höfling, C.-Y. Lu, and J.-W. Pan, “Near-transform-limited single photons from an efficient solid-state quantum emitter,” *Phys. Rev. Lett.* **116**, 213601 (2016).
- <sup>261</sup>J. C. Loredo, N. A. Zakaria, N. Somaschi, C. Anton, L. de Santis, V. Giesz, T. Grange, M. A. Broome, O. Gazzano, G. Coppola, I. Sagnes, A. Lemaitre, A. Aufferes, P. Senellart, M. P. Almeida, and A. G. White, “Scalable performance in solid-state single-photon sources,” *Optica* **3**, 433–440 (2016).
- <sup>262</sup>M. Reindl, J. H. Weber, D. Huber, C. Schimpf, S. F. Covre da Silva, S. L. Portalupi, R. Trotta, P. Michler, and A. Rastelli, “Highly indistinguishable single photons from incoherently excited quantum dots,” *Phys. Rev. B* **100**, 155420 (2019).
- <sup>263</sup>S. Kalliakos, Y. Brody, A. J. Bennett, D. J. Ellis, J. Skiba-Szymanska, I. Farrer, J. P. Griffiths, D. A. Ritchie, and A. J. Shields, “Enhanced indistinguishability of in-plane single photons by resonance fluorescence on an integrated quantum dot,” *Applied Physics Letters* **109**, 151112 (2016).
- <sup>264</sup>G. Kiršanskė, H. Thyrrstrup, R. S. Daveau, C. L. Dreeßen, T. Pregnolato, L. Midolo, P. Tighineanu, A. Javadi, S. Stobbe, R. Schott, A. Ludwig, A. D. Wieck, S. I. Park, J. D. Song, A. V. Kuhlmann, I. Söllner, M. C. Löbl, R. J. Warburton, and P. Lodahl, “Indistinguishable and efficient single photons from a quantum dot in a planar nanobeam waveguide,” *Phys. Rev. B* **96**, 165306 (2017).
- <sup>265</sup>L. Dusanowski, S.-H. Kwon, C. Schneider, and S. Höfling, “Near-unity indistinguishability single photon source for large-scale integrated quantum optics,” *Physical review letters* **122**, 173602 (2019).
- <sup>266</sup>P. Schnauber, A. Singh, J. Schall, S. I. Park, J. D. Song, S. Rodt, K. Srinivasan, S. Reitzenstein, and M. Davanco, “Indistinguishable photons from deterministically integrated single quantum dots in heterogeneous GaAs/Si<sub>3</sub>N<sub>4</sub> quantum photonic circuits,” *Nano Letters* **19**, 7164–7172 (2019).
- <sup>267</sup>R. J. Warburton, “Single spins in self-assembled quantum dots,” *Nature Materials* **12**, 483–493 (2013).
- <sup>268</sup>A. Faraon, I. Fushman, D. Englund, N. Stoltz, P. Petroff, and J. Vučković, “Coherent generation of non-classical light on a chip via photon-induced tunnelling and blockade,” *Nature Physics* **4**,

- 859–863 (2008).
- <sup>269</sup>A. P. Foster, D. Hallett, I. V. Iorsh, S. J. Sheldon, M. R. Godsland, B. Royall, E. Clarke, I. A. Shelykh, A. M. Fox, M. S. Skolnick, I. E. Itskevich, and L. R. Wilson, “Tunable Photon Statistics Exploiting the Fano Effect in a Waveguide,” *Phys. Rev. Lett.* **122**, 173603 (2019).
- <sup>270</sup>S. Sun, H. Kim, Z. Luo, G. S. Solomon, and E. Waks, “A single-photon switch and transistor enabled by a solid-state quantum memory,” *Science* **361**, 57–60 (2018).
- <sup>271</sup>A. Javadi, D. Ding, M. H. Appel, S. Mahmoodian, M. C. Löbl, I. Söllner, R. Schott, C. Papon, T. Pregolato, S. Stobbe, L. Midolo, T. Schröder, A. D. Wieck, A. Ludwig, R. J. Warburton, and P. Lodahl, “Spin-photon interface and spin-controlled photon switching in a nanobeam waveguide,” *Nature Nanotechnology* **13**, 398–403 (2018).
- <sup>272</sup>D. Ding, M. H. Appel, A. Javadi, X. Zhou, M. C. Löbl, I. Söllner, R. Schott, C. Papon, T. Pregolato, L. Midolo, A. D. Wieck, A. Ludwig, R. J. Warburton, T. Schröder, and P. Lodahl, “Coherent Optical Control of a Quantum-Dot Spin-Qubit in a Waveguide-Based Spin-Photon Interface,” *Phys. Rev. Applied* **11**, 031002 (2019).
- <sup>273</sup>P. Lodahl, S. Mahmoodian, S. Stobbe, A. Rauschenbeutel, P. Schneeweiss, J. Volz, H. Pichler, and P. Zoller, “Chiral quantum optics,” *Nature* **541**, 473–480 (2017).
- <sup>274</sup>I. Söllner, S. Mahmoodian, S. L. Hansen, L. Midolo, A. Javadi, G. Kirsanske, T. Pregolato, H. El-Ella, E. H. Lee, J. D. Song, S. Stobbe, and P. Lodahl, “Deterministic photon-emitter coupling in chiral photonic circuits,” *Nature Nanotechnology* **10**, 775–778 (2015).
- <sup>275</sup>R. J. Coles, D. M. Price, J. E. Dixon, B. Royall, E. Clarke, P. Kok, M. S. Skolnick, A. M. Fox, and M. N. Makhonin, “Chirality of nanophotonic waveguide with embedded quantum emitter for unidirectional spin transfer,” *Nature Communications* **7**, 11183 (2016).
- <sup>276</sup>L. Tang, J. Tang, W. Zhang, G. Lu, H. Zhang, Y. Zhang, K. Xia, and M. Xiao, “On-chip chiral single-photon interface: Isolation and unidirectional emission,” *Phys. Rev. A* **99**, 043833 (2019).
- <sup>277</sup>D. Martín-Cano, H. R. Haakh, and N. Rotenberg, “Chiral emission into nanophotonic resonators,” *Acs Photonics* **6**, 961–966 (2019).
- <sup>278</sup>R. Katsumi, Y. Ota, A. Osada, T. Tajiri, T. Yamaguchi, M. Kakuda, S. Iwamoto, H. Akiyama, and Y. Arakawa, “In situ wavelength tuning of quantum-dot single-photon sources integrated on a CMOS-processed silicon waveguide,” *Applied Physics Letters* **116**, 041103 (2020).
- <sup>279</sup>A. W. Elshaari, E. Bykzer, I. E. Zadeh, T. Lettner, P. Zhao, E. Schll, S. Gyger, M. E. Reimer, D. Dalacu, P. J. Poole, K. D. Jns, and V. Zwiller, “Strain-Tunable Quantum Integrated Photonics,” *Nano Letters* **18**, 7969–7976 (2018).
- <sup>280</sup>M. Petruzzella, S. Birindelli, F. M. Pagliano, D. Pellegrino, . Zobenica, L. H. Li, E. H. Linfield, and A. Fiore, “Quantum photonic integrated circuits based on tunable dots and tunable cavities,” *APL Photonics* **3**, 106103 (2018).
- <sup>281</sup>J. H. Weber, B. Kambs, J. Kettler, S. Kern, J. Maisch, H. Vural, M. Jetter, S. L. Portalupi, C. Becher, and P. Michler, “Two-photon interference in the telecom C-band after frequency conversion of photons from remote quantum emitters,” *Nature Nanotechnology* **14**, 23–26 (2019).
- <sup>282</sup>H. Vural, S. L. Portalupi, J. Maisch, S. Kern, J. H. Weber, M. Jetter, J. Wrachtrup, R. Löw, I. Gerhardt, and P. Michler, “Two-photon interference in an atom–quantum dot hybrid system,” *Optica* **5**, 367–373 (2018).
- <sup>283</sup>A. J. Bennett, R. B. Patel, C. A. Nicoll, D. A. Ritchie, and A. J. Shields, “Interference of dissimilar photon sources,” *Nature Physics* **5**, 715–717 (2009).
- <sup>284</sup>N. Prtljaga, C. Bentham, J. O’Hara, B. Royall, E. Clarke, L. R. Wilson, M. S. Skolnick, and A. M. Fox, “On-chip interference of single photons from an embedded quantum dot and an external laser,” *Applied Physics Letters* **108**, 251101 (2016).
- <sup>285</sup>S. V. Polyakov, A. Muller, E. B. Flagg, A. Ling, N. Borjemscaia, E. Van Keuren, A. Migdall, and G. S. Solomon, “Coalescence of Single Photons Emitted by Disparate Single-Photon Sources: The Example of InAs Quantum Dots and Parametric Down-Conversion Sources,” *Phys. Rev. Lett.* **107**, 157402 (2011).
- <sup>286</sup>T. Huber, M. Prilmüller, M. Sehner, G. S. Solomon, A. Predojević, and G. Weihs, “Interfacing a quantum dot with a spontaneous parametric down-conversion source,” *Quantum Science and Technology* **2**, 034016 (2017).
- <sup>287</sup>K. Konthasinghe, M. Peiris, and A. Muller, “Resonant light scattering of a laser frequency comb by a quantum dot,” *Phys. Rev. A* **90**, 023810 (2014).
- <sup>288</sup>H. Ollivier, I. Maillette de Buy Wenniger, S. Thomas, S. C. Wein, A. Harouri, G. Coppola, P. Hilaire, C. Millet, A. Lematre, I. Sagnes, O. Krebs, L. Lanco, J. C. Loredó, C. Antn, N. Somaschi, and P. Senellart, “Reproducibility of High-Performance Quantum Dot Single-Photon Sources,” *ACS Photonics* **7**, 1050–1059 (2020).
- <sup>289</sup>H. Du, F. S. Chau, and G. Zhou, “Mechanically-tunable photonic devices with on-chip integrated mems/nems actuators,” *Micromachines* **7**, 69 (2016).
- <sup>290</sup>M. Radulaski, R. Bose, T. Tran, T. Van Vaerenbergh, D. Kielpinski, and R. G. Beausoleil, “Thermally tunable hybrid photonic architecture for nonlinear optical circuits,” *ACS Photonics* **5**, 4323–4329 (2018).
- <sup>291</sup>M. Li, H. Liang, R. Luo, Y. He, J. Ling, and Q. Lin, “Photon-level tuning of photonic nanocavities,” *Optica* **6**, 860–863 (2019).
- <sup>292</sup>K. Hennessy, A. Badolato, A. Tamboli, P. Petroff, E. Hu, M. Atatüre, J. Dreiser, and A. Imamoglu, “Tuning photonic crystal nanocavity modes by wet chemical digital etching,” *Applied Physics Letters* **87**, 021108 (2005).
- <sup>293</sup>T. Yoshie, A. Scherer, J. Hendrickson, G. Khitrova, H. M. Gibbs, G. Rupper, C. Ell, O. B. Shchekin, and D. G. Deppe, “Vacuum Rabi splitting with a single quantum dot in a photonic crystal nanocavity,” *Nature* **432**, 200–203 (2004).
- <sup>294</sup>D. G. Gevaux, A. J. Bennett, R. M. Stevenson, A. J. Shields, P. Atkinson, J. Griffiths, D. Anderson, G. A. C. Jones, and D. A. Ritchie, “Enhancement and suppression of spontaneous emission by temperature tuning InAs quantum dots to photonic crystal cavities,” *Applied Physics Letters* **88**, 131101 (2006).
- <sup>295</sup>A. Faraon, D. Englund, I. Fushman, J. Vuković, N. Stoltz, and P. Petroff, “Local quantum dot tuning on photonic crystal chips,” *Applied Physics Letters* **90**, 213110 (2007).
- <sup>296</sup>A. Faraon and J. Vuković, “Local temperature control of photonic crystal devices via micron-scale electrical heaters,” *Applied Physics Letters* **95**, 043102 (2009).
- <sup>297</sup>J.-H. Kim, S. Aghaeimeibodi, C. J. K. Richardson, R. P. Leavitt, and E. Waks, “Super-Radiant Emission from Quantum Dots in a Nanophotonic Waveguide,” *Nano Letters* **18**, 4734–4740 (2018).
- <sup>298</sup>S. G. Carter, A. S. Bracker, M. K. Yakes, M. K. Zalalutdinov, M. Kim, C. S. Kim, C. Czarnocki, M. Scheibner, and D. Gammon, “Sensing flexural motion of a photonic crystal membrane with InGaAs quantum dots,” *Applied Physics Letters* **111**, 183101 (2017).
- <sup>299</sup>J. Q. Grim, A. S. Bracker, M. Zalalutdinov, S. G. Carter, A. C. Kozen, M. Kim, C. S. Kim, J. T. Mlack, M. Yakes, B. Lee, and D. Gammon, “Scalable in operando strain tuning in nanophotonic waveguides enabling three-quantum-dot superradiance,” *Nature Materials* **18**, 963–969 (2019).
- <sup>300</sup>S. M. Thon, H. Kim, C. Bonato, J. Gudat, J. Hagemeyer, P. M. Petroff, and D. Bouwmeester, “Independent electrical tuning of separated quantum dots in coupled photonic crystal cavities,” *Applied Physics Letters* **99**, 161102 (2011).
- <sup>301</sup>F. Pagliano, Y. Cho, T. Xia, F. van Otten, R. Johne, and A. Fiore, “Dynamically controlling the emission of single excitons in photonic crystal cavities,” *Nature Communications* **5**, 5786 (2014).
- <sup>302</sup>D. Hallett, A. P. Foster, D. L. Hurst, B. Royall, P. Kok, E. Clarke, I. E. Itskevich, A. M. Fox, M. S. Skolnick, and

- L. R. Wilson, "Electrical control of nonlinear quantum optics in a nano-photon waveguide," *Optica* **5**, 644–650 (2018).
- <sup>303</sup>M. Petruzzella, T. Xia, F. Pagliano, S. Birindelli, L. Midolo, Z. Zobenica, L. H. Li, E. H. Linfield, and A. Fiore, "Fully tunable, purcell-enhanced solid-state quantum emitters," *Applied Physics Letters* **107**, 141109 (2015).
- <sup>304</sup>S. Z. Butler, S. M. Hollen, L. Cao, Y. Cui, J. A. Gupta, H. R. Gutierrez, T. F. Heinz, S. S. Hong, J. Huang, A. F. Ismach, E. Johnston-Halperin, M. Kuno, V. V. Plashnitsa, R. D. Robinson, R. S. Ruoff, S. Salahuddin, J. Shan, L. Shi, M. G. Spencer, M. Terrones, W. Windl, and J. E. Goldberger, "Progress, Challenges, and Opportunities in Two-Dimensional Materials Beyond Graphene," *ACS Nano* **7**, 2898–2926 (2013).
- <sup>305</sup>Y.-M. He, G. Clark, J. R. Schaibley, Y. He, M.-C. Chen, Y.-J. Wei, X. Ding, Q. Zhang, W. Yao, X. Xu, C.-Y. Lu, and J.-W. Pan, "Single quantum emitters in monolayer semiconductors," *Nature Nanotechnology* **10**, 497–502 (2015).
- <sup>306</sup>A. K. Geim and I. V. Grigorieva, "Van der Waals heterostructures," *Nature* **499**, 419–425 (2013).
- <sup>307</sup>A. K. Geim and K. S. Novoselov, "The rise of graphene," *Nature Materials* **6**, 183–191 (2007).
- <sup>308</sup>F. Xia, H. Wang, and Y. Jia, "Rediscovering black phosphorus as an anisotropic layered material for optoelectronics and electronics," *Nature Communications* **5**, 4458 (2014).
- <sup>309</sup>A. J. Mannix, X.-F. Zhou, B. Kiraly, J. D. Wood, D. Alducin, B. D. Myers, X. Liu, B. L. Fisher, U. Santiago, J. R. Guest, M. J. Yacaman, A. Ponce, A. R. Oganov, M. C. Hersam, and N. P. Guisinger, "Synthesis of borophenes: Anisotropic, two-dimensional boron polymorphs," *Science* **350**, 1513–1516 (2015).
- <sup>310</sup>D. Xiao, G.-B. Liu, W. Feng, X. Xu, and W. Yao, "Coupled Spin and Valley Physics in Monolayers of MoS<sub>2</sub> and Other Group-VI Dichalcogenides," *Phys. Rev. Lett.* **108**, 196802 (2012).
- <sup>311</sup>M. Atatüre, D. Englund, N. Vamivakas, S.-Y. Lee, and J. Wrachtrup, "Material platforms for spin-based photonic quantum technologies," *Nature Reviews Materials* **3**, 38–51 (2018).
- <sup>312</sup>A. Srivastava, M. Sidler, A. V. Allain, D. S. Lembke, A. Kis, and A. Imamoglu, "Optically active quantum dots in monolayer WSe<sub>2</sub>," *Nature Nanotechnology* **10**, 491–496 (2015).
- <sup>313</sup>A. Gottscholl, M. Kianinia, V. Soltamov, S. Orlinskii, G. Mamin, C. Bradac, C. Kasper, K. Krambrock, A. Sperlich, M. Toth, I. Aharonovich, and V. Dyakonov, "Initialization and read-out of intrinsic spin defects in a van der Waals crystal at room temperature," *Nature Materials* (2020), 10.1038/s41563-020-0619-6.
- <sup>314</sup>M. Koperski, K. Nogajewski, A. Arora, V. Cherkez, P. Mallet, J.-Y. Veuillen, J. Marcus, P. Kossacki, and M. Potemski, "Single photon emitters in exfoliated WSe<sub>2</sub> structures," *Nature Nanotechnology* **10**, 503–506 (2015).
- <sup>315</sup>Q. H. Wang, K. Kalantar-Zadeh, A. Kis, J. N. Coleman, and M. S. Strano, "Electronics and optoelectronics of two-dimensional transition metal dichalcogenides," *Nature Nanotechnology* **7**, 699–712 (2012).
- <sup>316</sup>K. F. Mak and J. Shan, "Photonics and optoelectronics of 2D semiconductor transition metal dichalcogenides," *Nature Photonics* **10**, 216–226 (2016).
- <sup>317</sup>A. Splendiani, L. Sun, Y. Zhang, T. Li, J. Kim, C.-Y. Chim, G. Galli, and F. Wang, "Emerging Photoluminescence in Monolayer MoS<sub>2</sub>," *Nano Letters* **10**, 1271–1275 (2010).
- <sup>318</sup>J. S. Ross, P. Klement, A. M. Jones, N. J. Ghimire, J. Yan, D. G. Mandrus, T. Taniguchi, K. Watanabe, K. Kitamura, W. Yao, D. H. Cobden, and X. Xu, "Electrically tunable excitonic light-emitting diodes based on monolayer WSe<sub>2</sub> p-n junctions," *Nature Nanotechnology* **9**, 268–272 (2014).
- <sup>319</sup>C. Lee, H. Yan, L. E. Brus, T. F. Heinz, J. Hone, and S. Ryu, "Anomalous Lattice Vibrations of Single- and Few-Layer MoS<sub>2</sub>," *ACS Nano* **4**, 2695–2700 (2010).
- <sup>320</sup>K. F. Mak, K. He, J. Shan, and T. F. Heinz, "Control of valley polarization in monolayer MoS<sub>2</sub> by optical helicity," *Nature Nanotechnology* **7**, 494–498 (2012).
- <sup>321</sup>A. M. Jones, H. Yu, N. J. Ghimire, S. Wu, G. Aivazian, J. S. Ross, B. Zhao, J. Yan, D. G. Mandrus, D. Xiao, W. Yao, and X. Xu, "Optical generation of excitonic valley coherence in monolayer WSe<sub>2</sub>," *Nature Nanotechnology* **8**, 634–638 (2013).
- <sup>322</sup>C. Chiriac, D. G. Cahill, N. Nguyen, D. Johnson, A. Bodapati, P. Keblinski, and P. Zschack, "Ultralow Thermal Conductivity in Disordered, Layered WSe<sub>2</sub> Crystals," *Science* **315**, 351–353 (2007).
- <sup>323</sup>S.-Y. Kim, J. Kwak, C. V. Ciobanu, and S.-Y. Kwon, "Recent Developments in Controlled Vapor-Phase Growth of 2D Group 6 Transition Metal Dichalcogenides," *Advanced Materials* **31**, 1804939 (2019).
- <sup>324</sup>Y. Zhang, T.-R. Chang, B. Zhou, Y.-T. Cui, H. Yan, Z. Liu, F. Schmitt, J. Lee, R. Moore, Y. Chen, H. Lin, H.-T. Jeng, S.-K. Mo, Z. Hussain, A. Bansil, and Z.-X. Shen, "Direct observation of the transition from indirect to direct bandgap in atomically thin epitaxial MoSe<sub>2</sub>," *Nature Nanotechnology* **9**, 111–115 (2014).
- <sup>325</sup>T. Li and G. Galli, "Electronic Properties of MoS<sub>2</sub> Nanoparticles," *The Journal of Physical Chemistry C* **111**, 16192–16196 (2007).
- <sup>326</sup>T. Cheiwchanchamnangij and W. R. L. Lambrecht, "Quasiparticle band structure calculation of monolayer, bilayer, and bulk mos<sub>2</sub>," *Phys. Rev. B* **85**, 205302 (2012).
- <sup>327</sup>K. F. Mak, C. Lee, J. Hone, J. Shan, and T. F. Heinz, "Atomically Thin MoS<sub>2</sub>: A New Direct-Gap Semiconductor," *Phys. Rev. Lett.* **105**, 136805 (2010).
- <sup>328</sup>D. Xiao, G.-B. Liu, W. Feng, X. Xu, and W. Yao, "Coupled Spin and Valley Physics in Monolayers of MoS<sub>2</sub> and Other Group-VI Dichalcogenides," *Phys. Rev. Lett.* **108**, 196802 (2012).
- <sup>329</sup>T. Cao, G. Wang, W. Han, H. Ye, C. Zhu, J. Shi, Q. Niu, P. Tan, E. Wang, B. Liu, and J. Feng, "Valley-selective circular dichroism of monolayer molybdenum disulphide," *Nature Communications* **3**, 887 (2012).
- <sup>330</sup>K. F. Mak, K. L. McGill, J. Park, and P. L. McEuen, "The valley Hall effect in MoS<sub>2</sub> transistors," *Science* **344**, 1489–1492 (2014).
- <sup>331</sup>K. He, N. Kumar, L. Zhao, Z. Wang, K. F. Mak, H. Zhao, and J. Shan, "Tightly Bound Excitons in Monolayer WSe<sub>2</sub>," *Phys. Rev. Lett.* **113**, 026803 (2014).
- <sup>332</sup>Z. Ye, T. Cao, K. O'Brien, H. Zhu, X. Yin, Y. Wang, S. G. Louie, and X. Zhang, "Probing excitonic dark states in single-layer tungsten disulphide," *Nature* **513**, 214–218 (2014).
- <sup>333</sup>M. M. Ugeda, A. J. Bradley, S.-F. Shi, F. H. da Jornada, Y. Zhang, D. Y. Qiu, W. Ruan, S.-K. Mo, Z. Hussain, Z.-X. Shen, F. Wang, S. G. Louie, and M. F. Crommie, "Giant bandgap renormalization and excitonic effects in a monolayer transition metal dichalcogenide semiconductor," *Nature Materials* **13**, 1091–1095 (2014).
- <sup>334</sup>K. F. Mak, K. He, C. Lee, G. H. Lee, J. Hone, T. F. Heinz, and J. Shan, "Tightly bound trions in monolayer MoS<sub>2</sub>," *Nature Materials* **12**, 207–211 (2013).
- <sup>335</sup>Y. You, X.-X. Zhang, T. C. Berkelbach, M. S. Hybertsen, D. R. Reichman, and T. F. Heinz, "Observation of biexcitons in monolayer WSe<sub>2</sub>," *Nature Physics* **11**, 477–481 (2015).
- <sup>336</sup>Y.-M. He, G. Clark, J. R. Schaibley, Y. He, M.-C. Chen, Y.-J. Wei, X. Ding, Q. Zhang, W. Yao, X. Xu, C.-Y. Lu, and J.-W. Pan, "Single quantum emitters in monolayer semiconductors," *Nature Nanotechnology* **10**, 497–502 (2015).
- <sup>337</sup>C. Chakraborty, L. Kinnischtzke, K. M. Goodfellow, R. Beams, and A. N. Vamivakas, "Voltage-controlled quantum light from an atomically thin semiconductor," *Nature Nanotechnology* **10**, 507–511 (2015).
- <sup>338</sup>S. Schwarz, A. Kozikov, F. Withers, J. K. Maguire, A. P. Foster, S. Dufferwiel, L. Hague, M. N. Makhonin, L. R. Wilson, A. K. Geim, K. S. Novoselov, and A. I. Tartakovskii, "Electrically

- pumped single-defect light emitters in WSe<sub>2</sub>,” *2D Materials* **3**, 025038 (2016).
- <sup>339</sup>A. Branny, S. Kumar, R. Proux, and B. D. Gerardot, “Deterministic strain-induced arrays of quantum emitters in a two-dimensional semiconductor,” *Nature Communications* **8**, 15053 (2017).
- <sup>340</sup>C. Palacios-Berraquero, D. M. Kara, A. R. P. Montblanch, M. Barbone, P. Latawiec, D. Yoon, A. K. Ott, M. Loncar, A. C. Ferrari, and M. Atatüre, “Large-scale quantum-emitter arrays in atomically thin semiconductors,” *Nature Communications* **8**, 15093 (2017).
- <sup>341</sup>T. T. Tran, S. Choi, J. A. Scott, Z.-Q. Xu, C. Zheng, G. Seniutinas, A. Bendavid, M. S. Fuhrer, M. Toth, and I. Aharonovich, “Room-Temperature Single-Photon Emission from Oxidized Tungsten Disulfide Multilayers,” *Advanced Optical Materials* **5**, 1600939 (2017).
- <sup>342</sup>Y. Luo, N. Liu, X. Li, J. C. Hone, and S. Strauf, “Single photon emission in WSe<sub>2</sub> up 160 K by quantum yield control,” *2D Materials* **6**, 035017 (2019).
- <sup>343</sup>T. T. Tran, K. Bray, M. J. Ford, M. Toth, and I. Aharonovich, “Quantum emission from hexagonal boron nitride monolayers,” *Nature Nanotechnology* **11**, 37–41 (2016).
- <sup>344</sup>T. T. Tran, C. Elbadawi, D. Totonjian, C. J. Lobo, G. Grosso, H. Moon, D. R. Englund, M. J. Ford, I. Aharonovich, and M. Toth, “Robust Multicolor Single Photon Emission from Point Defects in Hexagonal Boron Nitride,” *ACS Nano* **10**, 7331–7338 (2016).
- <sup>345</sup>F. Hayee, L. Yu, J. L. Zhang, C. J. Ciccarino, M. Nguyen, A. F. Marshall, I. Aharonovich, J. Vuckovic, P. Narang, T. F. Heinz, and J. A. Dionne, “Revealing multiple classes of stable quantum emitters in hexagonal boron nitride with correlated optical and electron microscopy,” *Nature Materials* (2020), 10.1038/s41563-020-0616-9.
- <sup>346</sup>X. Liu and M. C. Hersam, “2D materials for quantum information science,” *Nature Reviews Materials* **4**, 669–684 (2019).
- <sup>347</sup>A. Dietrich, M. Bürk, E. S. Steiger, L. Antoniuk, T. T. Tran, M. Nguyen, I. Aharonovich, F. Jelezko, and A. Kubanek, “Observation of fourier transform limited lines in hexagonal boron nitride,” *Phys. Rev. B* **98**, 081414 (2018).
- <sup>348</sup>A. Dietrich, M. W. Doherty, I. Aharonovich, and A. Kubanek, “Solid-state single photon source with fourier transform limited lines at room temperature,” *Phys. Rev. B* **101**, 081401 (2020).
- <sup>349</sup>D. Wong, J. Velasco, L. Ju, J. Lee, S. Kahn, H.-Z. Tsai, C. Germany, T. Taniguchi, K. Watanabe, A. Zettl, F. Wang, and M. F. Crommie, “Characterization and manipulation of individual defects in insulating hexagonal boron nitride using scanning tunnelling microscopy,” *Nature Nanotechnology* **10**, 949–953 (2015).
- <sup>350</sup>A. Bommer and C. Becher, “New insights into nonclassical light emission from defects in multi-layer hexagonal boron nitride,” *Nanophotonics* **8**, 2041 – 2048 (2019).
- <sup>351</sup>N. V. Proscia, Z. Shotan, H. Jayakumar, P. Reddy, C. Cohen, M. Dollar, A. Alkauskas, M. Doherty, C. A. Meriles, and V. M. Menon, “Near-deterministic activation of room-temperature quantum emitters in hexagonal boron nitride,” *Optica* **5**, 1128–1134 (2018).
- <sup>352</sup>M. R. Rosenberger, C. K. Dass, H.-J. Chuang, S. V. Sivaram, K. M. McCreary, J. R. Hendrickson, and B. T. Jonker, “Quantum Calligraphy: Writing Single-Photon Emitters in a Two-Dimensional Materials Platform,” *ACS Nano* **13**, 904–912 (2019).
- <sup>353</sup>Z. Li, Y. Li, T. Han, X. Wang, Y. Yu, B. Tay, Z. Liu, and Z. Fang, “Tailoring MoS<sub>2</sub> ExcitonPlasmon Interaction by Optical SpinOrbit Coupling,” *ACS Nano* **11**, 1165–1171 (2017).
- <sup>354</sup>G. M. Akselrod, T. Ming, C. Argyropoulos, T. B. Hoang, Y. Lin, X. Ling, D. R. Smith, J. Kong, and M. H. Mikkelsen, “Leveraging Nanocavity Harmonics for Control of Optical Processes in 2D Semiconductors,” *Nano Letters* **15**, 3578–3584 (2015).
- <sup>355</sup>M. Nguyen, S. Kim, T. T. Tran, Z.-Q. Xu, M. Kianinia, M. Toth, and I. Aharonovich, “Nanoassembly of quantum emitters in hexagonal boron nitride and gold nanospheres,” *Nanoscale* **10**, 2267–2274 (2018).
- <sup>356</sup>X. Gan, Y. Gao, K. Fai Mak, X. Yao, R.-J. Shiue, A. van der Zande, M. E. Trusheim, F. Hatami, T. F. Heinz, J. Hone, and D. Englund, “Controlling the spontaneous emission rate of monolayer MoS<sub>2</sub> in a photonic crystal nanocavity,” *Applied Physics Letters* **103**, 181119 (2013).
- <sup>357</sup>G. Wei, T. K. Stanev, D. A. Czapslewski, I. W. Jung, and N. P. Stern, “Silicon-nitride photonic circuits interfaced with monolayer MoS<sub>2</sub>,” *Applied Physics Letters* **107**, 091112 (2015).
- <sup>358</sup>H. Chen, S. Nanz, A. Abass, J. Yan, T. Gao, D.-Y. Choi, Y. S. Kivshar, C. Rockstuhl, and D. N. Neshev, “Enhanced Directional Emission from Monolayer WSe<sub>2</sub> Integrated onto a Multiresonant Silicon-Based Photonic Structure,” *ACS Photonics* **4**, 3031–3038 (2017).
- <sup>359</sup>T. Cai, J.-H. Kim, Z. Yang, S. Dutta, S. Aghaeimeibodi, and E. Waks, “Radiative Enhancement of Single Quantum Emitters in WSe<sub>2</sub> Monolayers Using Site-Controlled Metallic Nanopillars,” *ACS Photonics* **5**, 3466–3471 (2018).
- <sup>360</sup>O. Iff, N. Lundt, S. Betzold, L. N. Tripathi, M. Emmerling, S. Tongay, Y. J. Lee, S.-H. Kwon, S. Höfling, and C. Schneider, “Deterministic coupling of quantum emitters in WSe<sub>2</sub> monolayers to plasmonic nanocavities,” *Opt. Express* **26**, 25944–25951 (2018).
- <sup>361</sup>Y. Luo, G. D. Shepard, J. V. Ardelean, D. A. Rhodes, B. Kim, K. Barmak, J. C. Hone, and S. Strauf, “Deterministic coupling of site-controlled quantum emitters in monolayer WSe<sub>2</sub> to plasmonic nanocavities,” *Nature Nanotechnology* **13**, 1137–1142 (2018).
- <sup>362</sup>N. V. Proscia, R. J. Collison, C. A. Meriles, and V. M. Menon, “Coupling of deterministically activated quantum emitters in hexagonal boron nitride to plasmonic surface lattice resonances,” *Nanophotonics* **8**, 2057 – 2064 (2019).
- <sup>363</sup>T. Cai, S. Dutta, S. Aghaeimeibodi, Z. Yang, S. Nah, J. T. Fourkas, and E. Waks, “Coupling Emission from Single Localized Defects in Two-Dimensional Semiconductor to Surface Plasmon Polaritons,” *Nano Letters* **17**, 6564–6568 (2017).
- <sup>364</sup>S. Dutta, T. Cai, M. A. Buyukkaya, S. Barik, S. Aghaeimeibodi, and E. Waks, “Coupling quantum emitters in WSe<sub>2</sub> monolayers to a metal-insulator-metal waveguide,” *Applied Physics Letters* **113**, 191105 (2018).
- <sup>365</sup>F. Peyskens, C. Chakraborty, M. Muneeb, D. Van Thourhout, and D. Englund, “Integration of single photon emitters in 2D layered materials with a silicon nitride photonic chip,” *Nature Communications* **10**, 4435 (2019).
- <sup>366</sup>D. White, A. Branny, R. J. Chapman, R. Picard, M. Brotons-Gisbert, A. Boes, A. Peruzzo, C. Bonato, and B. D. Gerardot, “Atomically-thin quantum dots integrated with lithium niobate photonic chips (Invited),” *Opt. Mater. Express* **9**, 441–448 (2019).
- <sup>367</sup>H. B. Dyer, F. A. Raal, L. D. Preez, and J. H. N. Loubser, “Optical absorption features associated with paramagnetic nitrogen in diamond,” *The Philosophical Magazine: A Journal of Theoretical Experimental and Applied Physics* **11**, 763–774 (1965).
- <sup>368</sup>R. M. Chrenko, H. M. Strong, and R. E. Tuft, “Dispersed paramagnetic nitrogen content of large laboratory diamonds,” *The Philosophical Magazine: A Journal of Theoretical Experimental and Applied Physics* **23**, 313–318 (1971).
- <sup>369</sup>A. Mainwood, “Substitutional impurities in diamond,” *Journal of Physics C: Solid State Physics* **12**, 2543–2549 (1979).
- <sup>370</sup>M. Werner and R. Locher, “Growth and application of undoped and doped diamond films,” *Reports on Progress in Physics* **61**, 1665–1710 (1998).
- <sup>371</sup>Z. Yang, M. Pelton, I. Fedin, D. V. Talapin, and E. Waks, “A room temperature continuous-wave nanolaser using colloidal quantum wells,” *Nature Communications* **8**, 143 (2017).
- <sup>372</sup>Y. Chen, A. Ryou, M. R. Friedfeld, T. Fryett, J. Whitehead, B. M. Cossairt, and A. Majumdar, “Deterministic Positioning of Colloidal Quantum Dots on Silicon Nitride Nanobeam Cavi-

- ties,” *Nano Letters* **18**, 6404–6410 (2018).
- <sup>373</sup>J. Martin, R. Wannemacher, J. Teichert, L. Bischoff, and B. Khler, “Generation and detection of fluorescent color centers in diamond with submicron resolution,” *Applied Physics Letters* **75**, 3096–3098 (1999).
- <sup>374</sup>F. Waldermann, P. Olivero, J. Nunn, K. Surmacz, Z. Wang, D. Jaksch, R. Taylor, I. Walmsley, M. Draganski, P. Reichart, A. Greentree, D. Jamieson, and S. Prawer, “Creating diamond color centers for quantum optical applications,” *Diamond and Related Materials* **16**, 1887–1895 (2007).
- <sup>375</sup>D. McCloskey, D. Fox, N. O’Hara, V. Usov, D. Scanlan, N. McEvoy, G. S. Duesberg, G. L. W. Cross, H. Z. Zhang, and J. F. Donegan, “Helium ion microscope generated nitrogen-vacancy centres in type Ib diamond,” *Applied Physics Letters* **104**, 031109 (2014).
- <sup>376</sup>Wee, Tse-Luen and Tzeng, Yan-Kai and Han, Chau-Chung and Chang, Huan-Cheng and Fann, Wunshain and Hsu, Jui-Hung and Chen, Kuan-Ming and Yu, Yueh-Chung, “Two-photon Excited Fluorescence of Nitrogen-Vacancy Centers in Proton-Irradiated Type Ib Diamond,” *The Journal of Physical Chemistry A* **111**, 9379–9386 (2007).
- <sup>377</sup>I. Kiflawi, A. T. Collins, K. Iakubovskii, and D. Fisher, “Electron irradiation and the formation of vacancy–interstitial pairs in diamond,” *Journal of Physics: Condensed Matter* **19**, 046216 (2007).
- <sup>378</sup>S. Becker, N. Raatz, S. Jankuhn, R. John, and J. Meijer, “Nitrogen implantation with a scanning electron microscope,” *Scientific Reports* **8**, 32 (2018).
- <sup>379</sup>A. Mainwood, “Nitrogen and nitrogen-vacancy complexes and their formation in diamond,” *Phys. Rev. B* **49**, 7934–7940 (1994).
- <sup>380</sup>A. T. Collins and I. Kiflawi, “The annealing of radiation damage in type Ia diamond,” *Journal of Physics: Condensed Matter* **21**, 364209 (2009).
- <sup>381</sup>G. Davies, “Charge states of the vacancy in diamond,” *Nature* **269**, 498–500 (1977).
- <sup>382</sup>X. Hu, Y. Dai, R. Li, H. Shen, and X. He, “The diffusion of vacancies near a diamond (001) surface,” *Solid State Communications* **122**, 45–48 (2002).
- <sup>383</sup>C. Santori, P. E. Barclay, K.-M. C. Fu, and R. G. Beausoleil, “Vertical distribution of nitrogen-vacancy centers in diamond formed by ion implantation and annealing,” *Phys. Rev. B* **79**, 125313 (2009).
- <sup>384</sup>A. Gippius, R. Khmelnskiy, V. Dravin, and S. Tkachenko, “Formation and characterization of graphitized layers in ion-implanted diamond,” *Diamond and Related Materials* **8**, 1631–1634 (1999).
- <sup>385</sup>J. W. Steeds, W. Sullivan, A. Wotherspoon, and J. M. Hayes, “Long-range migration of intrinsic defects during irradiation or implantation,” *Journal of Physics: Condensed Matter* **21**, 364219 (2009).
- <sup>386</sup>D. M. Toyli, C. D. Weis, G. D. Fuchs, T. Schenkel, and D. D. Awschalom, “Chip-Scale Nanofabrication of Single Spins and Spin Arrays in Diamond,” *Nano Letters* **10**, 3168–3172 (2010).
- <sup>387</sup>P. Spinicelli, A. Dréau, L. Rondin, F. Silva, J. Achard, S. Xavier, S. Bansropun, T. Debuisschert, S. Pezzagna, J. Meijer, V. Jacques, and J.-F. Roch, “Engineered arrays of nitrogen-vacancy color centers in diamond based on implantation of CN-molecules through nanoapertures,” *New Journal of Physics* **13**, 025014 (2011).
- <sup>388</sup>S. Pezzagna, D. Rogalla, H.-W. Becker, I. Jakobi, F. Dolde, B. Naydenov, J. Wrachtrup, F. Jelezko, C. Trautmann, and J. Meijer, “Creation of colour centres in diamond by collimated ion-implantation through nano-channels in mica,” *physica status solidi (a)* **208**, 2017–2022 (2011).
- <sup>389</sup>S. Sangtawesin, T. O. Brundage, Z. J. Atkins, and J. R. Petta, “Highly tunable formation of nitrogen-vacancy centers via ion implantation,” *Applied Physics Letters* **105**, 063107 (2014).
- <sup>390</sup>J. Orwa, K. Ganesan, J. Newnham, C. Santori, P. Barclay, K. Fu, R. Beausoleil, I. Aharonovich, B. Fairchild, P. Olivero, A. Greentree, and S. Prawer, “An upper limit on the lateral vacancy diffusion length in diamond,” *Diamond and Related Materials* **24**, 6–10 (2012).
- <sup>391</sup>V. M. Acosta, E. Bauch, M. P. Ledbetter, C. Santori, K.-M. C. Fu, P. E. Barclay, R. G. Beausoleil, H. Linget, J. F. Roch, F. Treussart, S. Chemerisov, W. Gawlik, and D. Budker, “Diamonds with a high density of nitrogen-vacancy centers for magnetometry applications,” *Phys. Rev. B* **80**, 115202 (2009).
- <sup>392</sup>T. Ishikawa, K.-M. C. Fu, C. Santori, V. M. Acosta, R. G. Beausoleil, H. Watanabe, S. Shikata, and K. M. Itoh, “Optical and Spin Coherence Properties of Nitrogen-Vacancy Centers Placed in a 100 nm Thick Isotopically Purified Diamond Layer,” *Nano Letters* **12**, 2083–2087 (2012).
- <sup>393</sup>K. Ohashi, T. Roskopf, H. Watanabe, M. Loretz, Y. Tao, R. Hauert, S. Tomizawa, T. Ishikawa, J. Ishi-Hayase, S. Shikata, C. L. Degen, and K. M. Itoh, “Negatively Charged Nitrogen-Vacancy Centers in a 5 nm Thin 12C Diamond Film,” *Nano Letters* **13**, 4733–4738 (2013).
- <sup>394</sup>C. A. McLellan, B. A. Myers, S. Kraemer, K. Ohno, D. D. Awschalom, and A. C. Bleszynski Jayich, “Patterned formation of highly coherent nitrogen-vacancy centers using a focused electron irradiation technique,” *Nano Letters* **16**, 2450–2454 (2016).
- <sup>395</sup>E. E. Kleinsasser, M. M. Stanfield, J. K. Q. Banks, Z. Zhu, W.-D. Li, V. M. Acosta, H. Watanabe, K. M. Itoh, and K.-M. C. Fu, “High density nitrogen-vacancy sensing surface created via He+ ion implantation of 12C diamond,” *Applied Physics Letters* **108**, 202401 (2016).
- <sup>396</sup>J. Meijer, B. Burchard, M. Domhan, C. Wittmann, T. Gaebl, I. Popa, F. Jelezko, and J. Wrachtrup, “Generation of single color centers by focused nitrogen implantation,” *Applied Physics Letters* **87**, 261909 (2005).
- <sup>397</sup>S. Pezzagna, B. Naydenov, F. Jelezko, J. Wrachtrup, and J. Meijer, “Creation efficiency of nitrogen-vacancy centres in diamond,” *New Journal of Physics* **12**, 065017 (2010).
- <sup>398</sup>J. F. Ziegler, “SRIM-2003,” *Nuclear Instruments and Methods in Physics Research Section B: Beam Interactions with Materials and Atoms* **219-220**, 1027–1036 (2004).
- <sup>399</sup>Y. Liu, G. Chen, M. Song, X. Ci, B. Wu, E. Wu, and H. Zeng, “Fabrication of nitrogen vacancy color centers by femtosecond pulse laser illumination,” *Opt. Express* **21**, 12843–12848 (2013).
- <sup>400</sup>Y.-C. Chen, B. Griffiths, L. Weng, S. S. Nicley, S. N. Ishmael, Y. Lekhai, S. Johnson, C. J. Stephen, B. L. Green, G. W. Morley, M. E. Newton, M. J. Booth, P. S. Salter, and J. M. Smith, “Laser writing of individual nitrogen-vacancy defects in diamond with near-unity yield,” *Optica* **6**, 662–667 (2019).
- <sup>401</sup>E. Murray, D. J. P. Ellis, T. Meany, F. F. Floether, J. P. Lee, J. P. Griffiths, G. A. C. Jones, I. Farrer, D. A. Ritchie, A. J. Bennett, and A. J. Shields, “Quantum photonics hybrid integration platform,” *Applied Physics Letters* **107**, 171108 (2015).
- <sup>402</sup>R. Katsumi, Y. Ota, A. Osada, T. Yamaguchi, T. Tajiri, M. Kakuda, S. Iwamoto, H. Akiyama, and Y. Arakawa, “Quantum-dot single-photon source on a CMOS silicon photonic chip integrated using transfer printing,” *APL Photonics* **4**, 036105 (2019).
- <sup>403</sup>Y.-C. Chen, P. S. Salter, S. Knauer, L. Weng, A. C. Frangeskou, C. J. Stephen, S. N. Ishmael, P. R. Dolan, S. Johnson, B. L. Green, G. W. Morley, M. E. Newton, J. G. Rarity, M. J. Booth, and J. M. Smith, “Laser writing of coherent colour centres in diamond,” *Nature Photonics* **11**, 77–80 (2017).
- <sup>404</sup>H. Nakamura, Y. Sugimoto, K. Kanamoto, N. Ikeda, Y. Tanaka, Y. Nakamura, S. Ohkouchi, Y. Watanabe, K. Inoue, H. Ishikawa, and K. Asakawa, “Ultra-fast photonic crystal/quantum dot all-optical switch for future photonic networks,” *Opt. Express* **12**, 6606–6614 (2004).
- <sup>405</sup>T. Pregnolato, X.-L. Chu, T. Schröder, R. Schott, A. D. Wieck, A. Ludwig, P. Lodahl, and N. Rotenberg, “Deterministic positioning of quantum dots in nanophotonic waveguides,” *arXiv preprint arXiv:1907.01426* (2019).
- <sup>406</sup>K. Tanabe, K. Watanabe, and Y. Arakawa, “III-V/Si hybrid photonic devices by direct fusion bonding,” *Scientific Reports*

- 2**, 349 (2012).
- <sup>407</sup>D. Ellis, A. Bennett, C. Dangel, J. Lee, J. Griffiths, T. Mitchell, T.-K. Paraiso, P. Spencer, D. Ritchie, and A. Shields, “Independent indistinguishable quantum light sources on a reconfigurable photonic integrated circuit,” *Applied Physics Letters* **112**, 211104 (2018).
- <sup>408</sup>I. E. Zadeh, A. W. Elshaari, K. D. Jns, A. Fognini, D. Dalacu, P. J. Poole, M. E. Reimer, and V. Zwiller, “Deterministic Integration of Single Photon Sources in Silicon Based Photonic Circuits,” *Nano Letters* **16**, 2289–2294 (2016).
- <sup>409</sup>A. Castellanos-Gomez, M. Buscema, R. Molenaar, V. Singh, L. Janssen, H. S. J. van der Zant, and G. A. Steele, “Deterministic transfer of two-dimensional materials by all-dry viscoelastic stamping,” *2D Materials* **1**, 011002 (2014).
- <sup>410</sup>R. Katsumi, Y. Ota, M. Kakuda, S. Iwamoto, and Y. Arakawa, “Transfer-printed single-photon sources coupled to wire waveguides,” *Optica* **5**, 691–694 (2018).
- <sup>411</sup>G. F. Schneider, V. E. Calado, H. Zandbergen, L. M. K. Vander-sypen, and C. Dekker, “Wedging transfer of nanostructures,” *Nano Letters* **10**, 1912–1916 (2010).
- <sup>412</sup>C. R. Dean, A. F. Young, I. Meric, C. Lee, L. Wang, S. Sorgenfrei, K. Watanabe, T. Taniguchi, P. Kim, K. L. Shepard, and J. Hone, “Boron nitride substrates for high-quality graphene electronics,” *Nature Nanotechnology* **5**, 722–726, <https://doi.org/10.1038/nnano.2010.172>.
- <sup>413</sup>P. J. Zomer, S. P. Dash, N. Tombros, and B. J. van Wees, “A transfer technique for high mobility graphene devices on commercially available hexagonal boron nitride,” *Applied Physics Letters* **99**, 232104 (2011).
- <sup>414</sup>C. Linghu, S. Zhang, C. Wang, and J. Song, “Transfer printing techniques for flexible and stretchable inorganic electronics,” *npj Flexible Electronics* **2**, 26 (2018).
- <sup>415</sup>J. Lee, I. Karnadi, J. T. Kim, Y.-H. Lee, and M.-K. Kim, “Printed Nanolaser on Silicon,” *ACS Photonics* **4**, 2117–2123 (2017).
- <sup>416</sup>L. Li, I. Bayn, M. Lu, C.-Y. Nam, T. Schröder, A. Stein, N. C. Harris, and D. Englund, “Nanofabrication on unconventional substrates using transferred hard masks,” *Scientific Reports* **5**, 7802 (2015).
- <sup>417</sup>K. Aoki, D. Guimard, M. Nishioka, M. Nomura, S. Iwamoto, and Y. Arakawa, “Coupling of quantum-dot light emission with a three-dimensional photonic-crystal nanocavity,” *Nature Photonics* **2**, 688–692 (2008).
- <sup>418</sup>H. Thyrestrup, G. Kirsanske, H. Le Jeannic, T. Pregolato, L. Zhai, L. Raahauge, L. Midolo, N. Rotenberg, A. Javadi, R. Schott, *et al.*, “Quantum optics with near-lifetime-limited quantum-dot transitions in a nanophotonic waveguide,” *Nano letters* **18**, 1801–1806 (2018).
- <sup>419</sup>R. S. Daveau, K. C. Balram, T. Pregolato, J. Liu, E. H. Lee, J. D. Song, V. Verma, R. Mirin, S. W. Nam, L. Midolo, *et al.*, “Efficient fiber-coupled single-photon source based on quantum dots in a photonic-crystal waveguide,” *Optica* **4**, 178–184 (2017).